Assessment Of Contaminant Flowpaths In Airside Economization And Analysis Of Thermal Performance At Tank And Server Level For Single-phase Immersion Cooled Data Centers

Dissertation

by

SATYAM SAINI

Submitted in Partial Fulfillment of the Requirements

for the Degree of Doctor of Philosophy at

The University of Texas at Arlington

MAY 2022

Supervising Committee:

Dr. Dereje Agonafer
Dr. Abdolhossein Haji-Sheikh
Dr. Miguel A. Amaya
Dr. Sunand Santhangopalan
Dr. Saket Karajgikar

Acknowledgments

To begin with, I owe huge gratitude to my parents who gave me the opportunity to move to the US to pursue my dream of higher education, and to all the sacrifices they have made for me. My wife, Alisha, has been my pillar of moral and emotional support in the ups and downs of my life. I cannot thank Dr.Agonafer enough for his guidance, mentorship, and valuable words of wisdom as an advisor throughout my Master's and Doctoral degree programs.

I would like to thank Dr. Haji Sheikh, Dr. Miguel Amaya, Dr. Sunand Santhangopalan and Dr. Saket Karajgikar for being the thesis committee members and providing me with their valuable inputs in improvising my research work.

My peers and colleagues have also played a vital role throughout my time in the EMNSPC research group. I have been very privileged to have my roommates Patik Bansode and Pardeep Shahi as my best research partners and for their immense contribution to my doctoral research. In addition to this, I have been able to work with many other like-minded and brilliant individuals within the EMNSPC team. My heartfelt regards also go towards Jimil Shah, who has also been my mentor during my master's degree and a valuable advisor even after he graduated from UTA.

Abstract

Risk Mitigation of Airborne Contaminants and Thermal Performance Enhancement for Airside Economized and Immersion-Cooled Hyperscale Data Centers

The University of Texas at Arlington, 2022

Supervising Professor: Dr.Dereje Agonafer

The last two decades of 2000 have seen an explosion of utilization and reliance on digital technologies and platforms. During this time, electronic devices have undergone intense miniaturization and a corresponding rise in power densities. In parallel to these developments, data center proliferation has been driven by the increasing utility of revolutionary technologies such as Machine Learning, Artificial Intelligence, e-commerce and, the Internet of Things. Data centers, thus, have become the core of the modern digital age. The primary bottleneck, however, due to extensive device miniaturization and data center proliferation has always been thermal management. Many of the aforementioned technologies require high-performance computing CPUs and GPUs platform clusters, that consume large amounts of power and dissipate an equally large amount of heat.

Air-cooling has been the most popular method of data center thermal management but is limited to low power processors since the cost and energy consumption to pump air for high power density racks becomes very large. As a result, data center administrators have resorted to energy-efficient air-cooling techniques like Direct/Indirect Airside Economization and Free Air-cooling. Both these techniques have proven to significantly reduce the Power Usage Effectiveness (PUE) of air-cooled data centers in geographies with favorable climatic conditions. Although these technologies aid in alleviating the concerns of high energy consumption they also have an inherent risk of exposing the IT equipment to harmful airborne particulate and gaseous contaminants. While the impact of gaseous contaminants has been well

documented in the literature, the same can't be said for the impact of particulate contaminants. This is because conducting controlled experiments where particles can be generated and behave similarly as in nature is extremely tough. This further makes it tough to assess the risks associated with particulate contamination and also thwarts the development of mitigation strategies.

The first part of this research investigates the distribution of these airborne particulates inside the IT equipment and data center space with the help of particle tracking using Computational Fluid Dynamics. This investigation aims at carrying out simplified modeling 3-D and 2-D models of data center space and IT Equipment with known boundary conditions of the airflow. Particle tracking models of a commercial CFD code ANSYS FLUENT are used to simulate the behavior of a known particle mass in the airflow. Based on the literature review on the most pervasive particulates, a range of particle sizes are simulated and tracked using the Lagrangian scheme. Analysis of the most vulnerable locations of particle deposition is made by assessing the regions with higher particle concentrations. Similarly, regions of high particle concentration are identified inside the IT Equipment for different server configurations and different velocity inlet boundary conditions. Mitigation strategies are suggested based on the analysis of particle concentrations for different configurations of IT Equipment. The CFD methodologies presented in these studies can be leveraged during the data center infrastructure design phase and also during the server mechanical design phase.

The second part of this study focuses on the design optimization of heat sinks and the analysis of the thermal performance of different server configurations at the tank level in single-phase immersion cooling. It has been seen that when data centers move from air to immersion cooling due to performance demands or energy constraints, they typically use the same server hardware for immersion cooling as it was in air cooling. Using air cooling hardware, especially air-cooled heat sinks in immersion cooling, can become a significant

bottleneck in achieving peak performance due to a limit on case temperatures. An in-depth numerical study on different multi-parametric optimization methodologies for heat sinks is conducted using OptiSLang for forced and natural convection for an open compute server design. The objective of this study is to address the heat sink optimization from dif The optimization is done at a constant pumping power and iterating the combination of pressure drop and thermal resistance minimization as objective functions. Heat sink parameters like fin count and fin thickness are varied first for a constant base thickness and then the base thickness is also varied with the other heat sink geometric parameters. This is done for both copper and aluminum heat sinks to analyze the differences between the two heat sink materials and choose the best option from both economic and thermal performance points of view. The optimization results also correlate the dependency of each of the geometric parameters of the heat sink types on the objective functions. It is observed that this dependency varies for both natural and forced convection. The results of this study will help develop standard methodologies for optimizing heat sinks for immersion cooling.

The second study in immersion cooling deals with analyzing the impact of flow boundary conditions of the immersion tank on the thermal performance of the immersed servers using CFD. Owing to the low flow rates in immersion-cooled servers, natural convection may play a significant role in cooling the primary heat-dissipating components. Under different flow rate conditions, it becomes extremely difficult to predict the balance between natural and forced convection cooling modes. This study quantifies this balance for different inlet flow boundary conditions and at various CPU power utilization levels. The flow path of the coolant is determined under these boundary conditions for a shadowed and a spread-core version of a commercially available high-power server. The temperature and velocity fields obtained using this numerical study will be, in the future, compared with the experimental results using Particle Image Velocimetry for validation.

Table of Contents

List of Illustrations

List of Tables

Chapter 1 Introduction

1.1 Introduction

Data centers have become the mainstay of growing digital economies around the world as more and more businesses have started to rely on data processing and storage-based applications. This is compounded by a boom in social networking businesses, cryptocurrency mining farms, streaming and content creating platforms, and computational applications requiring large datasets processing like Artificial Intelligence (AI) and Machine Learning (ML). The latter technologies, AI and ML, have particularly led to a demand for ultra-fast processing units that can solve complex data sets in the least possible time. These factors have led to unprecedented growth in data center proliferation over the last two decades across the globe and corresponding increase in rack power densities as shown in Figure 1-1. An estimate of this proliferation can be concluded from the fact that an increase of 550% has been observed in the global compute instances between 2010 and 2018. At the same time, the power consumption has increased by 6% only, owing to increasing high-efficiency data center deployments utilizing advanced cooling technologies [1]. Also, in recent years, there has been a push towards reducing carbon emissions and making new data center infrastructures more energy efficient.

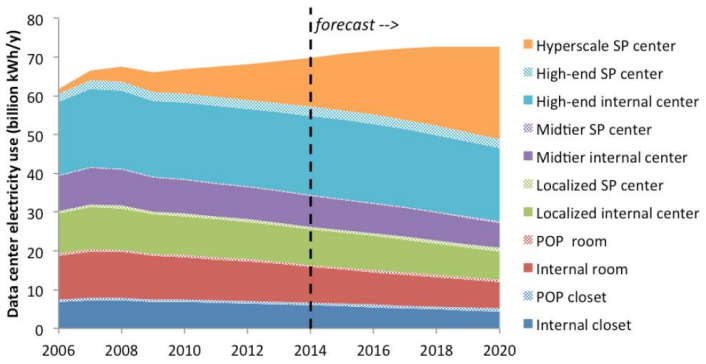

Figure 1-1: Overview of increasing data center power consumption use [2]

The data center industry is reaching an inflection point from a thermal management point of view due to increasing performance demands from every generation of new servers. The latest Thermal Design Power (TDPs) number from leading CPU and GPU manufacturers, accompanied by increasing memory and storage powers is challenging data centers to move away from air-cooling [3]. Thus it can be seen that while the use of efficient technologies has plateaued the impact of increasing data center energy demands, the fundamental challenge of server thermal management persists owed to increased processing demands.

A popular way to minimize energy consumption and reduce greenhouse gas emissions for air-cooled data centers is to minimize the reliance on compressor-based mechanical cooling. According to a 2015 report by the Environmental Protection Agency (EPA), the contribution of Information Technology Equipment (ITE) to global CO2 emissions was approximately 2% [4]. Therefore, to improve the data center efficiency for enterprise-level hyperscale data centers, using airside economizers (ASE) can be used to reduce cooling power energy consumption. Airside economization allows the data centers to bring the outside air completely or partially inside the data center under favorable temperature and humidity conditions. This reduces the utilization of energy for refrigeration-based cooling [5]. An airside economizer can be deployed in various combinations depending on the knowledge of the average annual ambient temperature and humidity conditions. When the outside conditions permit, complete intake of outside air is possible to cool down the ITE. However, this exposes the servers to airborne particulate and gaseous contaminants [6].

These particulate and gaseous contaminants can cause equipment failures in two ways. Firstly, the formation of electrical open circuits can lead to component failures. These electrical open circuits may occur due to, for example, corrosion of silver terminations on surface mount resistors in harsh gaseous environments of sulfur [7-10]. Sulfur reacts with the silver terminations of the resistors of the forming sulfides. This failure mechanism is very common

in polluted geographies where the ambient air has higher sulfur concentrations, for example, due to vehicular air pollution. Another common failure mechanism is electrical open circuits caused due to creep corrosion of cooper due to ion migration anodic-cathodic filamentation and ion migration. These failure mechanisms have been further accelerated as the components and features on server motherboards are being packed together more closely. This is because the path traveled for corrosion products reduced in electro-chemical products to bridge the gap between closely spaced features keeps reducing. If the airborne particulate matter that accumulates on the PCBs is hygroscopic, it can absorb moisture from data center air and become aqueous. If the aqueous solution of this hygroscopic matter is conductive, it can cause short-circuits inside the server. The difficulty in predicting the failure modes due to such particulate contamination is the intermittent nature of failures, as it can be ascertained what amount of deposition of matter will lead to a failure [11].

Figure 1-2 : Implementation of single-phase immersion cooling showing hot-swapping of server from dielectric fluid pool [12]

To tackle the issue of thermal management and overcome the issues related to the reliability of servers in harsh environments. An immersion-cooled data center deployment involves complete submersion of the servers in a thermally conductive dielectric fluid, typically of hydrocarbon origin [13]. Immersion cooling offers many advantages over traditional air-

cooling technologies such as higher thermal mass, low cost related to coolant transport to ITE, and protection of the ITE from harsh environments [14]. The primary advantage of immersion cooling lies in the fact that immersion-cooled ITE does not require server-level fans. This helps to immediately lower the data center PUE value which is defined as:

$$PUE = \frac{Total\ Facility\ Power}{ITE\ Power}$$

It can be comprehended from the above relation that in immersion cooling since there is no longer a need to have CRAC or CRAH units to cool the ITE, the overall facility energy falls. Typical PUE values for immersion-cooled data centers have been known to be around 1.03 [15]. As a comparison, the average PUE for data centers globally, based on a survey, for 2021 was 1.57 which is primarily because many data centers still rely on compressor-based air-cooling techniques [16]. Immersion cooling can be implemented in two ways: single-phase immersion cooling and two-phase immersion cooling. While two-phase immersion cooling is superior in terms of removing high heat fluxes from ITE, it currently faces challenges such as high fluid costs and fluid loss as the fluids are volatile [17]. Various thermal and non-thermal design considerations should be kept in mind while implementing single-phase immersion cooling such as material compatibility of server and tank components with the fluid and using optimized heat sinks for immersion.

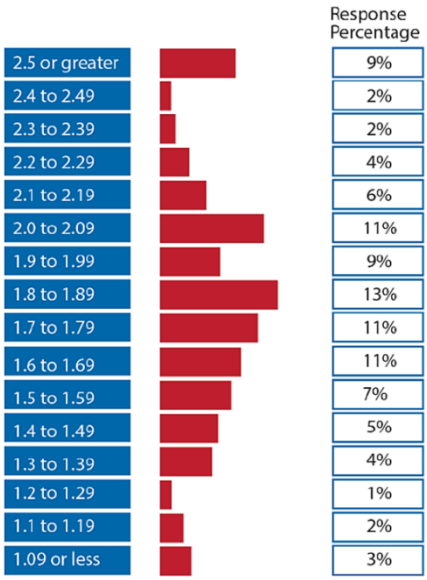

Figure 1-3: Results from a survey of data center PUE from 2019 showing the average PUE value is around 1.8 [16]

1.2 Scope of Work

The present investigation is divided into two parts. The objective of the first part of this investigation is to determine the airflow path and flow patterns of airborne particulates inside the data center and ITE. Experimental techniques of generating particles and visualizing them under precise boundary conditions for data centers is an expensive as well as an extremely tough task. Numerical modeling using programming languages is also known to require lengthy and tedious coding. Therefore, a commercially available Computational Fluid Dynamics (CFD) code was used to accomplish this task. This CFD code uses well-known particle flow models to simulate the discrete particle flow in a fluid domain. Simplified and detailed models of data center space and ITE were developed and a Discrete Phase Particle modeling scheme was used to simulate individual particles. A methodology was first developed and used for a simplified 3-D model of a data center space that was represented by using a set of boundary conditions. This methodology was then used to visualize the airflow paths of the contaminants inside ITE. The ITE was first modeled as 2-D geometries as features like heat sinks and Dual In-line Memory Modules (DIMMs) can increase the mesh count inside the server model to

large values. This would lead to a very large computational time. The CFD models of the 2-D simulations were also compared with 3-D CFD models to compare the amount of error between the two. The final part of this study was to design a 3-D model of a real-world data center and use the particle transport CFD methodology to analyze the particle flow paths. The 3-D model of this data center is designed as per the configuration for a modular data center with known boundary conditions. The results obtained from these studies analyze the severity of particle accumulation with the data center and ITE by calculating the mass that stays inside the fluid domain at a steady state. The ITE designs that are more susceptible to particle accumulation were thus identified. The impact of server mechanical design features was also determined. A similar methodology was followed at the data center level. The entire investigation is covered in Chapters 3, 4, and 5.

The second part of this study will focus on the thermal performance and reliability assessment in single-phase immersion-cooled servers. As discussed in the previous section, an optimized heat sink is necessary to achieve peak performance in immersion-cooled ITE. For the present investigation, an in-depth multi-objective and multi-design variable heat sink optimization study was conducted. The design variable used for optimizing the heat sink geometry in this study were the fin thickness, base thickness. Overall heat sink height and fin count. The objective functions or the constraints were set as minimization of pressure drop across the heat sink and heat sink thermal resistance. The optimization was done for both copper and aluminum heat sinks under forced as well as natural convection cooling modes.

This study also proposes an analysis of mixed convection flow behavior for immersion-cooled heat sinks using analytical and CFD methods. This will be done by analyzing a range of flow rates starting from pure natural convection to complete forced convection flow regimes. Dominant heat transfer modes will be quantified for the selected flow rate ranges. This study will help determine what type of heat sink solution is necessary based on the dominant heat

transfer regime so that optimum performance can be achieved from the processors. A reliability study of degradation of server components for bio-degradable immersion fluids is also proposed. A methodology will be developed to test various server components under different thermal aging conditions. The impact of prolonged immersion of components on aged and unaged samples will be tested based on the analysis of the mechanical properties of the components for different aging times and temperatures.

References

[1] Masanet, E., Shehabi, A., Lei, N., Smith, S. and Koomey, J., 2020. Recalibrating global data center energy-use estimates. *Science*, *367*(6481), pp.984-986

[2] Yevgeniy Sverdlik, 2016, "Here is How Much Energy all US Data Centers Consume," Data Center Knowledge, https://www.datacenterknowledge.com/archives/2016/06/27/heres-how-much-energy-all-us-data-centers-consume

[3] ASHRAE T.C. 9.9, Emergence and Expansion of Liquid Cooling in Mainstream Data Centers, White Paper by ASHRAE Technical Committee (TC) 9.9, Mission Critical Facilities, Data Centers, Technology Spaces, and Electronic Equipment, 2021, GA, USA

[4] Whitehead, B., Andrews, D., Shah, A. and Maidment, G., 2015. Assessing the environmental impact of data centres part 2: Building environmental assessment methods and life cycle assessment. *Building and Environment*, *93*, pp.395-405.

[5] Siriwardana, J., Jayasekara, S. and Halgamuge, S.K., 2013. Potential of air-side economizers for data center cooling: A case study for key Australian cities. *Applied Energy*, *104*, pp.207-219, https://doi.org/10.1016/j.apenergy.2012.10.046

[6] Shah, JM, Awe, O, Agarwal, P, Akhigbe, I, Agonafer, D, Singh, P, Kannan, N, & Kaler, M. "Qualitative Study of Cumulative Corrosion Damage of IT Equipment in a Data Center Utilizing Air-Side Economizer." *Proceedings of the ASME 2016 International Mechanical Engineering Congress and Exposition*. *Volume 10: Micro- and Nano-Systems Engineering and Packaging*. Phoenix, Arizona, USA. November 11–17, 2016. V010T13A052. ASME. https://doi.org/10.1115/IMECE2016-66199

[7] Singh, P, Klein, L, Agonafer, D, Shah, JM, & Pujara, KD. "Effect of Relative Humidity, Temperature and Gaseous and Particulate Contaminations on Information Technology Equipment Reliability." *Proceedings of the ASME 2015 International Technical Conference and Exhibition on Packaging and Integration of Electronic and Photonic Microsystems*

collocated with the ASME 2015 13th International Conference on Nanochannels, Microchannels, and Minichannels. Volume 1: Thermal Management. San Francisco, California, USA. July 6–9, 2015. V001T09A015. ASME. https://doi.org/10.1115/IPACK2015-48176

[8] Burnett, W. H., Sandroff, FS., and D'Egidio, S. M., 1992, "Circuit Failure Due to Fine Dust Mode Particulate Air Pollution," 18th International Symposium for Testing and Failure Analysis (ISTFA '92), Los Angeles, CA, Oct. 17–23, pp. 329–333

[9] Litvak, A., Gadgil, A. J., and Fisk, W. J., 2000, "Hygroscopic Fine Mode Particle Deposition on Electronic Circuits and Resulting Degradation of Circuit Performance: An Experimental Study," Indoor Air, 10, pp. 47–56

[10] Fu, H., Chen, C., Singh, P., Zhang, J., Kurella, A., Chen, X., Jiang, X., Burlingame, J., and Lee, S., 2012, "Investigation of Factors That Influence Creep Corrosion on Printed Circuit Boards," SMTA Pan Pacific Microelectronics Symposium, Kauai, HI, Feb. 14–16, Paper No. PP2012_WA1.4

[11] Saini, S., Shah, J. M., Shahi, P., Bansode, P., Agonafer, D., Singh, P., Schmidt, R., and Kaler, M. (September 15, 2021). "Effects of Gaseous and Particulate Contaminants on Information Technology Equipment Reliability—A Review." ASME. *J. Electron. Packag*. September 2022; 144(3): 030801. https://doi.org/10.1115/1.4051255

[12] GRC and Total Data Centre Solutions Partner to Expand Data Centre Liquid Immersion Cooling in Europe, 2020, Businesswire, https://www.businesswire.com/news/home/20201019005928/en/GRC-and-Total-Data-Centre-Solutions-Partner-to-Expand-Data-Centre-Liquid-Immersion-Cooling-in-Europe

[13] Kuncoro, I.W., Pambudi, N.A., Biddinika, M.K., Widiastuti, I., Hijriawan, M. and Wibowo, K.M., 2019, December. Immersion cooling as the next technology for data center

cooling: A review. In *Journal of Physics: Conference Series* (Vol. 1402, No. 4, p. 044057). IOP Publishing.

[14] Shah, J.M., 2018, *Characterizing contamination to expand ASHRAE envelope in airside economization and thermal and reliability in immersion cooling of data centers*, Doctoral dissertation, The University of Texas at Arlington, USA

[15] Eiland, R., Fernandes, J., Vallejo, M., Agonafer, D. and Mulay, V., 2014, May. Flow Rate and inlet temperature considerations for direct immersion of a single server in mineral oil. *Fourteenth Intersociety Conference on Thermal and Thermomechanical Phenomena in Electronic Systems (ITherm)*, 2014, pp. 706-714, doi: 10.1109/ITHERM.2014.6892350. s

[16] Uptime Institute 11th Annual Global Data Center Survey Shows Sustainability, Outage and Efficiency Challenges Amid Capacity Growth, Accessed January 5, 2021, https://uptimeinstitute.com/about-ui/press-releases/uptime-institute-11th-annual-global-data-center-survey#:~:text=PUE%20levels%20remain%20stagnant.,over%20the%20past%20five%20years.

[17] Data center cold wars – Part 2 Two-phase versus single-phase immersion cooling, https://www.grcooling.com/blog/two-phase-versus-single-phase-immersion-cooling/#:~:text=Efficiency%20%26%20Operating%20Expenses-,Two%2DPhase%20Cooling,to%201.03%20for%20single%2Dphase.

Chapter 2 Literature Review

2.1 Data Center Contamination

With increasing demands for cloud computing, high-performance computing solutions, efficient thermal management of datacom facilities has become even more challenging [1–3]. A large fraction of energy and resources are expended for continuous cooling of the Information technology equipment (ITE) to comply with special environmental requirements of temperature, humidity, and cleanliness for continuous reliable operation. Heat loads have become the defining characteristic and design criteria of data centers. This is evident from recent reports that projected 73 billion kWh of electricity consumption in 2020 [4]. These reports also estimated that because of the increased demand for information technology (IT) services, data centers alone accounted for an estimated 1.7%–2.2% of the total energy consumption in the U.S. and 1.1%–1.5% globally in 2010 [4,5]. When compressor-based air-cooling is used in data centers, the cooling power can account for approximately a third of total power consumption as seen in Refs. [6] and [7]. There has been, therefore, a constant effort to

resort to cooling technologies that can generate considerable cost savings by cooling power reduction. To address this concern of rising cooling power consumption, ASHRAE TC 9.9 expanded its recommended ranges for temperature and humidity to increase the number of hours for airside economization [8]. The recommended envelope in these guidelines specifies 18°C-27°C dry bulb temperature, 9°C to 15°C dew point temperature, and up to 60% relative humidity as shown in Fig. 1. The allowable envelopes in these guidelines also allow

brief excursions outside the recommended envelope to the allowable envelopes where the datacom equipment can operate at a higher inlet dry bulb temperature of 45°C and 90% Relative Humidity (RH). A reduction in cooling power consumption, thus, can be achieved by directly using outside air, using airside economizers to partially or completely cool down ITE

heat loads under favorable conditions [9,10]. An airside economizer is typically defined as “A duct and damper arrangement and automatic control system that together allows a cooling system to supply outdoor air to reduce or eliminate the need for mechanical cooling during mild or cold weather” [11]. Free air cooling is implemented when the amount of enthalpy in the air is sufficient and no additional conditioning is required for sufficiently cool and dry [12]. Figure 2 is a schematic showing the working of an airside economizer unit utilizing direct/indirect evaporative cooling. The reluctance in the implementation of airside economization from data center owners is due to the increased risk of exposure of ITE to particulate and gaseous contaminants. These contaminants can enter the data center either directly in the economizer mode or indirectly through media such as low-efficiency filters and makeup air. A study from Intel concludes that for 10 months in a free air-cooled data center, the humidity can vary between 4% and 90%. Since there is a minimum control over temperature, humidity, and airborne contaminant introduction in economizer mode, the ITE reliability can be easily compromised [13]. Among the airborne contaminants, highly reactive gases, and low deliquescence relative humidity (DRH) value particles are of primary concern. Gases like H2S, Cl2, NO2, SO2, and O3 have been identified to be most corrosive for electronics in presence of favorable temperature and humidity conditions [14]. Details on underlying failure modes and mechanisms due to these contaminants will be provided in the later sections of this paper. In presence of such contaminants, the surrounding environmental parameters of temperature, RH, and contamination can cause ITE failures via two main mechanisms. The first is electrical open circuits due to corrosion of silver terminals in surface mount resistors in the corrosive environment of sulfur-rich gases. The second common failure mode is due to copper creep corrosion causing electrical open circuits due to electrochemical migration (ECM) or cathodic-anodic filamentation [15–19]. These corrosion mechanisms and the rate of corrosion in any given environment can be affected by temperature, humidity, and

level, and type of particulate and gaseous contaminants [20–23]. The above-mentioned failure modes also led to new specifications for contamination limits accepted by the industry, which now place a lower limit on the DRH of dust [24,25]. To better understand these failure modes associated with data center particulate and gaseous contamination, it is essential to understand the relationship between environmental RH and settled the hygroscopic matter on the printed circuit boards (PCBs). Airborne particulate matter and hygroscopic gaseous corrosion products

are known to become wet and therefore ionically conductive and corrosive if the humidity in the environment rises above the DRH of the particulate matter. It is, therefore, necessary and informational to have a clear understanding of the terms critical relative humidity (CRH) and DRH. CRH is the value of the relative humidity at which the settled particulate matter starts adsorbing enough moisture to become electrically conductive. Whereas the relative humidity value at which the settled particulate matter becomes completely aqueous is termed as the DRH for the settled particle mixture. When the RH inside the data center, locally or globally, exceeds the DRH value of salts or accumulated particles on the PCB, the subsequent conductive solution formed leads to electrical short-circuiting due to a reduction in surface insulation resistance (SIR) between the closely spaced features on the PCBs [26].

2.2 Sources of Contaminants

The environment surrounding and within a server is defined by temperature, humidity, and gaseous and particulate contamination in the air [28, 29]. In free air cooling and economizer mode, it is easier for these contaminants to enter the data center white space and cause ITE failures, under favorable conditions over time. However, there is not adequate literature and statistics available directly correlating the impact of outdoor/indoor contaminant concentrations and ITE failure rates in data centers. This section provides an overview of the pervasive gaseous and particle contaminants and their sources.

Gaseous pollution today is caused primarily by fossil fuel burning, factories, commercial and domestic buildings, and automobiles. Over the years, three main pollutant gases found are throughout the industrialized world: sulfur dioxide (SO_2), ozone (O_3), and nitrogen dioxide (NO_2). Other gaseous contaminants of primary concern include chlorides (chlorine [Cl_2] and hydrogen chloride [HCl]), acetic acid (CH_3COOH), and formaldehyde ($HCHO$) [30]. The types of gases that most commonly cause corrosion are acidic gases such as hydrogen sulfide, sulfur and nitrous oxides, and hydrogen fluoride; caustic gases, such as ammonia; and oxidizing gases, such as ozone. Out of the three, acidic gases are of interest. It should be pointed out that, sulfur-bearing gases like SO_2 (sulfur dioxide) and H_2S (hydrogen sulfide), the major gaseous contaminants, are not directly responsible for corrosion but, in fact, by combining with NO_2 (nitrogen oxide) and O_3 (ozone) make the product with the former two gases more corrosive [30]. ASHRAE 1775-TRP (2015) [31] provides the details about typical values of the outdoor concentrations of these gaseous contaminants worldwide as seen in Table 1. These values can vary by both location and time of the year. Similar guidelines and pollutant classification are provided in ANSI/ISA-71.04-2013 for the most pervasive gaseous contaminants. These guidelines are classified based on the severity level affecting the ITE. As seen from Table 1 and Table 2, the values suggested by ASHRAE are around the same magnitude as the ISA guidelines for ITE. Although, these values represent the absolute impact of the gaseous pollutants on ITE corrosion rates without considering their synergistic effects. An estimate of the worldwide surface concentration levels for SO_2 was presented by Buchard et al. [32] over 10 months. As seen in Figure 2-1, the value of this concentration lies around the 40 ppb (parts per billion) mark which is similar to that given by ASHRAE 1775 TRP (2015). It is also seen that the concentration is higher during the winters, which also corresponds to the time for maximum free air cooling and economizer hours.

Table 1: ASHRAE RFP 1755-TRP typical outdoor pollutant concentrations worldwide

Pollutant	Outdoor Concentration in ppb	
	Minimum	Maximum
H_2S	4	140
NO_2	5	80
SO_2	4	40
Cl_2	1	10
O_3	5	60

Table 2: Contaminant Concentrations versus Severity Levels (ANSI/ISA-71.04-2013)

	G1 (Mild)	G2 (Moderate)	G3 (Harsh)	GX (Severe)
Gas	Concentration (ppb)			
H_2S	<3	<10	<50	50
SO_2, SO_3	<10	<100	<300	3000
Cl_2	<1	<2	<10	10
NO_x	<50	<125	<1250	1250
HF	<1	<2	<10	10
NH_3	<500	<10,000	<25,000	25,000
O_3	<2	<25	<100	100

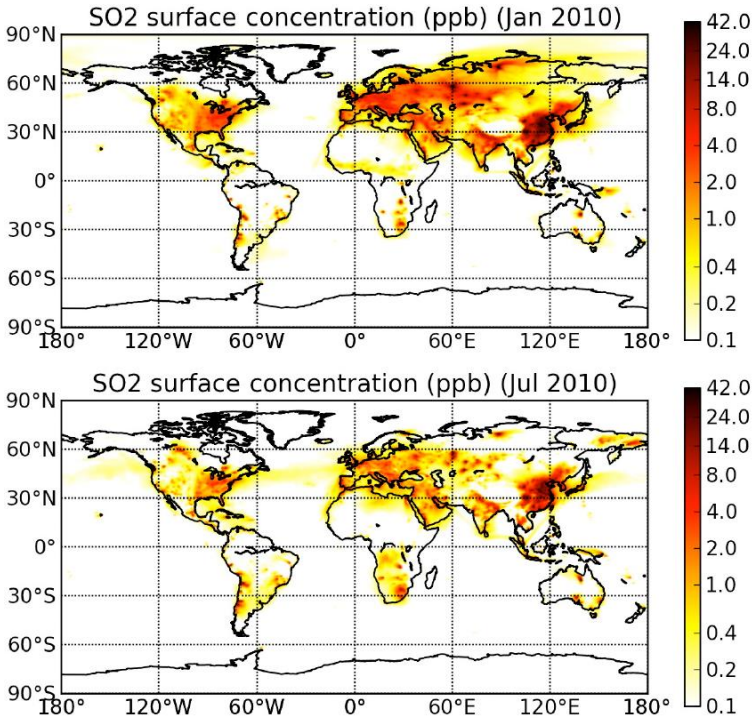

Figure 2-1 : Goddard Earth Observing System version 53GEOS-5/GOCART Monthly Mean of SO2 Surface-Level (Revised Run) for January and July 2010 [32]

On the other hand, particulate matter or dust is primarily classified into two groups: fine particles and coarse particles. Fine particles are defined as particles with a diameter less than or equal to 2.5μm such as those found in diesel particulate matter (DPM), motor vehicle exhaust and, smog. These fine particles are further classified into primary and secondary particles [33,34] where primary particles are those that are directly emitted from a specific source, such as volcanoes, forest fires, and construction sites. Secondary fine particles are formed because of photochemical reactions that take place in the atmosphere and make up most of the fine particulate pollution. These photochemical reactions occur due to the presence of oxides of sulfur and nitrogen that are emitted from automobiles and various industries. Carbonaceous material with a size of less than 0.1μm interacts with nitrogen dioxide and sulfur dioxide in a multistep photochemical process to result in the formation of nitric and sulfuric acids. Fertilizers generally containing ammonia, decayed biological matter, and other sources neutralize these acids thereby forming ammonium sulfate, ammonium nitrate, and ammonium hydrogen sulfate [35-39].

Coarse particles are typically related to a particle diameter range of 2.5-15μm. They include particulate matter such as sea salts, natural and artificial fibers, and plant pollen. Their major sources mainly include erosion of soil, flaking of biological materials, and minerals which are accelerated by winds [40]. The sea salt particles get airborne due to a mechanism known as sea spray, where the salts become airborne as aerosol particles. These particles are also capable of reacting with other pollutant molecules to form new salts and dissociate into free ions. Within the data center, coarse particles can also be found in the form of zinc whiskers from the undersides of the floor tiles or metallic ducts electroplates with zinc. This form of particles is, although, considered to be rare. Another such rare source of indoor particles can be the salts entering the airstream from humidifiers. The reason behind this can be high salt content in feedwater, especially the salts with low DRH values [25]. It can be concluded from these studies that most of the contaminants, both gaseous and particulate, originate outdoors from either manmade or natural causes. A particle pollution report by EPA (Environmental Protection Agency, USA) analyzed and reported $PM_{2.5}$ and PM_{10} levels for 4 years [41]. The major findings of the report suggest that the majority of $PM_{2.5}$ is attributed to regional pollution due to sulfate, VOC (Volatile Organic Compounds), and nitrate emissions from power plants and highways. This airborne particulate matter can be transported hundreds of miles away from the sources. This is consistent with the findings of one of the studies reviewed later in this paper which characterizes the dust found in a modular data center located in a polluted industrial area of Dallas, Texas. The above-discussed sources of typical contaminants that are found in a data center are tabulated in Table 3. The table summarizes the contaminants and their sources that might not be necessarily present in all the data centers. Also, most of the particle sources summarized here are due to natural sources and can be avoided if proper air filtration and indoor air monitoring guidelines are followed. The subsequent sections will review the studies

describing the most common failure modes and their mechanisms due to corrosive airborne or settled hygroscopic contaminants.

Table 3: Sources of some typical airborne contaminants [42]

Contaminant	Source
Zinc-whisker	Zinc coated ICT, steel building studs
Tin-whisker	Components and products with electroplated tin
Oxide flake off	Magnetic media
Natural and artificial fibers	Paper, cardboard, etc.
Water-soluble ionic salts	Chemical reaction
Sulfates, nitrates and sea salts	Wind
Lime Dust with Water	Concrete material
Dust	Farms (especially during plowing)
Toner Dust	Toner
Smoke	Cigarette, wind
Cellulose Fragments	Traditional ceiling tiles and space

2.3 Single-Phase Immersion Cooling

In the last decade, as the energy demands and processor power densities increased due to higher processing demands, traditional air cooling methods have been limited to cooling processors with lower Thermal Design Power (TDP) limits. With rising energy consumption and increasing complexity in thermal management, researchers have proposed various

strategies to enhance thermal performance [43, 44], increase power savings using different operation strategies of current cooling techniques [45, 46], or use liquid-based cooling technologies [47, 48]. Among the popular liquid-cooling technologies, Single-Phase Immersion Cooling stands out owing to its ease of deployment, low costs of dielectric fluids, and low-complexity cooling infrastructure [49]. Many of the present proprietary cooling solutions have established the efficacy of single-phase immersion cooling in terms of low Power Usage Effectiveness [50] values and enhanced reliability of server components [51]. A key direct advantage of complete submersion of servers in dielectric fluids is that it disconnects the server components from the harsh environment such as gaseous contaminants, reduces failures due to fan vibrations, and removes the necessity of cooling peripheral components as hot components are in direct contact with the coolant. Immersion cooling offers significant advantages as compared to air-cooling but requires careful thermal and non-thermal design considerations for air-cooled hardware. As an example, when immersing air-cooled hardware, fans should be removed from the server, hard drives need to be sealed, material compatibility issues should be addressed and the heat sink design should be optimized, which is the objective of this study.

To achieve consistently reliable and peak performance from Central Processing Unit (CPU) or (Graphics Processing Unit) GPU in immersion cooling, an optimized heat sink needs to be utilized, rather than using an air-cooled heat sink. Design optimizations for parallel plate-fin heat sinks have been widely studied including optimization of geometric properties [52, 53] and also from a single or multi-objective optimization point of view [54, 55]. Optimum geometric parameters such as fin spacing, fin thickness, base thickness, and fin count play an important role in maximizing the thermal performance of the heat sink as well as the processors. Current literature shows an increasing number of studies related to the optimization of heat

sink solutions for both air and liquid-cooled systems using various CFD-based and analytical methods.

Chen and Chen used a multi-objective and novel direction-based algorithm to optimize plate-fin heat sinks integrated with an impingement fan using a commercially available Multiphysics tool [56]. The optimized parallel plate heat sink showed both superior heat transfer performance and reduced weight. Fuzzy logic-based approaches have also been used to quantify the effect of heat sink design parameters on thermal performance [57]. Design parameters of a pin-fin heat sink such as fin spacing, pin-fin diameter, and height were investigated experimentally. Analysis of Variance (ANOVA) was then used to explore the effect of these design parameters on heat sink characteristics like thermal resistance, pressure drop, and average heat transfer coefficient. Response Surface Method (RSM) was used by Chaing and Chang [58] used to obtain optimum design parameters for pin-fin heat sinks to achieve higher thermal performance. Minimizing entropy generation rate as an objective function was done by Chen et al. [59]. They optimized a plate-fin heat sink for a CPU using a coded genetic algorithm for obtaining optimum design parameters for the heat sink. In terms of objective functions, Devi et al. [60] used a Taguchi-based non-gradient method for minimizing three objective functions namely, radiation emission, thermal resistance, and heat sink mass.

References

[1] Buyya, R., Vecchiola, C., and Selvi, S. T., 2013, "Mastering Cloud Computing: Foundations and Applications Programming," Morgan Kaufmann, Burlington, MA.

[2] Buyya, R., Beloglazov, A., and Abawajy, J., 2010, "Energy-Efficient Management of Data Center Resources for Cloud Computing: A Vision, Architectural Elements, and Open Challenges," Proceedings of the International Conference on Parallel and Distributed Processing Techniques and Applications (PDPTA 2010), Las Vegas, NV, July 12–15.

[3] Krug, L., Shackleton, M., and Saffre, F., 2014, "Understanding the Environmental Costs of Fixed Line Networking," Proceedings of the Fifth International Conference on Future Energy Systems, Cambridge, UK, June 11–13, pp. 87–95 .

[4] Shehabi, A., Smith, S. J., Sartor, D. A., Brown, R. E., Herrlin, M., Koomey, J. G., Masanet, E. R., Horner, N., Azevedo, I. L., and Lintner, W., 2016, "United States Data Center Energy Usage Report," Lawrence Berkeley National Laboratory, Berkeley, CA, Report No. LBNL-1005775.

[5] Koomey, J., 2011, "Growth in Data Center Electricity Use 2005 to 2010," A Report by Analytical Press, Completed at the Request of The New York Times, Analytics Press, El Dorado Hills, CA, p. 161.

[6] Rong, H., Zhang, H., Xiao, S., Li, C., and Hu, C., 2016, "Optimizing Energy Consumption for Data Centers," Renewable Sustain. Energy Rev., 58, pp. 674–691.

[7] Zhou, R., Wang, Z., Bash, C. E., and McReynolds, A., 2011, "Modeling and Control for Cooling Management of Data Centers With Hot Aisle Containment," ASME Paper No. IMECE2011-62506.

[8] ASHRAE, 2015, "Thermal Guidelines for Data Processing Environments," ASHRAE Datacom Series, 4th ed., ASHRAE Inc, Atlanta, GA.

[9] Patterson, M. K., Atwood, D., and Miner, J. G., 2009, “Evaluation of Air-Side Economizer Use in a Compute-Intensive Data Center,” ASME Paper No. InterPACK2009-89358.

[10] Lee, K. P., and Chen, H. L., 2013, “Analysis of Energy Saving Potential of Air-Side Free Cooling for Data Centers in Worldwide Climate Zones,” Energy Build., 64, pp. 103–112.

[11] ASHRAE ANSI/ASHRAE/IES Standard 90.1, 2019, “Energy Standard for Buildings Except for Low-Rise Residential Buildings,” ASHRAE, Atlanta, GA.

[12] OUC, 2019, “Economizers,”OUC, accessed Dec. 20, 2019, https://ouc.bizenergyadvisor.com/article/economizers

[13] Intel Information Technology, 2008, “Reducing Data Center Cost With an Air Economizer,” IT@Intel Brief; Computer Manufacturing; Energy Efficiency, accessed June 7, 2021, https://www.intel.com/content/dam/doc/technology-brief/data-center-efficiency-xeon-reducing-data-center-cost-with-air-economizerbrief.pdf

[14] ISA, 1985, “Environmental Conditions for Process Measurement and Control Systems: Airborne Contaminants,” ISA-The Instrumentation Systems, and Automation Society, Research Triangle Park, NC, Standard No. ISA-71.04- 1985.

[15] Cole, M., Hedlund, L., Hutt, G., Kiraly, T., Klein, L., Nickel, S., Singh, P., and Tofil, T., 2010, “Harsh Environment Impact on Resistor Reliability,” SMTAI Conference Proceedings, Orlando, FL, Oct. 24–28, pp. 1–9.

[16] Official Journal of the European Union, 2003, “Directive 2002/95/EC of the European Parliament and of the Council of 27 January 2003 on the Restriction of the Use of Certain Hazardous Substances in Electrical and Electronic Equipment,” Official Journal of the European Union, Luxembourg, pp. L37/19–23.

[17] Fu, H., Chen, C., Singh, P., Zhang, J., Kurella, A., Chen, X., Jiang, X., Burlingame, J., and Lee, S., 2012, “Investigation of Factors That Influence Creep Corrosion on Printed Circuit Boards,” SMTA Pan Pacific Microelectronics Symposium, Kauai, HI, Feb. 14–16, pp. 14–16.

[18] Fu, H., Chen, C., Singh, P., Zhang, J., Kurella, A., Chen, X., Jiang, X., Burlingame, J., and Lee, S., 2012, "Investigation of Factors That Influence Creep Corrosion on Printed Circuit Boards-Part 2," Proceedings of SMTA International, Olando, FL, Oct. 14–18, pp. 292–299.

[19] Ready, W. J., Turbini, L. J., Nickel, R., and Fischer, J., 1999, "A Novel Test Circuit for Automatically Detecting Electrochemical Migration and Conductive Anodic Filament Formation," J. Elect. Mater., 28(11), pp. 1158–1163.

[20] Ailor, W., Dean, S., and Haynie, F., 1974, "Corrosion in Natural Environments," Presented at the Seventy-Sixth Annual Meeting American Society For Testing and Materials, ASTM Special Technical Publication 558, Philadelphia, PA, June 24–29, pp. 7–21.

[21] Rice, D. W., Peterson, P., Rigby, E. B., Phipps, P. B. P., Cappell, R. J., and Tremoureux, R., 1981, "Atmospheric Corrosion of Copper and Silver," J. Electrochem. Soc., 128(2), pp. 275–284.

[22] W. H. Abbott, 1989, "The Corrosion of Copper and Porous Gold in Flowing Mixed Gas Environments," Proceedings of the Thirty Fifth Meeting of the IEEE Holm Conference on Electrical Contacts, Chicago, IL, Sept. 18–20, pp. 141–146.

[23] Leygraf, C., Wallinder, I. O., Tidblad, J., and Graedel, T., 2016, "Atmospheric Corrosion," John Wiley & Sons, New York.

[24] ASHRAE, T.C. 9.9, 2013, "Particulate and Gaseous Contamination in Datacom Environments" ASHRAE, Atlanta, GA.

[25] Muller, C., 2014, "Reliability Concerns for Data Center ITE: Contamination Issues, Standards Actions, and Case Studies," IPC APEX Conference & Exhibition, Las Vegas, NV, Mar. 23–27.

[26] Shah, J. M., 2016, "Reliability Challenges in Airside Economization and Oil Immersion Cooling," M.S. dissertation, The University of Texas at Arlington, Arlington, TX.

[27] Singh, P., Ruch, P., Saliba, S., and Muller, C., 2015, “Characterization, Prevention and Removal of Particulate Matter on Printed Circuit Boards,” IPC APEX, San Diego, CA.

[28] Geng, H., and Han, T., 2014, “Particulate and Gaseous Contamination in Data Centers,” Data Center Handbook, H. Geng, ed., John Wiley & Sons, New York, pp. 307–312.

[29] Purafil, 2020, “Causes of Corrosion and Corrosion Monitoring,” Purafil, Doraville, GA, accessed Jan. 19, 2020, https://www.purafil.com/causes-corrosioncorrosion-monitoring/

[30] Zhang, J., Zhang, R., Schmidt, R., Gilbert, J., and Guo, B., 2019, “Impact of Gaseous Contamination and High Humidity on the Reliable Operation of Information Technology Equipment in Data Centers (1755-TRP),” ASHRAE, Atlanta, GA, Report No. D-RP-1755.

[31] Buchard, V., Da Silva, A. M., Colarco, P., Krotkov, N., Dickerson, R. R., Stehr, J. W., Mount, G., Spinei, E., Arkinson, H. L., and He, H., 2014, “Evaluation of GEOS-5 Sulfur Dioxide Simulations During the Frostburg, MD 2010 Field Campaign,” Atmos. Chem. Phys., 14(4), pp. 1929–1941.

[32] Song, B., Azarisn, M. H., and Pecht, M. G., 2013, “Effect of Temperature and Relative Humidity on the Impedance Degradation of Dust-Contaminated Electronics,” J. Electrochem. Soc., 160 (3), pp. C97–C105.

[33] Seinfeld, J. H., and Pandis, S. N., 2016, “Atmospheric Chemistry and Physics: From Air Pollution to Climate Change,” John Wiley & Sons, New York.

[34] Zhao, P. S., Fan Dong, Di He, X. J. Zhao, W. Z. Zhang, Q. Yao, and H. Y. Liu., 2013, “Characteristics of Concentrations and Chemical Compositions for PM 2.5 in the Region of Beijing, Tianjin, and Hebei, China,” Atmos. Chem. Phys., 13, pp. 4631–4644.

[35] U. S. Environmental Protection Agency, 2014, “Air Trends 1995 Summary – Nitrogen Dioxide (NO2),” U. S. Environmental Protection Agency, Researech Park Triangle, NC, accessed Jan. 30, 2020, http://www.epa.gov/airtrends/aqtrnd95/no2.html

[36] Anand, R., 2018, “Development and Validation of the Deliquescent Relative Humidity Test Method for the Accumulated Particulate Matter Found in a Data Center Utilizing an Airside Economizer,” M.S. dissertation, The University of Texas at Arlington, Arlington, TX.

[37] Thirunavakkarasu, G., 2018, “Air Flow Pattern and Path Flow Simulation of Airborne Particulate Contaminants in a Cold-Aisle Containment High-Density Data Center Utilizing Airside Economization,” M.S. dissertation, The University of Texas at Arlington, Arlington, TX.

[38] Saini, S., 2018, “Airflow Path and Flow Pattern Analysis of Sub-Micron Particulate Contaminants in a Data Center with Hot Aisle Containment System Utilizing Direct Air Cooling,” M.S. dissertation, The University of Texas at Arlington, Arlington, TX.

[39] Comizzoli, R. B., Frankenthal, R. P., Lobnig, R. E., and Peins, G., 1993, “Corrosion of Electronic Materials and Devices by Submicron Atmospheric Particles,” Electrochem. Soc., Interface, 2(3), pp. 26–33.

[40] The United States Environmental Protection Agency, 2004, “The Particle Pollution Report-Current Understanding of Air Quality and Emissions through 2003,” The United States Environmental Protection Agency, Research Park Triangle, NC, Report No. EPA 454-R-04-002, pp. 1–12.

[41] Shah, J. M., Awe, O., Agarwal, P., Akhigbe, I., Agonafer, D., Singh, P., Kannan, N., and Kaler, M., 2017, “Qualitative Study of Cumulative Corrosion Damage of IT Equipment in a Data Center Utilizing Air-Side Economizer,” ASME Paper No. IMECE2016-66199.

[42] Singh, P., Cole, M., Kiraly, T., Tan, J., Rangaraj, R., Wood, G., and Chang, T., 2016, “Comparing Flowers of Sulfur and Mixed Flowing Gas Creep Corrosion Testing of Printed Circuit Boards,” SMTA International, Rosemont, IL, Sept. 25–29, pp. 25–29.

[43] Shahi, P., Agarwal, S., Saini, S., Niazmand, A., Bansode, P., & Agonafer, D., CFD Analysis on Liquid Cooled Cold Plate Using Copper Nanoparticles, *Proceedings of the ASME*

2020 International Technical Conference and Exhibition on Packaging and Integration of Electronic and Photonic Microsystems. *ASME 2020 International Technical Conference and Exhibition on Packaging and Integration of Electronic and Photonic Microsystems*. Virtual, Online. October 27–29, 2020. V001T08A007. ASME. https://doi.org/10.1115/IPACK2020-2592, 2020

[44] Niazmand, A., Murthy, P., Saini, S., Shahi, P., Bansode, P., & Agonafer, D., Numerical Analysis of Oil Immersion Cooling of a Server Using Mineral Oil and Al2O3 Nanofluid, *Proceedings of the ASME 2020 International Technical Conference and Exhibition on Packaging and Integration of Electronic and Photonic Microsystems*. *ASME 2020 International Technical Conference and Exhibition on Packaging and Integration of Electronic and Photonic Microsystems*. Virtual, Online. October 27–29, 2020. V001T08A009. ASME. https://doi.org/10.1115/IPACK2020-2662, 2020

[45] Shahi, P., Saini, S., Bansode, P., Agonafer, D., A Comparative Study of Energy Savings in a Liquid-Cooled Server by Dynamic Control of Coolant Flow Rate at Server Level, in *IEEE Transactions on Components, Packaging and Manufacturing Technology*, vol. 11, no. 4, pp. 616-624, doi: 10.1109/TCPMT.2021.3067045, 2021

[46] Shahi, P., Deshmukh, A. P., Hurnekar, H. Y., Saini, S., Bansode, P., Kasukurthy, R., and Agonafer, D., Design, Development, and Characterization of a Flow Control Device for Dynamic Cooling of Liquid-Cooled Servers, ASME. *J. Electron. Packag*., **vol** 144(4): 041008. https://doi.org/10.1115/1.4052324, 2022

[47] Niazmand, A., Chauhan, T., Saini, S., Shahi, P., Bansode, P.V., & Agonafer, D., CFD Simulation of Two-Phase Immersion Cooling Using FC-72 Dielectric Fluid, *Proceedings of the ASME 2020 International Technical Conference and Exhibition on Packaging and Integration of Electronic and Photonic Microsystems*. *ASME 2020 International Technical Conference and Exhibition on Packaging and Integration of Electronic and Photonic*

Microsystems. Virtual, Online. October 27–29, 2020. V001T07A009. ASME. https://doi.org/10.1115/IPACK2020-2595

[48] Hoang, C.H., Hoang, C.H., Tradat, M., Manaserh, Y., Ramakrisnan, B., Rangarajan, S., Hadad, Y., Schiffres, S. and Sammakia, B., A Review of Recent Developments in Pumped Two-Phase Cooling Technologies for Electronic Devices," in *IEEE Transactions on Components, Packaging and Manufacturing Technology*, vol. 11, no. 10, pp. 1565-1582, doi: 10.1109/TCPMT.2021.3117572, 2021

[49] Shah, J.M., Eiland, R., Siddarth, A. and Agonafer, D., Effects of mineral oil immersion cooling on IT equipment reliability and reliability enhancements to data center operations. In *2016 15th IEEE Intersociety Conference on Thermal and Thermomechanical Phenomena in Electronic Systems (ITherm)*, 31 May-3 June, pp. 316-325, IEEE, https://doi.org/10.1109/ITHERM.2016.7517566, 2016

[50] Eiland, R., Fernandes, J., Vallejo, M., Agonafer, D. and Mulay, V., "Flow Rate and inlet temperature considerations for direct immersion of a single server in mineral oil," *Fourteenth Intersociety Conference on Thermal and Thermomechanical Phenomena in Electronic Systems (ITherm)*, 2014, pp. 706-714, doi: 10.1109/ITHERM.2014.6892350, 2014

[51] Shah, J. M., Padmanaban, K., Singh, H., Duraisamy Asokan, S., Saini, S., and Agonafer, D., Evaluating the Reliability of Passive Server Components for Single-Phase Immersion Cooling, ASME. *J. Electron. Packag.*, 144(2): 021109. https://doi.org/10.1115/1.4052536, 2022

[52] Yazicioğlu, B. and Yüncü, H., 2007. Optimum fin spacing of rectangular fins on a vertical base in free convection heat transfer. *Heat and Mass Transfer*, *44*(1), pp.11-21, https://doi.org/10.1007/s00231-006-0207-6, 2007

[53] Jang, D., Yu, S.H. and Lee, K.S., 2012. Multidisciplinary optimization of a pin-fin radial heat sink for LED lighting applications. *International Journal of Heat and Mass Transfer*, *55*(4), pp. 515-521, https://doi.org/10.1016/j.ijheatmasstransfer.2011.11.016, 2012

[54] Kim, D.K., Thermal optimization of plate-fin heat sinks with fins of variable thickness under natural convection, *International journal of heat and mass transfer*, *55*(4), pp.752-761, https://doi.org/10.1016/j.ijheatmasstransfer.2011.10.034, 2012

[55] Subasi, A., Sahin, B. and Kaymaz, I., Multi-objective optimization of a honeycomb heat sink using Response Surface Method. *International Journal of Heat and Mass Transfer*, *101*, pp.295-302, https://doi.org/10.1016/j.ijheatmasstransfer.2016.05.012, 2016

[56] Chen, C.T. and Chen, H.I., 2013. Multi-objective optimization design of plate-fin heat sinks using a direction-based genetic algorithm. *Journal of the Taiwan Institute of chemical Engineers*, *44*(2), pp.257-265, https://doi.org/10.1016/j.jtice.2012.11.012, 2013.

[57] Chiang, K.T., Chang, F.P. and Tsai, T.C., 2006. Optimum design parameters of Pin-Fin heat sink using the grey-fuzzy logic based on the orthogonal arrays. *International communications in heat and mass transfer*, *33*(6), pp.744-752, https://doi.org/10.1016/j.icheatmasstransfer.2006.02.011, 2006

[58] Chiang, K.T. and Chang, F.P., 2006. Application of response surface methodology in the parametric optimization of a pin-fin type heat sink. *International communications in heat and mass transfer*, *33*(7), pp.836-845, https://doi.org/10.1016/j.icheatmasstransfer.2006.04.011, 2006

[59] Chen, C.T., Wu, C.K. and Hwang, C., 2008. Optimal design and control of CPU heat sink processes. *IEEE Transactions on components and Packaging Technologies*, *31*(1), pp.184-195, https://doi.org/10.1109/TCAPT.2008.916855, 2008

[60] Devi, S.P., Manivannan, S. and Rao, K.S., 2012. Comparison of nongradient methods with hybrid Taguchi-based epsilon constraint method for multiobjective optimization of cylindrical

fin heat sink. *The International Journal of Advanced Manufacturing Technology*, *63*(9-12), pp.1081-1094, DOI 10.1007/s00170-012-3985-7, 2012

Chapter 3 CFD Investigation of Dispersion of Airborne Contaminants in a Raised Floor Data Center

[41]

3.1 Introduction

To cope with rising computation and cloud storage demands, data center proliferation has been increasing unabatedly. Rising computational needs have also increased power densities at the chip level, causing a corresponding spike in the cooling demands. While novel cooling technologies like indirect and direct liquid cooling and immersion-cooling, evaporative cooling [27-29,36,39], have been shown to dissipate high heat fluxes, cloud providers like Google, Microsoft and Facebook have achieved PUE close to 1.1 using free air cooling at ideal locations. [1-3] Still, the majority of the data center administrators refrain from resorting to frees aircooling methods owing to overhead costs of filters and dehumidification devices installation and the threat of introducing particulate and gaseous contaminants into the data center white space.

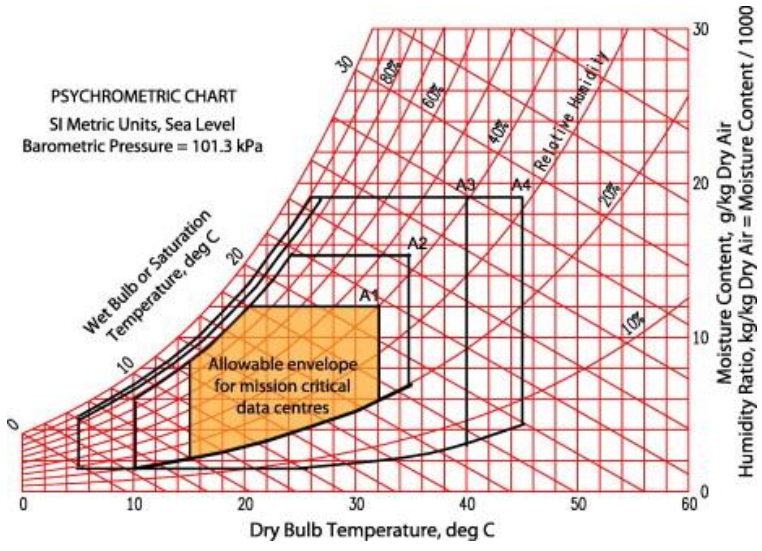

Figure 3-1 : Psychrometric chart for ASHRAE recommended and allowable classes

The ASHRAE T.C.9.9 subcommittee on Mission Critical Facilities, Data Centers, Technology Spaces and Electronic equipment has defined temperature and humidity ranges to ensure reliable operation of IT equipment [9-14]. They areaccepted by ITE manufacturers and their clients to be as follows: 18°C to 27°C (64.4°F to 80.6°F) dry bulb temperature, 5.5°C to 15°C (41.9°F to 59°F) dew point temperature, and less than 60% relative humidity. This recommended envelope was expanded by ASHRAE Thermal Guidelines for Data Processing Environments 2008, thereby, allowing short excursions into the allowable regions A1-A3, as shown in Figure 3-1, and an increase in the number of economizer hours. This exposes the IT equipment to the threat of gaseous and particulate contaminants. Two main failure modes associated with IT equipment failure because of surrounding the environment are: electrical open circuits resulting from corrosion of surface mount components due to gaseous contaminants and electrical short circuits due to copper creep corrosion, electrochemical migration and settled hygroscopic matter. While much has been studied about the failure modes due to the presence of corrosive gases in the data center environment, less attention has been paid to failures because of particulate contaminants owing to the intermittent nature of the failures. 2011 The Gaseous and Particulate Contaminants Guidelines for Data Centers [23] recommends keeping the data centers clean as per ISO Class 8 by the following means of filtration:

• The room air may be continuously filtered with MERV 8 filters, as recommended by ASHRAE Standard 127 (ASHRAE 2007).

• For data centers using airside economizers, the air entering the data center may be filtered with MERV 11 or MERV 13 filters as recommended by ASHRAE (2009b).

The mechanism involved failure due to settled ionic particulate matter is moisture absorption from the surrounding humid air. Such hygroscopic matter forms a conductive

aqueous solution above its DRH value, thus, reducing the Surface Insulation Resistance of the PCB and causing short-circuiting of closely spaced PCB features due to ion migration. The abovementioned concerns point towards a planned effort in addressing these concerns through experimental and numerical studies of the impacts of particulate contamination at the server level.

The present investigation addresses the impacts of particulate contamination in data centers by utilizing a numerical approach to determine the flow patterns of submicron-particulate contaminants. Because of a lack of literature on particle transport studies in the data centers, an in-depth literature review was done on particle transport and particle dispersion studies in ducts and ducts with obstructions. Conclusions were made about the dominating forces involved and accurate numerical models to be used by correlating the flow and particle transport characteristics valid for the present investigation. 6SigmaRoom, a commercially available data center CFD code, was used to predict accurate pressure and velocity boundary conditions of the flow through a floor tile in a raised floor data center. The particle transport study was then conducted in ANSYS FLUENT where, for a rectangular flow domain representing volumetric flow rate through a floor tile. A transient Discrete Phase Modeling approach was used to track particle diameters between 1 μm-10 μm, and realizable ke model was used to model flow turbulence as per the literature review. Particles were injected in the form of 2-D surface injections at the inlet and a low-pressure boundary condition was used to represent server inlet. Particle tracks and average volume fractions were obtained based on varying particle diameters and particle residence time in the flow.

3.2 Numerical Method

Particle-laden flow is a common phenomenon for many practical daily indoor and technical applications. CFD enables detailed prediction of complex fluid flows by discretizing

complex geometries into smaller regions and numerically solving the desired flow characteristics in these individual discretized regions. Commercially available CFD codes have made it easier to visualize complicated flow phenomena like particle-particle interactions and particle-flow interactions.

Lagrange-Euler approach has been proven to solve multiphase particle-laden flows. This approach uses RANS equations to solve the continuous or carrier phase and the dispersed or particle phase is resolved by Lagrangian tracking. The CFD code was chosen based on its extensive abilities in resolving particle-particle, particle-flow interactions and accurate mathematical models in simulating turbulence involved in particle flow. As described in ANSYS FLUENT Theory guide [32,33], the continuous phase is calculated using the RANS equations as given below:

$$\nabla . \bar{u} = 0 \qquad (1)$$

$$\frac{\partial u}{\partial t} + \rho\,(\bar{u}.\nabla)\bar{u} = -\nabla\bar{p} + \eta\Delta\bar{u} - \nabla.\overline{\tau^{RS}} + \bar{f}_D \qquad (2)$$

Where $\bar{u}$ and $\bar{p}$ are the average velocities of continuous (air) and discrete (particle) phase. The second term on the left-hand side in equation (2) represents the Reynolds Stresses which are modeled using the eddy-viscosity approach. In this study, realizable RNG κ-ε model was used to model kinetic energy and turbulent dissipation. Equations (3), (4) and, (5) are solved to obtain the particle force balance and particle trajectories of particles of mass m_p.

$$m_p \frac{d\overrightarrow{u_p}}{dt} = \sum \bar{F}_i \qquad (3)$$

$$\sum \overline{F_i} = \overline{F_D} + \overline{F_B} + \overline{F_G} \tag{4}$$

$$m_p \frac{d\overrightarrow{u_p}}{dt} = m_p \frac{\vec{u} - \vec{u}_p}{\tau_r} + m_p \frac{\vec{u}(\rho_p - \rho)}{\rho_p} + \vec{F} \tag{5}$$

The particles were assumed to be smooth and spherical, therefore, spherical drag law was activated, and default values of the coefficients were used for particles greater than 1µm. For sub-micron particles, as explained in theory guide, Stoke Cunningham drag law was used, which is given by equations 6, 7 and 8.

$$\overline{F_D} = \frac{3}{4} \frac{\rho}{\rho_p} \frac{d_p}{m_p} C_D(\vec{u} - \vec{u}_p)|\vec{u} - \vec{u}_p| \tag{6}$$

$$F_D = \frac{18\mu}{d_p^2 \rho C_C} \tag{7}$$

$$C_C = 1 + \frac{2\lambda}{d_p}(1.257 + 0.4) \tag{8}$$

The particle relaxation time was used for predicting particle trajectories using the force balance on the particle in the Lagrangian time frame as given in equation (5). This describes the deacceleration of particles due to the drag force and was solved using equation (9).

$$\tau_r = \frac{\rho_p d_p^2}{18\mu} \frac{24}{C_d Re} \tag{9}$$

Here Re is the relative Reynolds number and is calculated by:

$$Re_p = \frac{\left|\vec{u} - \overrightarrow{u_p}\right| \rho d_p}{\mu} \tag{10}$$

As the particles considered in this study are of small diameter, the torque or particle rotation was not considered. For sub-micron particles, it has been concluded from the literature that their dispersion is dominated by Brownian Force which is calculated using equation (11). The particle lifts for particle diameters greater than 1μm can be solved using equation (12).

$$F_{bi} = \zeta_i \sqrt{\frac{216\rho\nu\sigma T}{\pi\rho_p^2 d_p^5 C_c \Delta t}} \tag{11}$$

$$\vec{F} = m_p \frac{2K v^{\frac{1}{2}} \rho d_{ij}}{\rho_p d_p (d_{lk} d_{kl})^{\frac{1}{4}}} (\vec{u} - \vec{u}_p) \tag{12}$$

The Discrete Random Walk Model or eddy lifetime model can be used to model particle interaction with discrete fluid phase turbulent eddies which are classified by random velocity fluctuations given by u', v', w' and are calculated as given below in equations (13)-(15) where ζ is a normally distributed random number. The value of the RMS (Root Mean Square)

fluctuating components on the right-hand side of these equations is calculated by equation (16) using known values of kinetic energy turbulence at each point in the flow.

$$u' = \zeta\sqrt{\overline{u'^2}} \tag{13}$$

$$v' = \zeta\sqrt{\overline{v'^2}} \tag{14}$$

$$w' = \zeta\sqrt{\overline{w'^2}} \tag{15}$$

The characteristic lifetime of an eddy is given by equation (16). The same can be calculated using equation (17) as random variation about T_L, fluid Lagrangian integral time, r is a uniform random number greater than zero and less than 1 and C_L is the integral time scale constant.

$$\tau_e = 2T_L \tag{16}$$

$$\tau_e = -T_L \ln(r) \tag{17}$$

$$T_L = C_L \frac{k}{\epsilon} \tag{18}$$

3.3 Methodology

After an in-depth literature review of existing literature on particle transport in ducts, a set of assumptions was formulated that would simplify the current model giving near accurate results. A pressure-based solver was used for solving carrier fluid flow and pressure velocity coupling is achieved using the SIMPLE algorithm [38]. Based on the generated flow field, a defined number of particles were injected and were tracked as they traveled through the flow domain.

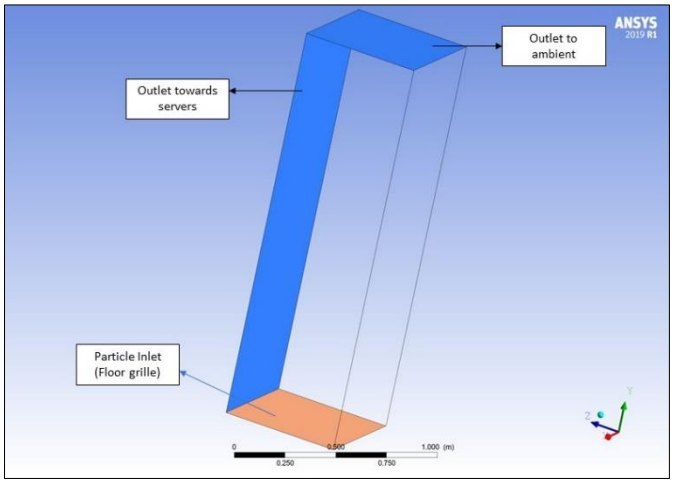

Figure 3-2: Boundary conditions used in the CFD study

The flow domain was designed in ANSYS DM as a rectangular channel extruded as a fluid representing the flow through a floor tile. Figure 3-2 shows the set of boundary conditions used in the CFD study, where a 0 Pa gauge pressure boundary condition was used for the outlet to ambient and -0.1 Pa for the outlet towards the servers. The meshing was done using an integrated mesher in the CFD code. As there were no obstructions curvatures within the flow domain, a fine quality mesh was homogenously generated consisting of 747,921 nodes. To visualize accurate boundary conditions, 6SigmaRoom was used to model airflow through floor tiles in a raised floor data center. This was done to realize the effect of neighboring floor tiles on the airflow through any specific tile. A server rack filled with 42 1U servers was modeled in front of a row of five floor tiles with an open area of 29%. 2-D contours of velocity through

the floor tiles and pressure contours at the rack inlet were obtained. The obtained values of the velocity and pressure were then used in the CFD code.

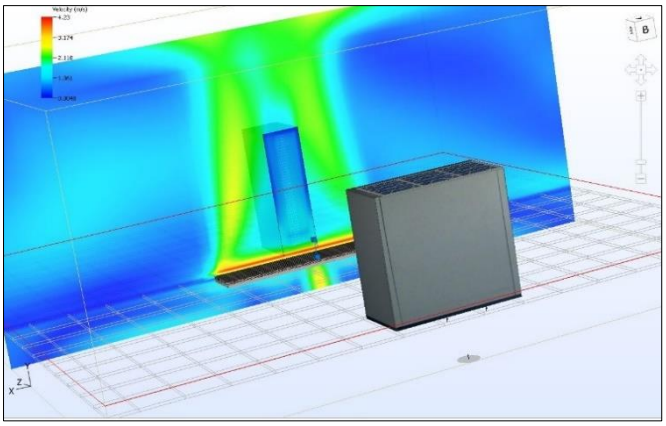

Figure 3-3: Velocity profile through floor tile in 6SigmaRoom

As seen in Figure 3-3, a rather constant velocity contour can be seen in front of the server rack with a maximum outlet velocity of 4m/s from the floor tile. As seen from the pressure distribution in the front of the rack in Figure 3-4, the boundary condition at the outlet towards the servers in FLUENT was given as -0.1 Pa of gauge pressure.

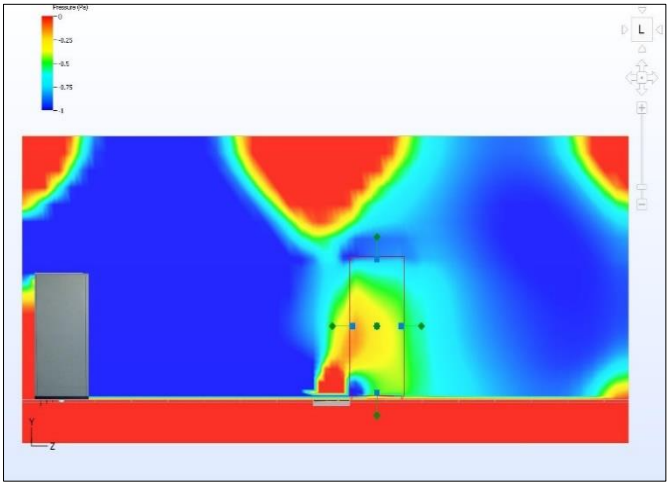

Figure 3-4: Pressure variation as seen in front of the rack in 6Sigma Room with a minimum pressure of -1 Pa

To validate the particle transport approach used, a validation study was conducted by simulating particle dispersion across a 2D square cylindrical obstruction in a channel flow as described by Jafari et al [34]. As most of the particle transport studies in the reviewed literature use numerical techniques to model particle transport, it was necessary to determine if the

models available in the CFD code could give near similar results to numerical exact solutions. The reviewed study numerically modeled particle transport and deposition by correlating the flow Stokes number for laminar flow. Similar mathematical models for forces and flow were activated in ANSYS and a transient simulation was run with a time step of 0.01 seconds for 1000 time steps. This allowed the flow to sufficiently fill the entire domain and aided in visualizing the vortex shedding across the bluff body as seen in Figure 9. This study concluded that particle dispersion is dominated by Brownian motion for sub-micron particles and by inertia forces for particle sizes of larger diameters.

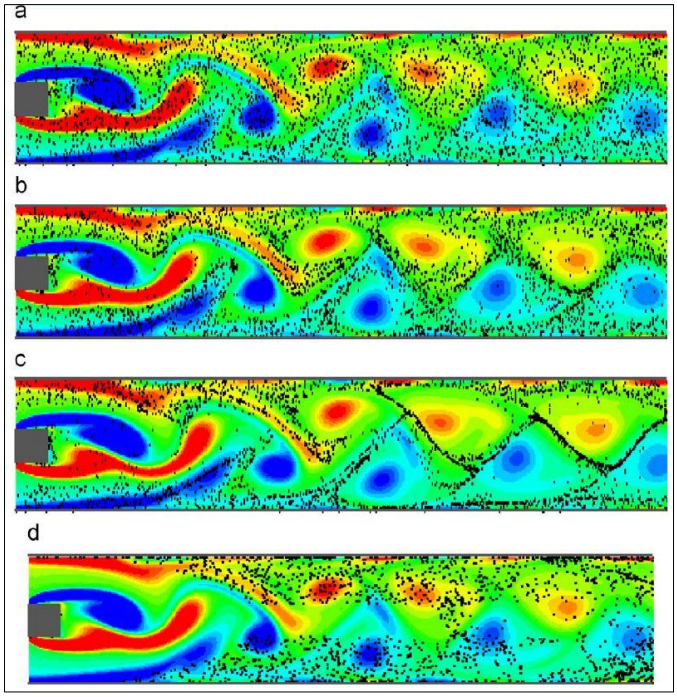

Figure 3-5: Particle traces as obtained for validation case

The particle dispersion is also selectively distributed based on particle size. Smaller particles were unaffected due to the presence of the vortices, as can be seen in Figure 3-5. While the heavier particles are distributed on the periphery of the shed vortices. This is because inertial particles tend to move towards low vorticity regions because of the vortex generated centrifugal forces. Using the same design parameters and geometries, particle dispersion was obtained in the CFD code. The comparison of both the reviewed study and current study can

be seen below, and a similar pattern is observed in present simulations as seen below in Figure 3-6.

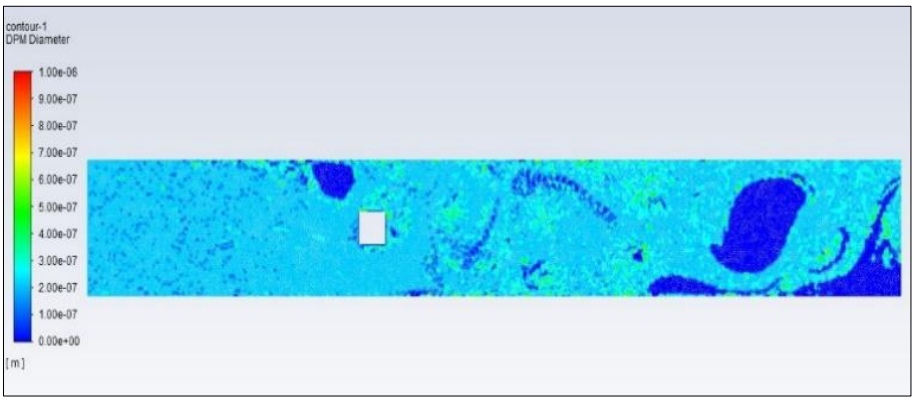

Figure 3-6: Particle traces as obtained for validation case

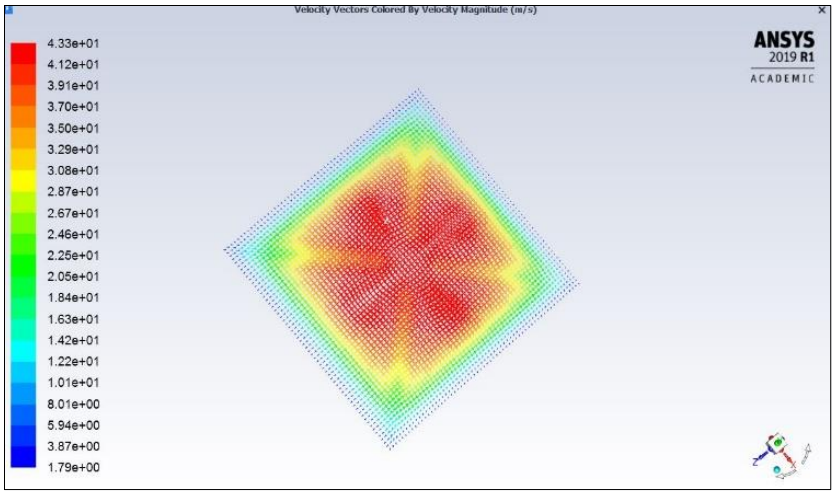

Figure 3-7: Velocity vectors of air at the outlet for base flow simulation

The final flow domain was imported to the CFD code and appropriate flow models and boundary conditions were activated. The particles were injected as surface injections where particles were then released from each facet of the surface. Here, the facet value of a variable is defined as the computed arithmetic average of the adjacent cell values of the variable. A total flow rate of 1e-04 kg/m^3 was used so that a sufficient number of particles can be generated and tracked. The maximum, minimum and mean diameters of the injections were specified for size distribution. The particle properties were selected using anthracite (ρ=1550kg/m^3) as an inert particle from the software material library and relevant force balance laws were activated. Two-way coupling was used in which the continuous flow field was solved first, after which the

discrete phase trajectories are calculated. After this, the continuous phase was solved again based on interphase momentum exchange (as no heat and mass transfer is considered in this study) and discrete phase trajectories were then recalculated for a modified flow field. This process was repeated until a converged solution was obtained. For the current study, a DPM iteration interval of 10 was selected, which means that a discrete phase iteration was performed every tenth continuous phase iteration. A time step size of 0.1 seconds was chosen with a total number of iterations equal to 100 and maximum iterations per time step equal to 10.

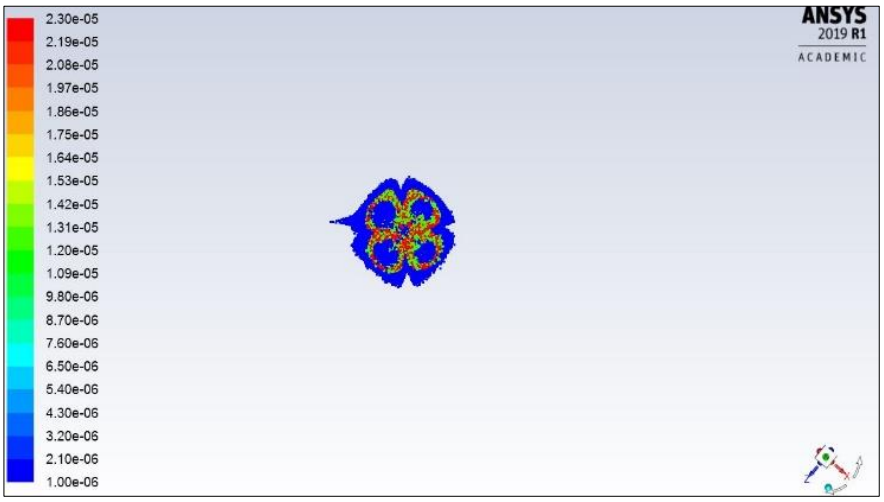

Figure 3-8: Particle concentration contour for various particle diameters at the outlet

Multiple simulations were run after completing the validation case. The first case simulated in the present study was that of a rectangular channel with all four sides of the channel in a symmetry boundary condition. This was done to validate the approach that without any influence of gravity, all the particles must follow the flow streamlines of air/continuous fluid. Figure 3-8 shows the velocity profile of the flow as seen at the domain outlet. Comparing the velocity contour to the particle concentration, it can be concluded that the assumption made about particle following the flow streamlines holds. Also, from the knowledge of fluid dynamics, for a flow in a rectangular duct, the maximum flow velocity should occur at the center of the duct.

A similar flow and selective concentration pattern were observed for the particles, in this case, irrespective of their diameters. Unlike succeeding simulations, the effects of buoyancy and Brownian motion were ignored for the base simulation. Another base simulation with a particle diameter less than 1µm was also performed which showed the same flow pattern and was, therefore, not included in the results to avoid the repeated presentation of similar patterns.

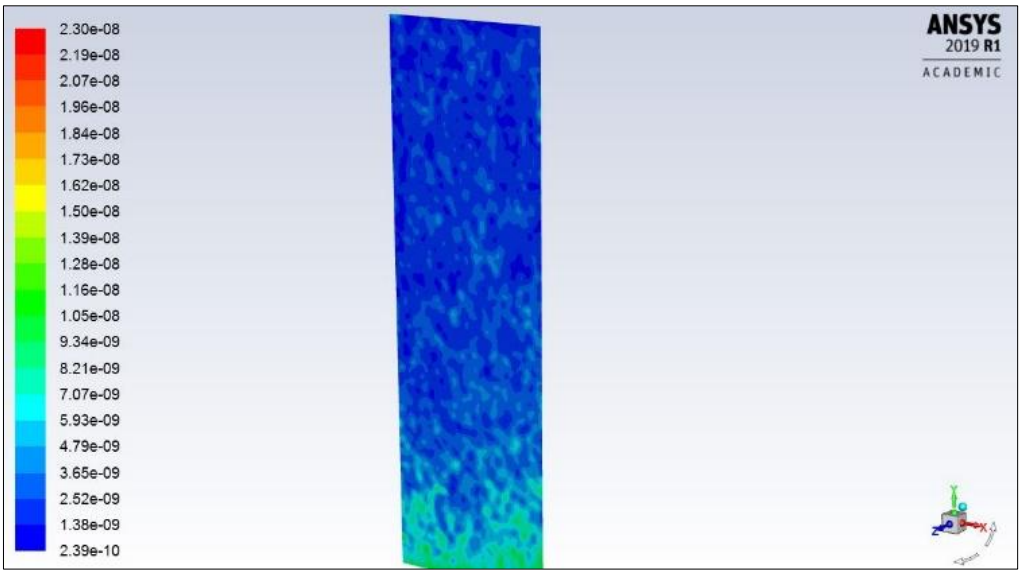

Figure 3-9: Particle concentration distribution on server side for low-density particles

The next and final set of simulations was performed by defining a second low-pressure outlet in the flow domain depicting the floor tile side facing the rack inlet. The value of the pressure was chosen from 6SigmaRoom by populating a server inlets. It was assumed that all the servers operated under a constant load, hence creating a constant pressure drop across the width of the rack. The other three sides of the flow domain were given a symmetry boundary condition. Physically, the symmetry boundary condition, in this case, can be interpreted as a floor tile present at the center of a cabinet row with no effect on its airflow from any of the neighboring tiles. Unlike the previous case, the effects of particle buoyancy and Brownian motion were also considered. Figure 3-10 shows the instantaneous distribution of particles based on particle diameters.

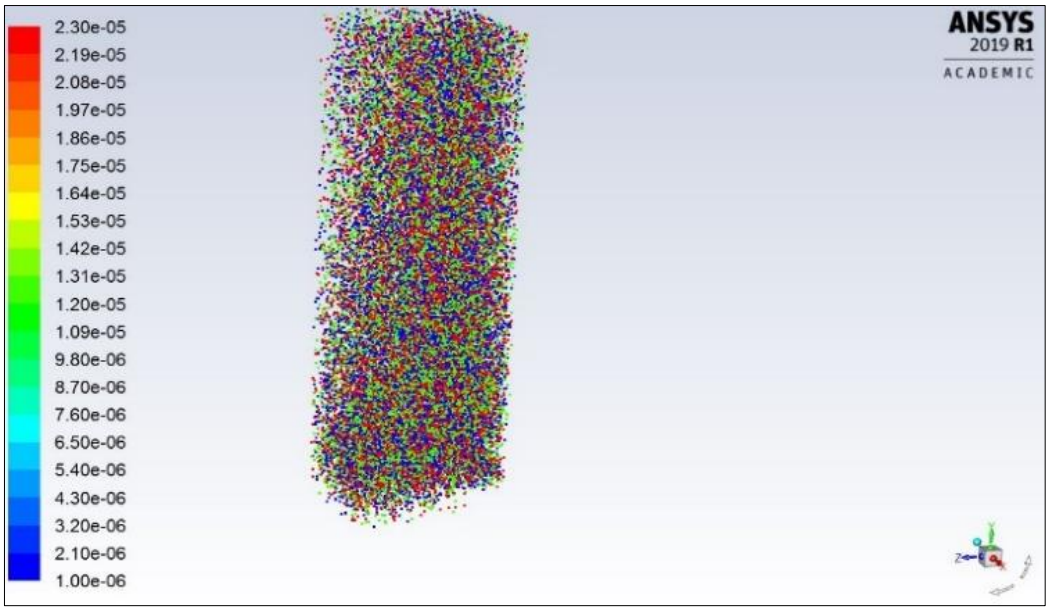

Figure 3-10: Real time Particle diameter distribution in flow domain after complete simulation

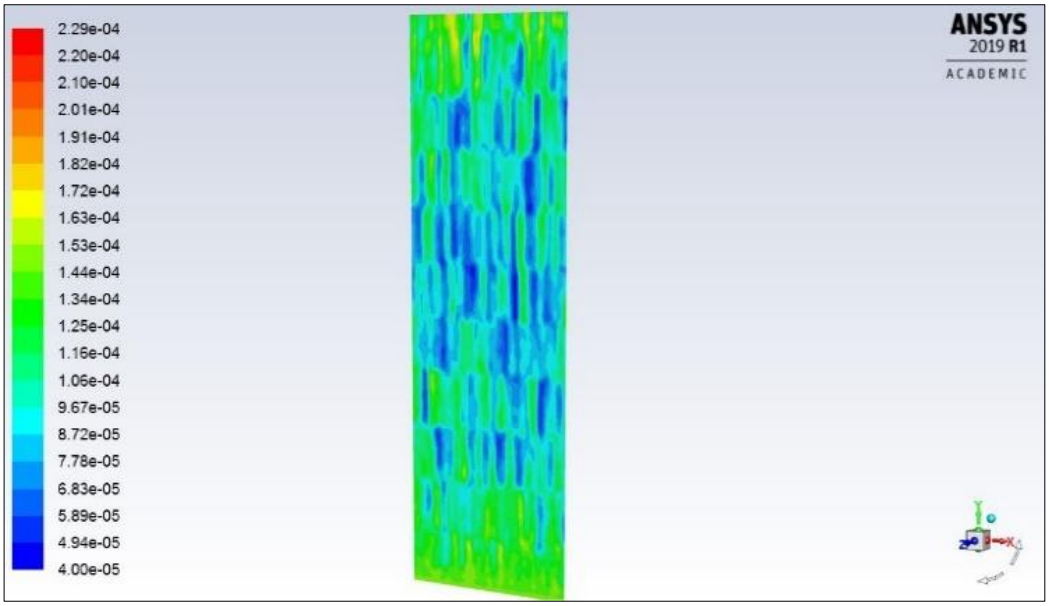

Figure 3-11: Particle concentration of dense particles on the server inlet side

Figure 13 shows the concentration distribution of low-density particles as observed at the flow domain side facing the server inlets. Comparing this to Figure 3-11, the distribution of particles is more pronounced at the bottom and top ends of the flow domain faces. Finally, the density of the particles was increased to 8800 kg/m^3 to see how a large variation in density of the inert particles will affect the particle tracks obtained under the same boundary conditions.

Figure 3-11 and Figure 3-12 show overall particle concentration by total mass and concentration variation by diameters on the domain face towards the rack inlet respectively. Most of the particle mass was retained at the bottom of the domain and escaped through the outlet facing the servers. The particle diameter distribution at the final time step shows that most of the particles that escaped the outlet facing the servers were of diameters less than the mean diameter considered in this simulation. The inequality in the parentheses represents mean diameter in the simulation bounded by minimum and maximum diameters (1e-07µm <5e-07 µm <1e-06 µm).

Table 4: Particle summary for low-density particles

Property	**Server side**	**Top outlet**
Mass transfer	1.77e-04 kg	7e-04 kg
No. of particles escaped	6.4e+05	2.6e+08
Max. time before escaping	2.19 sec	2.15 sec

Table 5: Particle summary for high-density particles

Property	**Server side**	**Top outlet**
Mass transfer	1.77e-04 kg	7e-04 kg
No. of particles escaped	1.6e+06	1.8e+06
Max. time before escaping	2.1 sec	1.83 sec

The bulk distribution within the fluid domain of particle diameters was observed to be slightly different than that of lighter particles. This was observed from the fact that a greater number of particles escaped out from the inlet itself when compared to the particles of low

density. Since a lot of elements in the flow domain were reported by the solver having reverse flow because of a low-pressure outlet, as concluded from the validation case, the heavier particles can be trapped in their vicinity and stay in the flow domain for longer times. Particle summary was obtained in post-processing which showed that a total of 3.4e12 particles were ejected from the floor tile for 10 seconds for low-density particles. Table 1 shows the number of particles and mass transferred from the two outlets considered in the flow domain. The total mass and the number of particles escaped from the top outlet is almost four times greater than the outlet facing the servers. This means that less than 10e-07 of the total particles injected and tracked by the solver went towards the IT equipment. Although this number might seem small, as the literature suggests the failures related to particulates are intermittent and happen after sufficient particulate accumulation and favorable environmental conditions. For high-density particles, the total particle count injected in the flow domain was around 1.9e+11. The fraction of particles escaping towards the server side was an order of magnitude more than that obtained for lighter particles. Also, the total number of particles escaping both the outlets were similar.

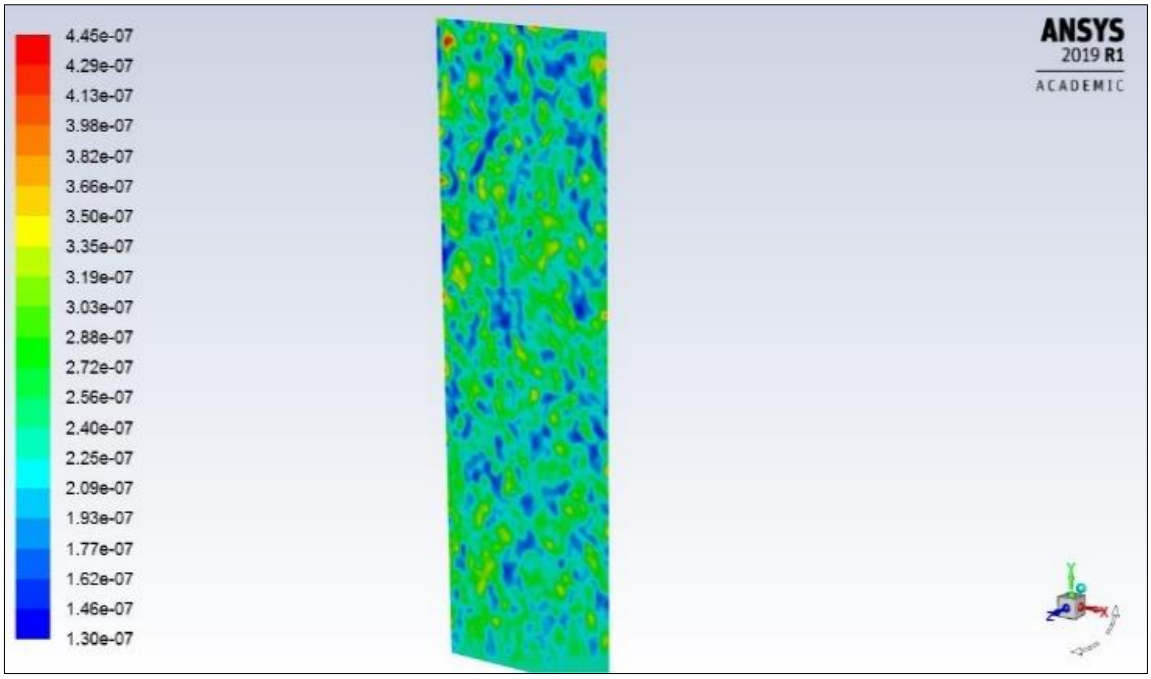

Figure 3-12: Particle diameter distribution at the side facing server inlets for high-density particles

3.4 Conclusion and Future Work

Particle transport of particulate contaminants was studied for a simplified model of a raised floor data center using CFD. Particle distribution was obtained for various boundary conditions within the flow domain and two different particle densities. The approach was validated as per existing particle dispersion studies in the literature. It was observed that particle sizes or particle mass is the dominant factor that dictates particle dispersion. For lighter or lower diameter particles, the dispersion was rather random. Also, the particle concentration plots obtained show that particle deposition will be more pronounced around the bottom servers due to low-pressure regions. This observation might need actual experimental validation, where either outflow or pressure variation can be measured at the rack level in an actual data center. The particle escape regions were inferred to be located towards the bottom of the flow domain, implying that the maximum particle concentration or deposition should be found in the servers located at the bottom of the flow domain.

In a real flow inside IT equipment, when the vortices formed due to impedance inside the server eventually lose their energy, the particles carried by them will be deposited at that location. For servers, where the flow is enclosed and is generally incident on multiple obstructions, it can be predicted that the stagnation points of the flow on these obstructions will be most vulnerable to particle deposition. It can be further extrapolated that if some of these particles are ionic in nature, there can be a high probability of equipment failure due to short-circuiting. Further simulations of particle flow within the server will give a better interpretation of the deposition and dispersion phenomenon within the server. Various raised floor data center cooling strategies and local airflow delivery methods through floor tiles [37] will also affect the particle distribution. This necessitates the requirement of further detailed simulations of the floor tile itself to get a better idea of special distribution and dispersion of the particulate

contaminants. Particle distribution will also be dependent on particle shape based on variation in drag and lift forces [40] which should also be taken into account for future studies.

This study is preliminary work in conducting a detailed study of the particle-laden airflow through the server rack as well as individual IT equipment. A detailed model of the combined floor tile and server rack will be created by experimentally determining the pressure drops across the server rack and inlet and outlet velocities. The effect of changes in particle particulate characteristics like particle density, diameters, and particle coagulation will be seen. The objectives of these subsequent studies are to determine the percentage deposition occurring inside the server and using CFD, predicting the locations of these depositions based on flow characteristics inside the server. User-defined functions can be compiled and imported into the CFD solver to study particle deposition which is directly related to particle's Stokes number.

REFERENCES

[1] https://www.opencompute.org/blog/cooling-an-ocp-data-center-in-a-hot-and-humid-climate

[2] Google. Efficiency: How We Do It, 2014

[3] Microsoft. Microsoft Shares Video Tour of its Cloud Datacenters,2011

[4] Longmire, E. K., and Eaton, J. K. (1992). Structure of a Particle-Laden Round Jet, *J. Fluid Mech.* 236:217–257.

[5] Lazaro, B. J., and Lasheras, J. C. (1992). Particle Dispersion in the Developing Free Shear Layer, Part 1—Unforced Flow, *J. Fluid Mech.* 235:143–178.

[6] Crowe, C. T., Chung, J. N., and Trout, T. R. (1988). Particle Mixing in Free Shear Flows, *Progress in Energy and Combustion Science* 14:171–194.

[7] Uthuppan, J., Aggarwal, S. K., Grinstein, F. F., and Kailasanath, K. (1994). Particle Dispersion in a Transitional Axisymmetric Jet: A Numerical Simulation, *AIAA J.* 32:2004–2014.

[8] Aggarwal, S. K. (1994). Relationship Between the Stokes Number and Intrinsic Frequencies in Particle-Laden Flows, *AIAA J.* 32:1322–1325.

[9] Chang, E., and Kailasanath, K. (1996). Simulation of Dynamics in a Confined Shear Flow, *AIAA J.* 34:1160–1166

[10] Alletto, M., & Breuer, M. (2012). One-way, two-way and four-way coupled LES predictions of a particle-laden turbulent flow at high mass loading downstream of a confined bluff body. *International Journal of Multiphase Flow*, *45*, 70–90.

[11] van Vliet, E., Singh, M., Schoonenberg,W., van Oord, J., van der Plas,D., & Deen, N. (2013). *Development and validation of Lagrangian-Eulerian multi-phase model for simulating the argon stirred steel flow in a ladle with slag*. Proceedings of the 5th International Conference on Modelling and Simulation of Metallurgical Processes in Steelmaking, STEELSIM. Ostrava, Czech Republic.

[12] Sardina, G., Schlatter, P., Brandt, L. P., & Casciola, C. (2012). Wall accumulation and spatial localization in particle-laden wall flows. *Journal of Fluid Mechanics*, *699*, 50–78.

[13] Wang, B., Manhart, M., & Zhang, H. (2011). Analysis of inertial particle drift dispersion by direct numerical simulation of two-phase wall-bounded turbulent flows. *Engineering Applications of Computational Fluid Mechanics*, *5*(3), 341–348.

[14] Vreman, A. (2015). Turbulence attenuation in particle-laden flow in smooth and rough channels. *Journal of Fluid Mechanics*, *773*, 103–136

[15] Pui DYH, Romay-Novas F, Liu BYH. Experimental study of particle deposition in bends of circular cross-section. Aerosol Sci Technol 1997;7:301–15

[16] Zhang H, Ahmadi G. Aerosol particle transport and deposition in vertical and horizontal turbulent duct flows. J Fluid Mech 2000;406:55–80.

[17] Zhao Bin, Wu Jun. Modeling particle fate in ventilation system—Part II: Case study. Build Environ 2009;44:612–20.

[18] D. J. Brandon & S. K. Aggarwal (2001) A Numerical Investigation of Particle Deposition on a Square Cylinder Placed in a Channel Flow, Aerosol Science & Technology, 34:4, 340-352

[19] Franziska Greifzu, Christoph Kratzsch, Thomas Forgber, Friederike Lindner & Rüdiger Schwarze (2016) Assessment of particle-tracking models for dispersed particle-laden flows

implemented in OpenFOAM and ANSYS FLUENT, Engineering Applications of Computational Fluid Mechanics, 10:1, 30-43, DOI: 10.1080/19942060.2015.1104266

[20] Gao, R., and Li, A. (2012). Dust Deposition in Ventilation and Air-Conditioning Duct Bend Flows. *Energy Convers. Manage.*, 55:49–59

[21] Jimil M. Shah, "Characterizing contamination to expand ASHRAE envelope in airside economization and thermal and reliability in immersion cooling of data centers", PhD dissertation, The University of Texas at Arlington, May 2018

[22] Jimil M. Shah, "Reliability challenges in airside economization and oil immersion cooling", UTA-THESIS, 2016-05-16, Shah, Jimil Manojbhai, 0000-0003-2297-7413.

[21] Prabjit Singh, Levente Klein, Dereje Agonafer, Jimil M. Shah and Kanan D. Pujara, "Effect of Relative Humidity, Temperature and Gaseous and Particulate Contaminations on ITE Reliability, DOI: 10.1115/IPACK2015-48176, ASME InterPACK 2015, San Francisco, CA.

[22] Shah, Jimil & Awe, Oluwaseun & Gebrehiwot, Betsegaw & Agonafer, Dereje & Singh, P & Kannan Mestex, Naveen & Kaler Mestex, Mike. (2017). Qualitative Study of Cumulative Corrosion Damage of ITE in a Data Center Utilizing Air-side Economizer Operating in Recommended and Expanded ASHRAE Envelope. Journal of Electronic Packaging. 139. 021002. 10.1115/1.4036363

[23] ASHARE. 2011. 2011 Gaseous and Particulate Guidelines for Data Centers, Atlanta, GA, USA.

[24] Seymour, M.J., A. A. M. A., and Jiang, J., 2000. "Cfd based airflow modelling to investigate the effectiveness of control methods intended to prevent the transmission of airborne organisms". Air Distribution in Rooms, (ROOMVENT 2000).

[25] Jones, P., and Whittle, G., 1992. “Computational fluid dynamics for building air flow prediction- current status and capabilities”. Building and Environment, 27(3), pp. 321–338.

[26] Chen, Q., and Zhang, Z., 2005. “Prediction of particle transport in enclosed environment”. China Particuology, 3(6), pp. 364–372.

[27] Jimil M. Shah, Chinmay Bhatt, Pranavi Rachamreddy, Ravya Dandamudi, Satyam Saini, Dereje Agonafer, 2019, “Computational Form Factor Study of a 3rd Generation Open Compute Server for Single-Phase Immersion Cooling,” ASME Conference Paper No. IPACK2019-6602

[28] Dhruvkumar Gandhi, Uschas Chowdhury, Tushar Chauhan, Pratik Bansode, Satyam Saini, Jimil M. Shah and Dereje Agonafer, 2019, “Computational analysis for thermal optimization of server for single phase immersion cooling”, ASME Conference Paper No. IPACK2019-6587

[29] Pravin A Shinde, Pratik V Bansode, Satyam Saini, Rajesh Kasukurthy, Tushar Chauhan, Jimil M Shah and Dereje Agonafer, 2019, “Experimental analysis for optimization of thermal performance of a server in single phase immersion cooling”, ASME Conference Paper No. IPACK2019-6590

[30] Jimil M. Shah, Roshan Anand, Satyam Saini, Rawhan Cyriac, Dereje Agonafer, Prabjit Singh, Mike Kaler, 2019, “Development of A Technique to Measure Deliquescent Relative Humidity of Particulate Contaminants and Determination of the Operating Relative Humidity of a Data Center, ASME Conference Paper No. IPACK2019-6601

[31] Gautham Thirunavakkarasu, Satyam Saini, Jimil Shah, Dereje Agonafer,2018, **“**Airflow pattern and path flow simulation of airborne particulate contaminants in a high-density Data Center utilizing Airside Economization”, ASME Conference Paper No. IPACK2018-8436

[32] *ANSYS® ANSYS FLUENT Theory Guide, Chapter 16, Release 2019 R1*

[33] *ANSYS® ANSYS FLUENT User's Guide, Chapter24, Release 2019 R1*

[34] Jafari, Saeed & Salmanzadeh, Mazyar & Rahnama, Mohammad & Ahmadi, Goodarz. (2010). Investigation of particle dispersion and deposition in a channel with a square cylinder obstruction using the lattice Boltzmann method. Journal of Aerosol Science. 41. 198-206. 10.1016/j.jaerosci.2009.10.005.

[35] Patankar, S. V., & Spalding, D. B. (1972). A calculation procedure for heat, mass and momentum transfer in threedimensional parabolic flows. *International Journal of Heat and Mass Transfer*, *15*, 1787–1806.

[36] Dakshinamurthy, H. N., Siddarth, A., Guhe, A., Kasukurthy, R., Hoverson, J., & Agonafer, D. (2019, January). Accelerated Degradation Testing of Rigid Wet Cooling Media to Analyse the Impact of Calcium Scaling. In *ASME 2018 International Mechanical Engineering Congress and Exposition*. American Society of Mechanical Engineers Digital Collection.

[37] Mohsenian, G., Khalili, S., & Sammakia, B. (2019, May). A Design Methodology for Controlling Local Airflow Delivery in Data Centers Using Air Dampers. In *2019 18th IEEE Intersociety Conference on Thermal and Thermomechanical Phenomena in Electronic Systems (ITherm)* (pp. 905-911). IEEE.

[38] Patankar, S. V., & Spalding, D. B. (1972). A calculation procedure for heat, mass and momentum transfer in threedimensional parabolic flows. *International Journal of Heat and Mass Transfer*, *15*, 1787–1806

[39] Kumar, A., Shahi, P., & Saha, S. K. Experimental Study of Latent Heat Thermal Energy Storage System for Medium Temperature Solar Applications.

[40] Sarker, M. R. H., Chowdhury, A. R., & Love, N. (2017). Prediction of gas–solid bed hydrodynamics using an improved drag correlation for nonspherical particles. *Proceedings of the Institution of Mechanical Engineers, Part C: Journal of Mechanical Engineering Science*, *231*(10), 1826-1838.

[41] S. Saini, P. Shahi, P. Bansode, A. Siddarth and D. Agonafer, "CFD Investigation of Dispersion of Airborne Particulate Contaminants in a Raised Floor Data Center," *2020 36th Semiconductor Thermal Measurement, Modeling & Management Symposium (SEMI-THERM)*, 2020, pp. 39-47, doi: 10.23919/SEMI-THERM50369.2020.9142865.

Chapter 4 CFD modeling of the Distribution of Airborne Particulate Contaminants Inside Data Center Hardware

4.1 Introduction

With a significant increase in computational demand over the last decade due to developments in AI (Artificial Intelligence) and machine learning, bitcoin mining, cloud computing, etc., data center proliferation has skyrocketed. While novel cooling techniques like dielectric fluid immersion cooling and indirect liquid cooling are being used to dissipate significantly high heat fluxes, air cooling still dominates the data center cooling industry and it will continue to do so. Since the HVAC systems are accountable for a major part of energy consumption in typical air-cooled data centers, it becomes imperative to improve the efficiency of the cooling systems. One of the many causes of inefficiencies in an air-cooled data center is the power consumption of cooling hardware like CRACs and chilled water systems.

Conventional data centers that are located in cold geographies, operate year-round using mechanical cooling without taking the advantage of seasonal or local climatic conditions to cool the IT equipment. Airside economization accomplishes this by bringing outside air at low ambient temperature and relative humidity to reduce the work done by mechanical compressors in the CRAC units for a major part of the year, thus, saving energy expenditure. The ASHRAE T.C.9.9 subcommittee on Mission Critical Facilities, Data Centers, Technology Spaces and Electronic equipment defines temperature and humidity range guidelines to ensure reliable operation of IT equipment [1-6]. They are accepted by ITE manufacturers and their clients to be as follows: 18°C to 27°C (64.4°F to 80.6°F) dry bulb temperature, -9°C to 15°C

(41.9°F to 59°F) dew point temperature, and less than 60% relative humidity. The recommended envelope was expanded by ASHRAE Thermal Guidelines for Data Processing Environments 2008, thereby, allowing short excursions into the allowable regions A1-A3, and an increase in the number of economizer hours.

While companies like Microsoft and Facebook have been able to achieve PUE values as low as 1.1 using free air-cooling methods in geographies with favorable climatic conditions throughout the year, many data center administrators are still reluctant to implement airside economization [6-9]. This is owed to the inherent risk of bringing in particulate and gaseous contaminants along with the outside air. Improvement in computational performance is achieved with a reduction in transistor channel lengths, thus, increasing packaging densities. The net impact of this scaling down results in a subsequent increase in the probability of contamination related failures as higher packaging densities require higher velocities for cooling. Literature suggests that higher velocities increase the particle accumulation rate as well, thus making the closely packed features on PCBs more susceptible to failures related to settled hygroscopic matter. Under the influence of particulate and gaseous contaminants, electronic components and PCBs fail in two ways: Electrical open circuits caused due to corrosion, for example, of silver terminations in surface mount resistors due to the presence of sulfur-bearing gases [10-14]; Electrical short-circuits due to copper creep corrosion, ECM (Electro Chemical Migration), and cathodic-anodic filamentation [12]. These failure modes led to new industry-accepted specifications for contamination limits, which now place a lower limit on the DRH of dust [15, 16]. Also, research by ASHRAE Technical Committee (TC) 9.9 for Mission Critical Facilities, Technology Spaces, and Electronic Equipment led to the publication of a white paper [21] and a book among the Datcom Series [17] on contamination guidelines for data centers and the formulation of new gaseous contamination limits used to update ISA Standard 71.04-2013 [18]. This research also led to the publication of an iNEMI

position paper [19] on gaseous contamination as well as current efforts to update the Chinese data center design guide GB 50174-2008 [20] to include gaseous contamination limits.

The challenging part of simulating particle flow inside the servers is the presence of a multitude of bluff bodies of varying geometries that produce eddies that produce numerous adverse pressure gradients around these objects. This study is an extension of the authors' previously published work where a simplified model of a raised floor data center space was developed to visualize particle transport at room level [21]. A similar approach was used where a transient CFD analysis was done for simplified 2-D models of the servers with large obstructions like heat sinks, DIMMs were created for different server configurations. The flow and particle transport models were studied from existing literature, as presented below, on particle transport in ducts and 2-D channels with/without obstructions. This enabled the authors to significantly simplify the problem and formulate a set of assumptions that closely matched the flow characteristics inside a real server. The particle dispersion results were reported by analyzing the time spent by a specified particle mass flow rate in the flow domain, the particle mass entering and leaving the domain at steady state, and average instantaneous particle volume fraction in the domain.

4.2 Methodology

To generalize the CFD results of particle dispersion, a set of assumptions was formulated that would most closely match flow parameters and conditions in a typical air-cooled data center. The range of particle diameter considered in this study is between 10µm-0.01µm with a mean diameter of 5µm. A total of 15 different diameters were generated between this range to judge the dispersion of well-distributed particle sizes in the flow domain. The study initially began with 3-D models of servers of 1U and 2U form factor as shown in Figure 4-1, with detailed design of heat sinks, power distribution unit, and DIMMs modeled as blocks. After

extracting the fluid volume, a refined mesh was generated with approximately 45 million elements. This led to high computation time because of which the modeling was done only in 2-D. Various cases that have been simulated are tabulated in Table 6. These cases were simulated with two-particle densities and two different flow velocities. The particle densities chosen were 1550 kg/m^3 and 4000 kg/m^3, and the velocities were chosen to be 0.8 m/sec and 2.5 m/sec. The densities and were chosen based on data from literature of most pervasive and corrosive ionic salts and particulate matter. For velocities, the literature on airflow in data centers was referred. These cases were simulated both with and without the effect of gravitational force. The gravitation component was activated for simulations of blade servers and the case where the flow domain is visualized from the side to judge the impact of streamwise obstructions. The same was not activated while judging the impact of obstruction shapes, as would be seen if a server is viewed from the top when its cover is open. The flow domains were designed in ANSYS DM and the dimensions and design of the servers were inspired by widely used open compute servers in the industry.

Table 6: Description of simulated cases

S.No.	Case Type
1	2 Heat Sinks inline
2	2 heat sinks side by side
3	Heat sink with round edge
4	Heat Sink with sharp edges
5	Blade server
6	Staggered Heat sink arrangement
7	Heat sink with cutout

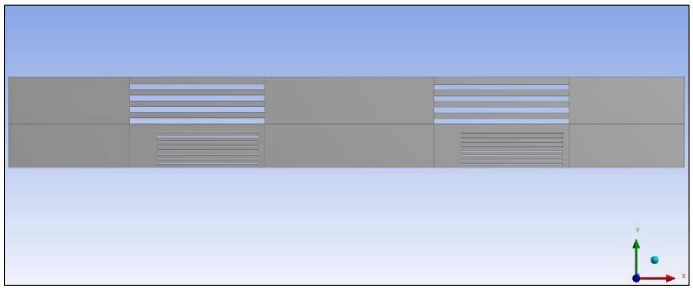

(a)

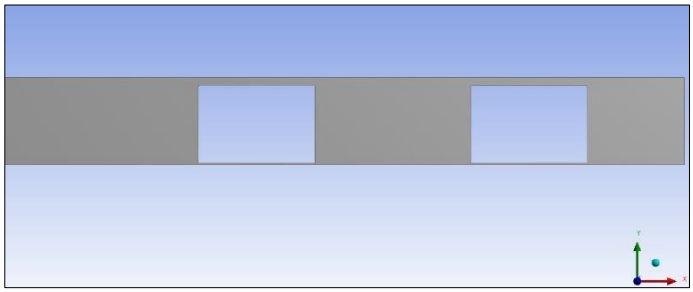

(b)

Figure 4-1: Examples of the simplified 2-D geometries of servers used for simulations showing (a) heat sink and dimms (b) heat sinks in line from side view

To reduce the simulation time while ensuring good results, the symmetric geometries were modeled with a symmetry boundary condition which also reduced the mesh count significantly. To ensure fast and reliable CFD simulation results, a fine quality mesh is paramount. For all the cases designed in the present study, consistent meshing operations were used in all the server designs. As turbulent flows in ducts are dominated by boundary layer effects, especially flows with bluff bodies and large obstructions, the mesh needs to be sufficiently dense near the walls. This is decided by the distance of the first cell from the wall based on the y^+ value in the flow, where the y^+ value is calculated using parameters like flow Reynolds number, hydraulic diameter, etc. For the present case, the y^+ was kept below 3 by adding 10 inflation layers within a total thickness of 1 mm from the walls as shown in Figure 4-2. Mesh metrics like total skewness and mesh orthogonality were used to determine the mesh quality. For the CFD code

used, a good mesh should have a skewness value closer to zero and orthogonality of less than 1. A uniform all quads structured grid was obtained for most of the cases with an average skewness of 0.08 and an orthogonality value of 0.9. The cases with multiple geometries were sliced to form sweepable faces for a structured grid. The maximum mesh count among all the cases was 439,000 which is significantly lower than that obtained in the 3-D model case.

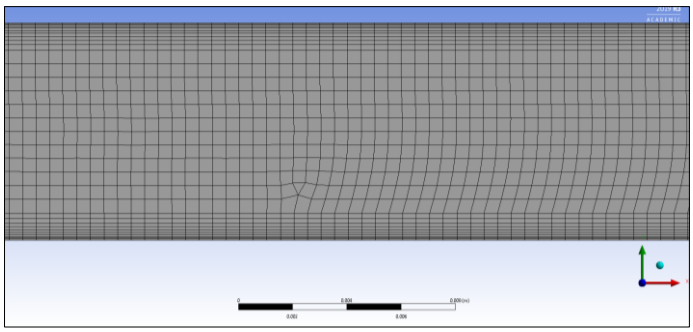

Figure 4-2: Inflation layers created at the walls to capture near wall velocity gradients and particle concentrations

For the current study, the effect of temperature and humidity were neglected as the main objective was to analyze and report particle dispersion and predict the most vulnerable locations of particle deposition. A transient analysis was done where a total simulation time of 5 seconds was used to fill the entire flow domain with enough particles to track. The particles were injected as surface injections at the inlet where particles were then released from each facet of the surface. Here, the facet value of a variable is defined as the computed arithmetic average of the adjacent cell values of the variable. The maximum, minimum, and mean diameters of the injections were specified. A constant mass flow rate was chosen 1e-16 kg/sec was chosen and for size distribution. The initial velocity of particles was also chosen to be the same as for the flow velocity. For particle specific flow models, two-way coupling was used in which the continuous flow field was solved first, after which the discrete phase trajectories are calculated. After this, the continuous phase was solved again based on interphase momentum exchange (as no heat and mass transfer is considered in this study) and discrete phase

trajectories were then recalculated for a modified flow field. This process was repeated until a converged solution was obtained. For the current study, a DPM iteration interval of 10 was selected, which means that a discrete phase iteration was performed every tenth continuous phase iteration. A time step size of 0.01 seconds was chosen with a total number of iterations equal to 500 and maximum iterations per time step equal to 20 to achieve convergence for each time step.

4.3 Results and Discussion

A total of 16 simulation cases were solved for different categories of server geometries and flow conditions based on varying particle density and velocity. To judge the probability of particle deposition, the elapsed residence time of particles within the flow domain, and total particle mass escaping the outlet was analyzed. As mentioned earlier, a mass flow rate of 1e-16 kg/sec was injected in the flow domain, meaning that a total particle mass of 5e-16 kg passed through the domain. The results are broadly divided into 5 different case categories as presented in the coming sections and repetitiveness of results was avoided by consolidating the particle summary in tables. The drag coefficient monitor was used to determine if the flow has reached steady-state or not. This was done as absolute convergence or monitoring of residuals is not necessarily an indicator of converged solution for highly turbulent flows with bluff bodies. The effect of gravity was neglected for some cases as the flow inside the servers is only dominated by forced convection.

4.3.1 Sharp-edged heat sink v/s curved edge

A lot of heat sinks are manufactured with curved edges, especially for servers requiring very high airflow rates, to reduce the overall pressure drop in the system. This decelerates the flow at the corners, keeping the turbulent mixing between the fins for effective heat removal.

In this case, 2-D geometries were designed with the dimensions equivalent to that of a 2U server and a heat sink height of 7.8 cm.

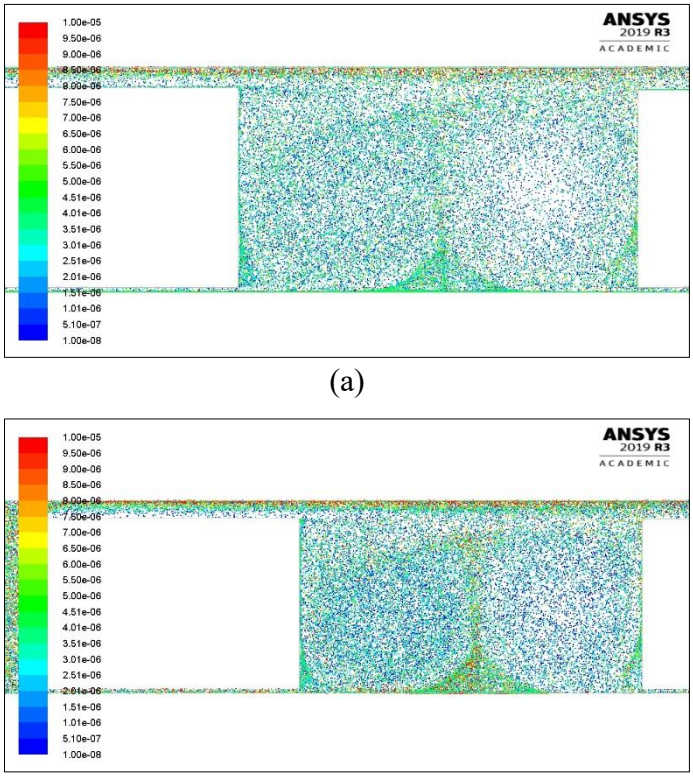

(a)

(b)

Figure 4-3: Particle diameters in the flow domain for dispersion from (a) sharp and (b) round edged heat sinks

As seen in Figures 4-3 (a) and (b), for sharp-edged heat sink more particle diameters were present on the heat sink in sharp edge than in the case of the round edge heat sink. Also, as opposed to that, more particle diameters were present between heat sinks in case round-cornered than sharp edge heat sink Furthermore, a greater number of the particles moved towards the top of the server for the round edge heat sink. A comparison of particle flow parameters is given in Table 7 and Table 8. It can be concluded that more particles stay in the flow domain for sharp-cornered heat sinks. This can be attributed to the fact that sharp edges tend to shed more vortices, trapping the particles of larger diameters in the around them due to the centrifugal forces. This has also been reported in the published literature.

Table 7: Particle summary for sharp edge heat sink

Parameter	Value
Total mass injected	5e-20 kg
Escaped Outlet	3.9e-16 kg
Max time in domain	2.36e-1 sec
Min time in the domain	4.93 sec

Table 8: Particle summary for round edge heat sink

Parameter	Value
Total mass injected	5e-20 kg
Escaped Outlet	4.5e-20 kg
Min time in the domain	2.30e-01 sec
Max time in the domain	4.64 sec

4.3.2 Heat sinks side by side v/s in line

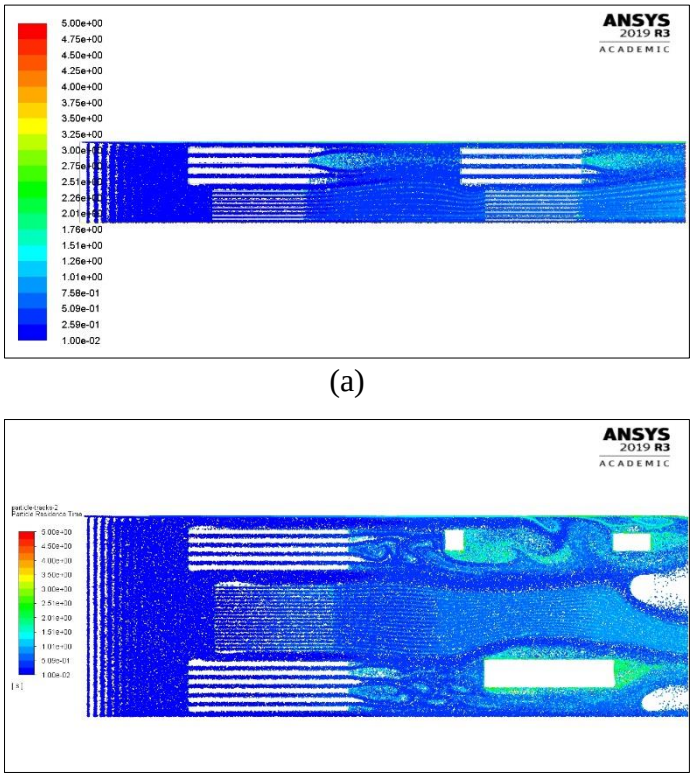

Figure 4-4: Particle residence time in the flow domain for (a) in-line heat sinks (b) side by side heat sinks

As mentioned earlier in this study, it is imperative to generalize the results obtained from these simulations for the most common server geometries. The geometries shown in Figure 4-4 were decided based on a general survey by the authors for storage products offered by leading server manufacturers. Symmetry boundary condition was used for bottom walls in both cases. Additional obstructions were added to observe the effect of varying geometrical shapes within the server. These geometrical features also represent other components within the server like power distribution trays inside the chassis, smaller heat sinks for chipsets, etc. As seen in the figure above, high particle residence time was obtained at the walls of in-line heat sinks towards the rear end of the server. Other locations of relatively higher residence time were between the heat sink and the DIMMs. Another inference that can be made from Figure 4-4 (b) is that solid obtructions behind the heat sinks with greater depth do not create large turbulent eddies or any vortex shedding when compared to square or circular obstructions. It can thus be pointed out

that there might be a greater probability of finding settled particulate matter towards the rear end of the servers of similar geometries. These regions mostly contain drive backplanes, power supplies, drive fillers, etc. Table 9 and Table 10 show the comparison particle summary for both the cases discussed in this section. Here, it can be noted that for both the cases, the maximum time spent by the particles in the flow domain was identical, but the average time was more in case of heat sinks located side by side.

Table 9: Particle summary for in-line heat sinks high density

Parameter	Value
Total mass injected	5e-16 kg
Escaped Outlet	4.3e-16 kg
Min time in the domain	3.9e-01 sec
Max time in the domain	4.9 sec

Table 10: Particle summary for heat sinks arranged side by side high density

Parameter	Value
Total mass injected	5e-16 kg
Escaped Outlet	4.2e-16 kg
Min time in the domain	4.1e-01 sec
Max time in the domain	4.9 sec

4.3.3 Blade Servers

As mentioned earlier, the effect of gravity can be neglected when considering the case of forced convection. This might not be completely true for the case of blade servers, where a chassis form factor of up to 8U is present in enclosures. In these cases, gravitational effects can have a significant impact on particle deposition within the enclosure. Table 11 and Table 12

show the impact of varying density within a blade server. It was observed that more particles are trapped for a longer period within the fins of the heat sinks as the effect of gravity is included as compared to the previous case for the inline case in Figure 4-4 (a).

Table 11: Particle transfer summary for low-density particles in a blade server

Parameter	Value
Total mass injected	5e-16 kg
Escaped Outlet	4.3e-16 kg
Min time in the domain	3.8e-01 sec
Max time in the domain	4.6 sec

Table 12: Particle transfer summary for high-density particles in a blade server

Parameter	Value
Total mass injected	5e-16 kg
Escaped Outlet	4.2e-16 kg
Min time in the domain	3.8e-01 sec
Max time in the domain	4.5 sec

4.3.4 Effect of velocity

To assess the impact of increasing inlet velocity on particle accumulation, two different values of velocities were chosen from published literature [48]. The particle residence time plots depict that for lower velocity value, particles spend more time in the flow domain and for high velocity, particles spend more time on the surfaces. This phenomenon holds when compared to the conclusions made by Frankenthal et al [45]. No deposition on top or bottom wall for high velocity was observed until the flow reaches the second set of DIMMs. The comparison of residence time and mass transfer through the outlet in both cases is shown in Tables 13 and 14.

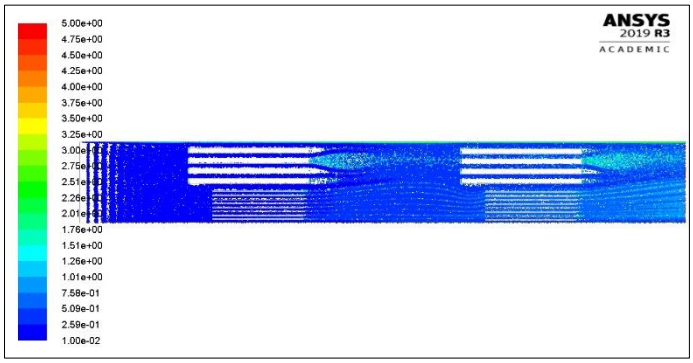

(a)

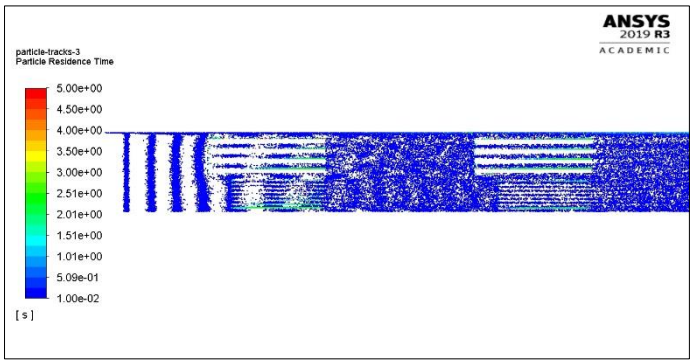

(b)

Figure 4-5: Particle residence time in the flow domain for in-line heat sinks (a) low velocity (b) high velocity

Table 13: Particle transfer summary for low-velocity flow with high-density particles

Parameter	**Value**
Total mass injected	5e-16 kg
Escaped Outlet	4.2e-16 kg
Min time in the domain	3.8e-01
Max time in the domain	4.5 sec

Table 14: Particle transfer summary for high-velocity flow with high-density particles

Parameter	**Value**
Total mass injected	5e-16 kg

Escaped Outlet	4.8e-16 kg
Min time in the domain	1.4e-01
Max time in the domain	4.6 sec

4.3.5 Effect of the heat sink cutout

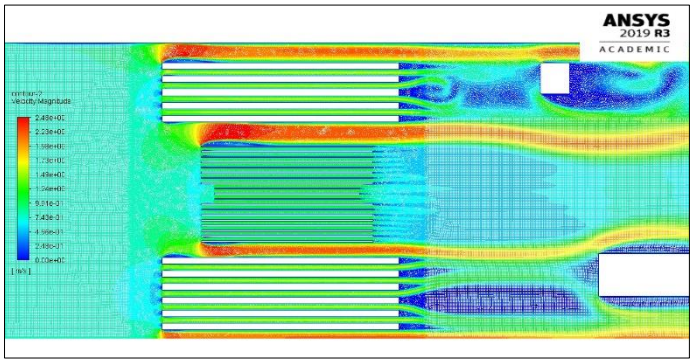

Figure 4-6: Flow velocity contour for heat sink cutout case

Cutouts can be provided on narrow as well as high form factor heat sinks to reduce pressure drops. To observe the effect of change of geometry within the heat sink, a heat sink cutout was provided at the center of the sink as shown in Figure 4-6. As it can be seen in Table 15 and Table 16, the heat sink cutout caused a reduction in total mass escaping the outlet meaning more particles are trapped within the flow domain. Although the total reduction might seem a very small number, this can be significantly higher over hours of operation. This increase in particle count within the flow domain might be due to a reduction in total static pressure value around the fins which might cause a local deposition of particles in the surrounding region. This was also observed in particle residence time plots.

Table 15: Particle transfer summary for heat sink cutout, low density

Parameter	**Value**
Total mass injected	5e-16 kg
Escaped Outlet	4.2e-16 kg

Min time in the domain	4.1e-01 sec
Max time in the domain	4.9 sec

Table 16: Particle summary for heat sink without cutout, low density

Parameter	Summary
Total mass injected	5e-16 kg
Escaped Outlet	4.4e-16 kg
Min time in the domain	4.1e-01 sec
Max time in the domain	4.98 sec

4.4 Conclusion and Future Work

Particle transport and dispersion within simplified data center storage systems were studied using CFD. Predictions for particle accumulation were made based on analysis of total elapsed time that the particles spend before escaping from the flow domain and by analyzing the difference of mass transferred between inlet and outlet of the flow domains. Based on the nature of flow obstructions present within the server, it was observed that while there might be little accumulation near thin features like DIMMS and heat sinks, the presence of other components and smaller features can significantly increase it. Also, for features with aspect ratios of any dimension closer to 1 may have significant particle accumulation around it. On the contrary, features with larger length offer significantly less flow resistance and may be less vulnerable to deposition. Critical components, as per failure rates are concerned, are usually hard drives. Most of the storage servers today have separate hard drive bays. The servers where the hard drives are located towards the rear end might be more prone to exposure to particulates. It was also seen that higher velocities tend to increase accumulation on flat surfaces like fins and the DIMMs, therefore, for computational servers that are air-cooled, they might experience

increased exposure to particles when the data center is operating in free air cooling mode. While novel cooling methods like phase-change, direct immersion cooling, and liquid cooling [49-52] are mostly being used for high-performance computing, most storage systems based data centers will continue to use air cooling. Therefore, it becomes imperative to address the challenge of particulate contamination for economizer based or free air-cooled data centers.

This study was a first step towards establishing a predictive approach to how the particles might behave after entering the data center equipment while economizer or free air-cooling mode is on. Based on conclusions drawn from this study, further investigations will be conducted at a larger scale where the spatial distribution of particles will be determined in a data center with multiple rows of racks. The simulations can be made complicated by varying pressure across each of these rows to represent a more realistic scenario. The effects of temperature and, therefore, thermophoresis force can be included by treating particles as volatile and reacting species as they move through the flow domain. A 2-D study is already being conducted by the authors to simulate the chemical reaction that occurs at the material level in presence of ionic species in the flow by varying the humidity and temperature of the flow domain.

REFERENCES

[1] Koomey, Jonathan. "Growth in data center electricity use 2005 to 2010." *A report by Analytical Press, completed at the request of The New York Times* 9 (2011): 161.

[2] Prabjit Singh, Levente Klein, Dereje Agonafer, Jimil M. Shah and Kanan D. Pujara, "Effect of Relative Humidity, Temperature and Gaseous and Particulate Contaminations on ITE Reliability, DOI: 10.1115/IPACK2015-48176, ASME InterPACK 2015, San Francisco, CA

[3] Shah, Jimil & Awe, Oluwaseun & Gebrehiwot, Betsegaw & Agonafer, Dereje & Singh, P & Kannan Mestex, Naveen & Kaler Mestex, Mike. (2017). "Qualitative Study of Cumulative Corrosion Damage of ITE in a Data Center Utilizing Air-side Economizer Operating in Recommended and Expanded ASHRAE Envelope". Journal of Electronic Packaging. 139. 021002. 10.1115/1.4036363.

[4] Thermal Guidelines for Data Processing Environments, ASHRAE Datacom Series, 1st Edition, 2004, ASHRAE, Atlanta, GA, USA.

[5] Thermal Guidelines for Data Processing Environments, ASHRAE Datacom Series, 2nd Edition, 2008, ASHRAE, Atlanta, GA, USA.

[6] Thermal Guidelines for Data Processing Environments, ASHRAE Datacom Series, 3rd Edition, 2012, ASHRAE, Atlanta, GA, USA

[7] https://www.opencompute.org/blog/cooling-an-ocp-data-center-in-a-hot-and-humid-climate

[8] Google. Efficiency: How We Do It, 2014

[9] Microsoft. Microsoft Shares Video Tour of its Cloud Datacenters,2011

[10] Burnett W. H., F. S. Sandroff and S. M. D'Egidio, "Circuit failure due to fine dust mode particulate air pollution," ISTFA '92, The 18th Int'l Symposium for Testing & Failure Analysis, Los Angeles, CA, 17-23 Oct 1992, 329-333.

[11] Cole, M., L. Hedlund. T; Kiraly, S. Nickel, P. Singh and T. Tofil, "Harsh Environmental Impact on Resistor Reliability", SMTA Int'l Conf, Proc., 24 Oct 2010.

[12] Directive 2002/95/EC of the European Parliament and of the Council of 27 January 2003 on the Restriction of the use of Certain Hazardous Substances on Electrical and Electronic Equipment Official Journal L 037, February 13, 2003, 19-23.

[13] Fu, H., C. Chen, P. Singh, J. Zhang. A. Kurella, X. Chen, X. Jiang, J. Burlingame and S. Lee, "Investigation of Factors that Influence Creep Corrosion on Printed Circuit Boards," SMTA Pan Pacific Microelectronics Symposium, Kauai, 14-16 Feb 2012.

[14] Fu, H., C. Chen, P. Singh, J. Zhang. A. Kurella, X. Chen, X. Jiang, J. Burlingame and S. Lee, "Investigation of Factors that Influence Creep Corrosion on Printed Circuit Boards, Part 2", SMTAI 2012.

[15] ASHRAE Technical Committee 9.9. 2009. "2009 Particulate and Gaseous Contamination Guidelines for Data Centers."

[16] Muller, Chris. (2014). "Reliability Concerns for Data Center ITE: Contamination Issues, Standards Actions, and Case Studies".

[17] ASHRAE. 2013. "Particulate and Gaseous Contamination in Datacom Environments", 2nd Ed. Atlanta: American Society of Heating, Refrigerating, and Air-Conditioning Engineers, Inc.

[18] ISA. 2013. ANSI/ISA 71.04-2013: Environmental Conditions for Process Measurement and Control Systems: Airborne Contaminants. Research Triangle Park: International Society for Automation.

[19] iNEMI. 2012. iNEMI Position Statement on the Limits of Temperature, Humidity and Gaseous Contamination in Data Centers and Telecommunication Rooms to Avoid Creep Corrosion on Printed Circuit Boards.

[20] China National Standard GB 50174-2008: Code for Design of Electronic Information System.

[21] Satyam Saini, Pardeep Shahi, Pratik Bansode, Ashwin Siddarth, Dereje Agonafer "CFD Investigation of Dispersion of Airborne Particulate Contaminants in a Raised Floor Data Center", SEMI-THERM 36, March 16-20, 2020

[22] Jimil M. Shah, Roshan Anand, Satyam Saini, Rawhan Cyriac, Dereje Agonafer, Prabjit Singh, Mike Kaler, 2019, Development of A Technique to Measure Deliquescent Relative Humidity of Particulate Contaminants and Determination of the Operating Relative Humidity of a Data Center**,** ASME Conference Paper No. IPACK2019-6601

[23] Gautham Thirunavakkarasu, Satyam Saini, Jimil Shah, Dereje Agonafer,2018, Airflow pattern and path flow simulation of airborne particulate contaminants in a high-density Data Center utilizing Airside Economization, ASME Conference Paper No. IPACK2018-8436

[24] Seymour, M.J., A. A. M. A., and Jiang, J., 2000. “Cfd based airflow modelling to investigate the effectiveness of control methods intended to prevent the transmission of airborne organisms”. Air Distribution in Rooms, (ROOMVENT 2000).

[25] Jones, P., and Whittle, G., 1992. “Computational fluid dynamics for building air flow prediction- current status and capabilities”. Building and Environment, 27(3), pp. 321–338.

[26] Chen, Q., and Zhang, Z., 2005. “Prediction of particle transport in enclosed environment”. China Particuology, 3(6), pp. 364–372.

[27]. Longmire, E. K., and Eaton, J. K. (1992). Structure of a Particle-Laden Round Jet, *J. Fluid Mech.* 236:217–257.

[28] Lazaro, B. J., and Lasheras, J. C. (1992). Particle Dispersion in the Developing Free Shear Layer, Part 1—Unforced Flow, *J. Fluid Mech.* 235:143–178.

[29]. Crowe, C. T., Chung, J. N., and Trout, T. R. (1988). Particle Mixing in Free Shear Flows, *Progress in Energy and Combustion Science* 14:171–194.

[30] Uthuppan, J., Aggarwal, S. K., Grinstein, F. F., and Kailasanath, K. (1994). Particle Dispersion in a Transitional Axisymmetric Jet: A Numerical Simulation, *AIAA J.* 32:2004–2014.

[31] Aggarwal, S. K. (1994). Relationship Between the Stokes Number and Intrinsic Frequencies in Particle-Laden Flows, *AIAA J.* 32:1322–1325.

[32] Chang, E., and Kailasanath, K. (1996). Simulation of Dynamics in a Confined Shear Flow, *AIAA J.* 34:1160–1166

[33] D. J. Brandon & S. K. Aggarwal (2001) A Numerical Investigation of Particle Deposition on a Square Cylinder Placed in a Channel Flow, Aerosol Science & Technology, 34:4, 340-352

[34] Alletto, M., & Breuer, M. (2012). One-way, two-way and four-way coupled LES predictions of a particle-laden turbulent flow at high mass loading downstream of a confined bluff body. *International Journal of Multiphase Flow*, *45*, 70–90.

[35] van Vliet, E., Singh, M., Schoonenberg,W., van Oord, J., van der Plas,D., & Deen, N. (2013). *Development and validation of Lagrangian-Eulerian multi-phase model for simulating the argon stirred steel flow in a ladle with slag*. Proceedings of the 5th International Conference

on Modelling and Simulation of Metallurgical Processes in Steelmaking, STEELSIM. Ostrava, Czech Republic.

[36] Sardina, G., Schlatter, P., Brandt, L. P., & Casciola, C. (2012). Wall accumulation and spatial localization in particle-laden wall flows. *Journal of Fluid Mechanics*, *699*, 50–78.

[37] Wang, B., Manhart, M., & Zhang, H. (2011). Analysis of inertial particle drift dispersion by direct numerical simulation of two-phase wall-bounded turbulent flows. *Engineering Applications of Computational Fluid Mechanics*, *5*(3), 341–348.

[38] Vreman, A. (2015). Turbulence attenuation in particle-laden flow in smooth and rough channels. *Journal of Fluid Mechanics*, *773*, 103–136

[39] Franziska Greifzu, Christoph Kratzsch, Thomas Forgber, Friederike Lindner & Rüdiger Schwarze (2016) Assessment of particle-tracking models for dispersed particle-laden flows implemented in OpenFOAM and ANSYS FLUENT, Engineering Applications of Computational Fluid Mechanics, 10:1, 30-43, DOI: 10.1080/19942060.2015.1104266

[40] Sippola, M. R., 2002, "Particle Deposition in Ventilation Ducts," Lawrence Berkeley National Lab (LBNL), Berkley, CA, Report No. LBNL-52189.

[41] Pui DYH, Romay-Novas F, Liu BYH. Experimental study of particle deposition in bends of circular cross-section. Aerosol Sci Technol 1997;7:301–15

[42] Zhang H, Ahmadi G. Aerosol particle transport and deposition in vertical and horizontal turbulent duct flows. J Fluid Mech 2000;406:55–80.

[43] Zhao Bin, Wu Jun. Modeling particle fate in ventilation system—Part II: Case study. Build Environ 2009;44:612–20.

[44] Gao, R., and Li, A. (2012). Dust Deposition in Ventilation and Air-Conditioning Duct Bend Flows. *Energy Convers. Manage.*, 55:49–59

[45] Comizzoli, R. B., Frankenthal, R. P., Lobnig, R. E., and Peins, G., 1993, “Corrosion of Electronic Materials and Devices by Submicron Atmospheric Particles,” Electrochem. Soc., Interface, 2(3), pp. 26–33.

[46] *ANSYS® ANSYS FLUENT Theory Guide, Chapter 16, Release 2019 R3*

[47] *ANSYS® ANSYS FLUENT User’s Guide, Chapter24, Release 2019 R3*

[48] Ibrahim, Mahmoud, et al. "Thermal mass characterization of a server at different fan speeds." *13th InterSociety Conference on Thermal and Thermomechanical Phenomena in Electronic Systems*. IEEE, 2012.

[49] Shah, J. M., Eiland, R., Rajmane, P., Siddarth, A., Agonafer, D., and Mulay, V. (April 10, 2019). "Reliability Considerations for Oil Immersion-Cooled Data Centers." ASME. J. Electron. Packag. June 2019; 141(2): 021007. https://doi.org/10.1115/1.4042979

[50]Ramdas, Shrinath, Rajmane, Pavan, Chauhan, Tushar, Misrak, Abel, and Agonafer, Dereje. "Impact of Immersion Cooling on Thermo-Mechanical Properties of PCB’s and Reliability of Electronic Packages." Proceedings of the ASME 2019 International Technical Conference and Exhibition on Packaging and Integration of Electronic and Photonic Microsystems. ASME 2019 International Technical Conference and Exhibition on Packaging and Integration of Electronic and Photonic Microsystems. Anaheim, California, USA. October 7–9,2019.V001T02A011.ASME.https://doi.org/10.1115/IPACK2019-6568

[51] Shahi, Pardeep, 2016, “Experimental Analysis of PCM based Thermal Storage System for Solar Power Plant,” M.S. thesis, Indian Institute of Technology- Mumbai.

[52] Kumar, Ashish, Pardeep Shahi, and Sandip K. Saha. "Experimental Study of Latent Heat Thermal Energy Storage System for Medium Temperature Solar Applications."

[53] Dehkordi, B. G., Fallah, S., & Niazmand, A. (2014). Investigation of harmonic instability of laminar fluid flow past 2D rectangular cross sections with 0.5–4 aspect ratios. *Proceedings of the Institution of Mechanical Engineers, Part C: Journal of Mechanical Engineering Science*, *228*(5), 828–839. https://doi.org/10.1177/0954406213491906

[54] Saini, S, Adsul, KK, Shahi, P, Niazmand, A, Bansode, P, & Agonafer, D. "CFD Modeling of the Distribution of Airborne Particulate Contaminants Inside Data Center Hardware." Proceedings of the ASME 2020 International Technical Conference and Exhibition on Packaging and Integration of Electronic and Photonic Microsystems. ASME 2020 International Technical Conference and Exhibition on Packaging and Integration of Electronic and Photonic Microsystems. Virtual, Online. October 27–29, 2020. V001T08A005. ASME. https://doi.org/10.1115/IPACK2020-2590

Chapter 5 Simplified and Detailed Analysis of Data Center Particulate Contamination at Server and Room Level Using CFD

5.1 Introduction

Data center energy consumption continues to rise with increasing computational, storage, and networking demands due to developments in AI (Artificial Intelligence) and machine learning, bitcoin mining, and cloud computing. While cooling technologies like dielectric fluid immersion cooling (single-phase and two-phase) [1-3] and direct-to-chip liquid cooling using cold plates [4,5] are being used to dissipate significantly high heat fluxes, air cooling still dominates the data center cooling industry, and it might continue as such.

Class[a]	Equipment Environmental Specifications for Air Cooling						
	Product Operations[b,c]					Product Power Off[c,d]	
	Dry-Bulb Temperature[e,g] °C	Humidity Range, Non-Condensing[h,i,k,l]	Maximum Dew Point[k] °C	Maximum Elevation[e,j,m] m	Maximum Temperature Change[f] in an Hour (°C)	Dry-Bulb Temperature °C	Relative Humidity[k] %
Recommended (Suitable for all 4 classes)							
A1 to A4	18 to 27	-9°C DP to 15°C DP and 60% RH					
Allowable							
A1	15 to 32	-12°C DP & 8% RH to 17°C DP and 80% RH[k]	17	3050	5/20	5 to 45	8 to 80
A2	10 to 35	-12°C DP & 8% RH to 21°C DP and 80% RH[k]	21	3050	5/20	5 to 45	8 to 80
A3	5 to 40	-12°C DP & 8% RH to 24°C DP and 85% RH[k]	24	3050	5/20	5 to 45	8 to 80
A4	5 to 45	-12°C DP & 8% RH to 24°C DP and 90% RH[k]	24	3050	5/20	5 to 45	8 to 80
B	5 to 35	8% to 28°C DP and 80% RH[k]	28	3050	NA	5 to 45	8 to 80
C	5 to 40	8% to 28°C DP and 80% RH[k]	28	3050	NA	5 to 45	8 to 80

Figure 5-1: ASHRAE 2015 temperature guidelines showing the recommended and allowable ranges for temperature and humidity for data centers

Conventional air-cooled data centers operate year-round using mechanical cooling without taking the advantage of seasonal or local climatic conditions to cool the IT equipment.

Airside economization or free air cooling can accomplish this by bringing outside air at low ambient temperature and relative humidity to reduce the compressor work partly or completely for a major part of the year, thus, saving energy expenditure. The ASHRAE T.C.9.9 subcommittee on Mission Critical Facilities, Data Centers, Technology Spaces and Electronic equipment expanded the recommended thermal and humidity envelopes, thereby, allowing short excursions into the allowable regions A1-A4, as shown in Figure 5-1, and an increase in the number of economizer hours. While companies like Microsoft and Facebook have been able to achieve PUE values as low as 1.1 using free air-cooling methods in geographies with favorable climatic conditions throughout the year, many data center administrators are still reluctant to implement airside economization [6-9]. This is owed to the inherent risk of introducing fine particulate and corrosive gaseous contaminants along with the outside air. For data centers using airside economization for cooling, ASHRAE recommends a MERV (Minimum Efficiency Reporting Value) 11-13 filters for outside air filtration and MERV 8 filters for continuously filtering data center indoor air [10]. A summary of the contaminant arresting efficiency of various MERV filters is shown in Figure 5-2.

MERV RATING CHART

Standard 52.5 Minimum Efficiency Reporting Value	Dust Spot Efficiency	Arrestance	Typical Controlled Contaminant	Typical Applications and Limitations	Typical Air Filter/Cleaner Type
20	n/a	n/a	< 0.30 pm particle size	Cleanrooms	≥99.999% eff. On .10-.20 pm Particles
19	n/a	n/a	Virus (unattached)	Radioactive Materials	Particles
18	n/a	n/a	Carbon Dust	Pharmaceutical Man.	Particulates
17	n/a	n/a	All Combustion smoke	Carcinogenetic Materials	≥99.97% eff. On .30 pm Particles
16	n/a	n/a	.30-1.0 pm Particle Size	General Surgery	**Bag Filter**- Nonsupported
15	>95%	n/a	All Bacteria	Hospital Inpatient Care	microfine fiberglass or synthetic media, 12-36 in. deep, 6-12 pockets
14	90-95%	>98%	Most Tobacco Smoke	Smoking Lounges	**Box Filter**- Rigid Style Cartridge Filters 6 to 12" deep m ay use lofted or paper media.
13	89-90%	>98%	Proplet Nuceli (Sneeze)	Superior Commercial Buildings	
12	70-75%	>95%	1.0-3.0 pm Particle Size Legionella	Superior Residential	**Bag Filter**- Nonsupported microfine fiberglass or synthetic media, 12-36 in. deep, 6-12 pockets
11	60-65%	>95%	Humidifier Dust Lead Dust	Better Commercial Buildings	**Box Filter**- Rigid Style Cartridge Filters 6 to 12" deep m ay use lofted or paper media.
10	50-55%	>95%	Milled Flour Auto Emissions	Hospital Laboratories	
9	40-45%	>90%	Welding Fumes		
8	30-35%	>90%	3.0-10.0 pm Particle Size Mold Spores	Commercial Buildings	**Pleated Filters**- Disposable, extended surface area, thick with cotton-polyester blend media, cardboard frame
7	25-30%	>90%	Hair Spray Fabric Protector	Better Residential	**Cartridge Filters**- Graded density viscous coated cube or pocket filters, synthetic media
6	<20%	85-90%	Dusting Aids Cement Dust	Industrial Workplace	**Throwaway**- Disposable synthetic panel filter.
5	<20%	80-85%	Pudding Mix	Paint Booth Inlet	
4	<20%	75-80%	>10.0 pm Particle Size Pollen	Minimal Filtration	**Throwaway**- Disposable fiberglass or synthetic panel filter.
3	<20%	70-75%	Dust Mites Sanding Dust	Residential	**Washable**- Aluminum Mesh
2	<20%	65-70%	Spray Paint Dust Textile Fibers	Window A/C Units	**Electrostatic**- Self charging woven panel filter.
1	<20%	<65%	Carpet Fibers		

Figure 5-2: Summary of different MERV filter efficiency and their particle arrestance efficiency at varying particle diameters

The issue being investigated this study is utilizing tools like CFD for data center particle flow visualization and addressing the lack of studies that specifically look into issue data center contamination. It is extremely difficult to otherwise, conduct tightly controlled experiments with particle visualization and particle generating equipment, where the cost can reach in hundreds of thousands of dollars for the state of the art equipment. The authors, therefore, propose using CFD tools that use well established particle and flow interaction correlations to simulate the contaminant flow in data center flow boundary conditions. The challenging part of simulating particle flow inside the servers and data center is the presence of a multitude of

bluff bodies of varying geometries that produce eddies that produce numerous adverse pressure gradients around these objects. Based on an extensive literature review, it was identified that a knowledge gap exists in terms of an approach to identify discrete locations of particle accumulation inside the IT equipment and at the data center level. The issue of data center contamination due to settled particulate matter has been mostly discussed in the form of case studies, from a risk assessment point of view, and mostly addresses the best practices to mitigate harmful contaminants [11, 12]. The current literature is dominated by empirical studies that have investigated the failure modes and failure mechanisms, dominated by corrosion studies at PCB level and interconnect level. Particle-laden flow, in general, has been studied widely for commercial buildings and indoor residential environments owing to the high risk to the occupants [13-15].

The results investigated in this study are divided into two main sections: particle flow patterns at the IT equipment level and particle flow pattern analysis at room level. This study is an extension of the authors' previously published work where a simplified model of a raised floor data center space was developed to visualize particle transport at room level [16]. A similar approach was used in the current study, where a transient CFD analysis was done for simplified 2-D and 3-D models of the servers with large obstructions like heat sinks, DIMMs were created for different server configurations. The flow and particle transport models were studied from existing literature on particle transport in ducts and 2-D channels and 3-D ducts with and without obstructions. This enabled the authors to significantly simplify the problem and formulate a set of assumptions that closely matched the flow characteristics inside a real server. The particle dispersion results were reported by analyzing the time spent by a specified particle mass flow rate in the flow domain, the particle mass entering and leaving the domain at a steady-state, and the average instantaneous particle volume fraction in the domain. Further analysis was also done to identify and compare various geometries and heat sink configurations

from a thermal point of view to ascertain the trade-offs in thermal performance and particle accumulation.

5.2 Methodology

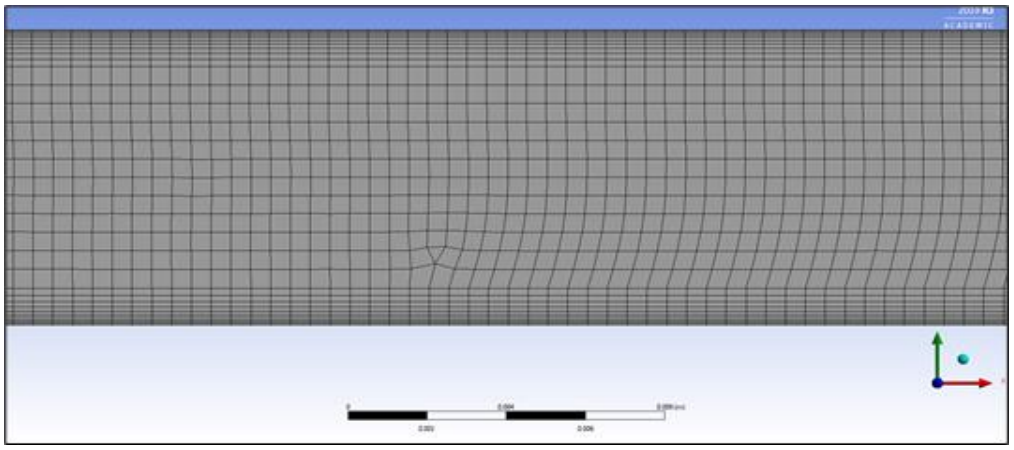

Figure 5-3: Inflation layers created at the walls to capture near-wall velocity gradients and particle concentrations

To generalize the CFD results of particle dispersion, a set of assumptions was formulated that would most closely match flow parameters and conditions in a typical air-cooled data center. The overall simulation setup including the inputs required for particle-phase, turbulence model used, and type of boundary conditions applied, stays the same for 2-D, 3-D as well as room-level simulations. The range of particle diameter considered in this study is between 10µm-0.01µm with a mean diameter of 5µm. A total of 15 different diameters were generated between this range to judge the dispersion of well-distributed particle sizes in the flow domain. Various cases that have been simulated are tabulated in Table 17 and an example of simplified 2-D geometries analyzed is shown in Figure 5-3. These cases were simulated with two-particle densities and two different flow velocities. The particle densities chosen were 1550 kg/m3 and 4000 kg/m3, and the velocities were chosen to be 0.8 m/sec and 2.5 m/sec. The densities and were chosen based on data from literature of most pervasive and corrosive ionic salts and particulate matter [19]. The cases with multiple geometries were sliced to form sweepable faces for a structured grid as shown in Figure 5-4. The maximum mesh

count among all the 2-D cases was 439,000 which is significantly lower than that obtained in the 3-D model case. For 3-D simulations, using similar meshing operations, the maximum grid count of 2.6 million was obtained.

Table 17: Description of simulated cases

S.No.	Case Type
1	2 Heat Sinks inline
2	2 heat sinks side by side
3	Heat sink with round edge
4	Heat Sink with sharp edges
5	Blade server
6	Staggered Heat sink arrangement
7	Heat sink with cutout

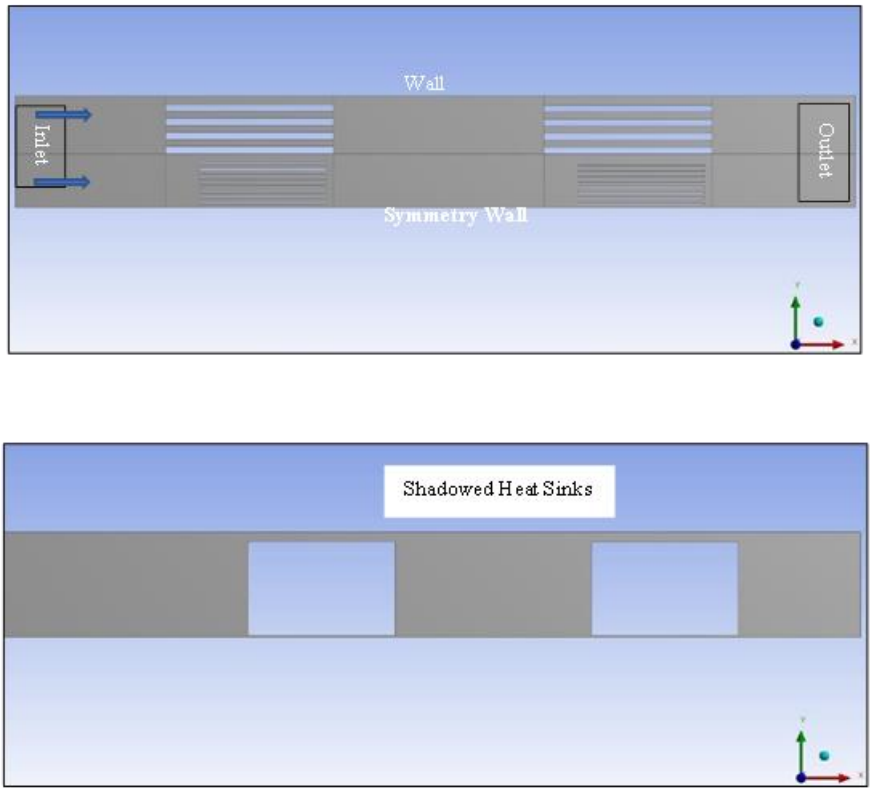

Figure 5-4: Examples of the simplified 2-d geometries of servers and boundary conditions used for simulations showing (Top) heat sink and DIMMs (bottom) heat sinks in line from the side view

5.3 Results and Discussion

The results presented in this section are divided into results from 2-D simulations, results obtained from 3-D simulations, and results for room-level simulations. The results obtained from 2-D simulations were also compared with 3-D simulations to quantify the discrepancy between the results.

5.4 Results for ITE in 2-D

5.4.1 Sharp-edged Heat Sink v/s Curve Edged

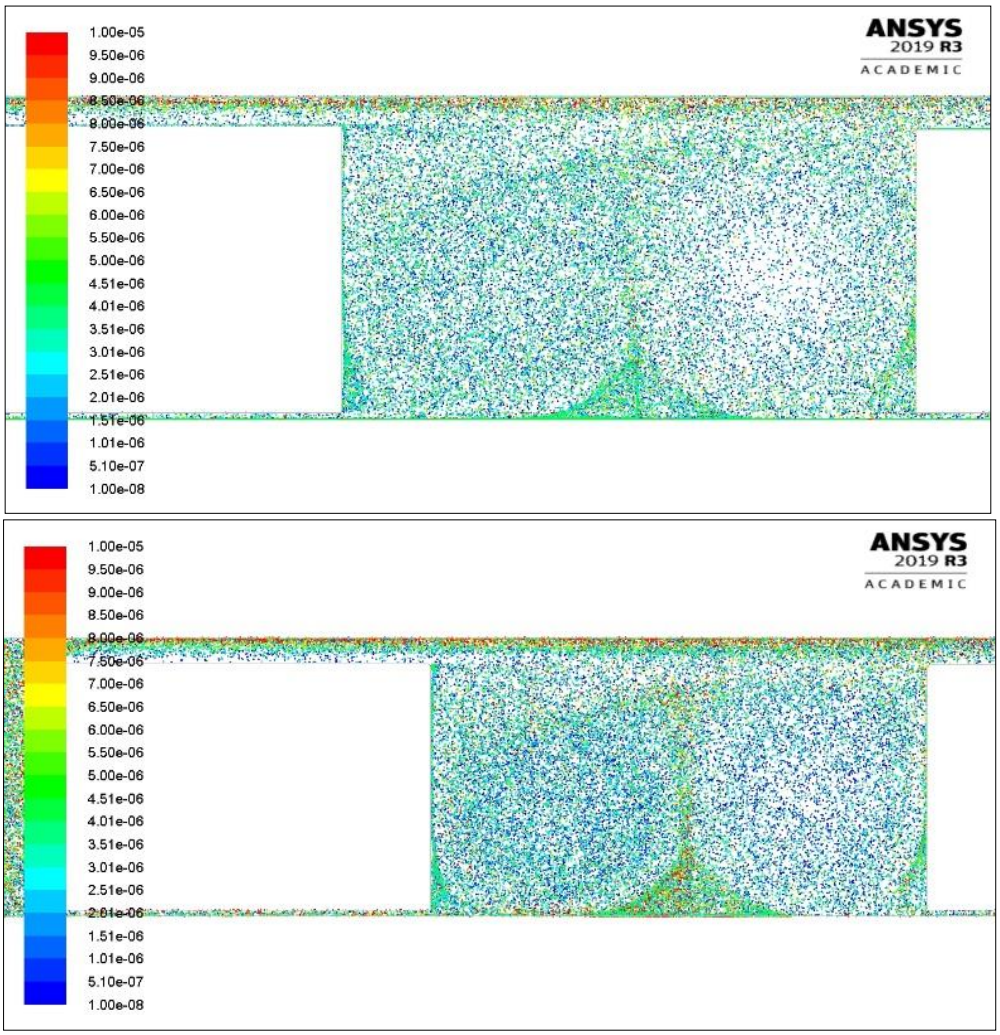

Figure 5-5: Particle diameters in the flow domain for dispersion from (top) sharp and (bottom) round-edged heat sinks

A lot of heat sinks are manufactured with curved edges, especially for servers requiring very high airflow rates, to reduce the overall pressure drop in the system. This decelerates the

flow at the corners, keeping the turbulent mixing between the fins for effective heat removal. In this case, 2-D geometries were designed with dimensions equivalent to that of a 2U server and a heat sink height of 7.8 cm. As seen in Figure 5-5, for sharp-edged heat sink more particle diameters were present on the heat sink in sharp edge than in the case of the round edge heat sink. Also, as opposed to that, more particle diameters were present between heat sinks in case round-cornered than sharp edge heat sink Furthermore, a greater number of the particles moved towards the top of the server for the round edge heat sink. A comparison of particle flow parameters is given in Table 18. It can be concluded that more particles stay in the flow domain for sharp-cornered heat sinks. This can be attributed to the fact that sharp edges tend to shed more vortices, trapping the particles of larger diameters around them due to the centrifugal forces. This has also been reported in the published literature.

Table 18: Particle summary for the sharp edge and curved edge heat sink

Sharp Edge	
Parameter	**Value**
Total mass injected	5e-20 kg
Escaped Outlet	3.9e-16 kg
Max time in domain	2.36e-1 sec
Min time in the domain	4.93 sec
Curved Edge	
Parameter	**Value**
Total mass injected	5e-20 kg
Escaped Outlet	4.5e-20 kg
Min time in the domain	2.30e-01 sec
Max time in the domain	4.64 sec

5.4.2 Heat sink side by side v/s in-line

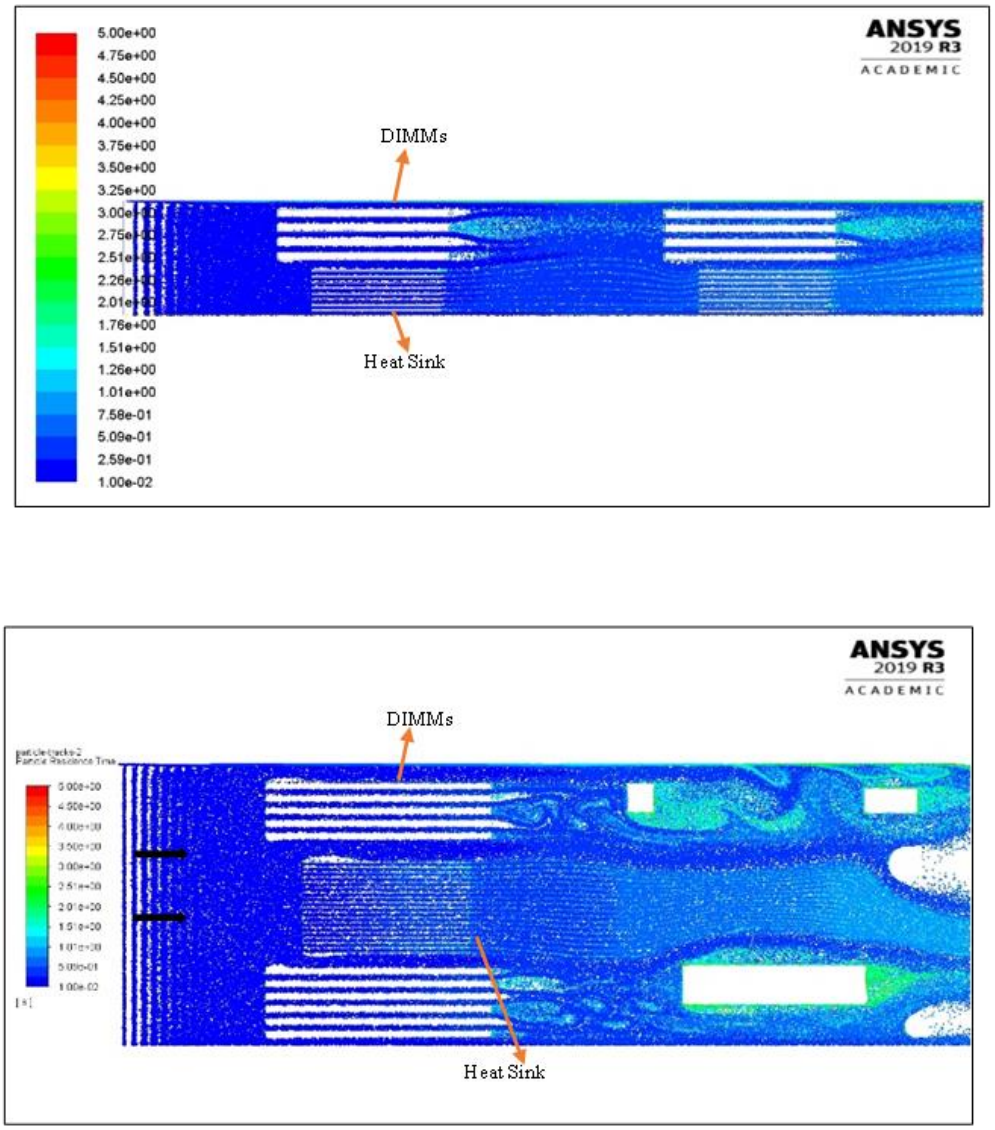

Figure 5-6: Particle residence time in the flow domain for (top) in-line heat sinks (bottom) side by side heat sinks

As seen in Figures 5-6, high particle residence time was obtained at the walls of in-line heat sinks towards the rear end of the server. Other locations of relatively higher residence time were between the heat sink and the DIMMs. Another inference that can be made from Figure 28 (b) is that solid obstructions behind the heat sinks with greater depth do not create large turbulent eddies or any vortex shedding when compared to square or circular obstructions. It can thus be pointed out that there might be a greater probability of finding settled particulate

matter towards the rear end of the servers of similar geometries. These regions mostly contain drive backplanes, power supplies, drive fillers, etc. Table 19 shows the comparison particle summary for both the cases discussed in this section. Here, it can be noted that for both cases, the maximum time spent by the particles in the flow domain was identical, but the average time was more in the case of heat sinks located side by side.

Table 19: Particle summary for heat sinks arranged side by side high density and inline

Inline Heat Sinks	
Parameter	**Value**
Total mass injected	5e-16 kg
Escaped Outlet	4.3e-16 kg
Min time in the domain	3.9e-01 sec
Max time in the domain	4.9 sec
Side by Side Heat Sinks	
Parameter	**Value**
Total mass injected	5e-16 kg
Escaped Outlet	4.2e-16 kg
Min time in the domain	4.1e-01 sec
Max time in the domain	4.9 sec

5.4.3 Effect of Velocity

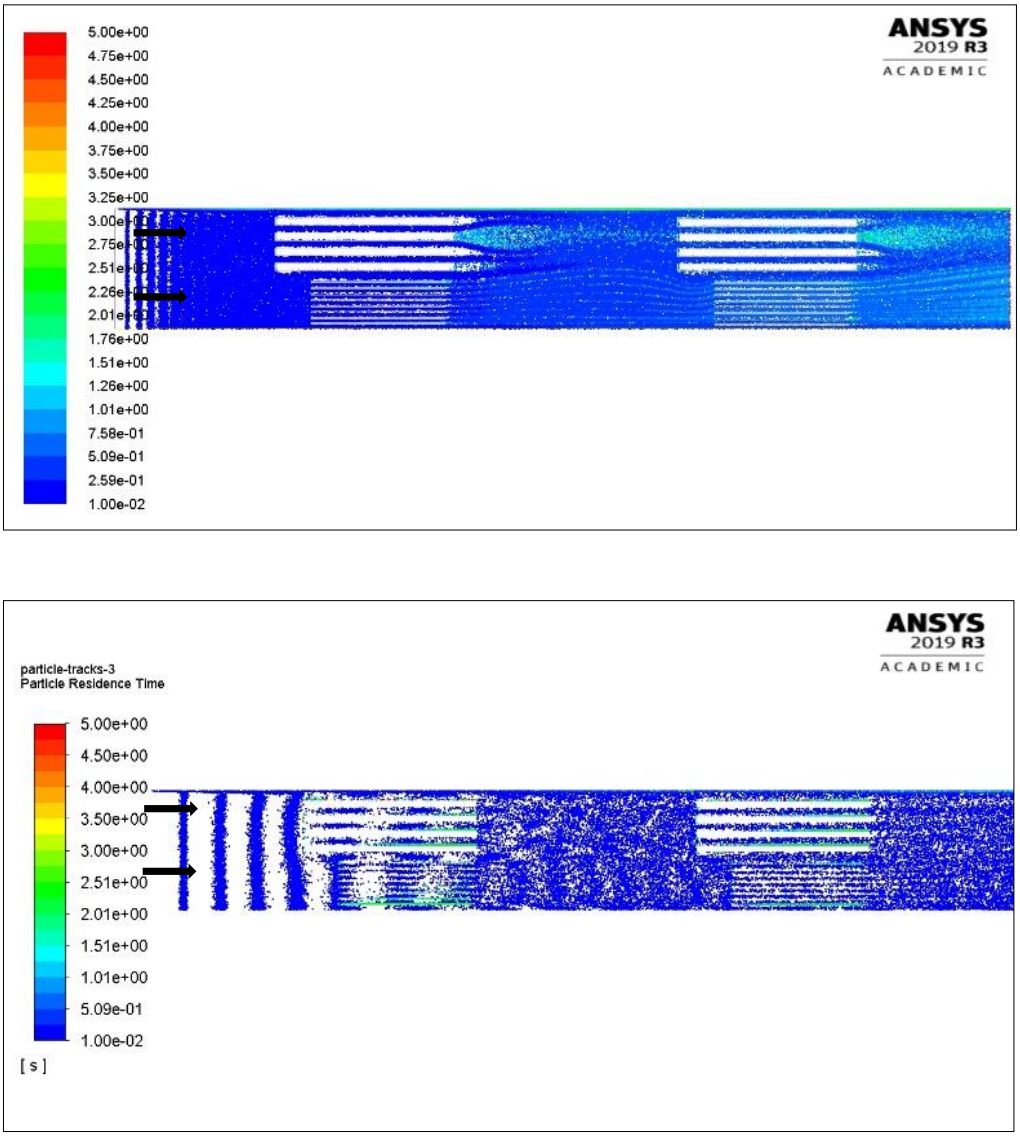

Figure 5-7: Particle residence time in the flow domain for in-line heat sinks (top) low velocity (bottom) high velocity

Figure 5-7 shows the impact of increasing inlet velocity on particle accumulation, two different values of velocities were chosen from published literature [20]. The particle residence time plots depict that for lower velocity values, particles spend more time in the flow domain and for high velocity, particles spend more time on the surfaces. This phenomenon holds when compared to the conclusions made by Frankenthal et al [21]. No deposition on the top or bottom wall for high velocity was observed until the flow reaches the second set of DIMMs. The

comparison of residence time and mass transfer through the outlet in both cases is shown in Table 20.

Table 20: Particle transfer summary for low and high-velocity particles

Low Velocity	
Parameter	**Value**
Total mass injected	5e-16 kg
Escaped Outlet	4.2e-16 kg
Min time in the domain	3.8e-01 sec
Max time in the domain	4.5 sec
High Velocity	
Total mass injected	5e-16 kg
Escaped Outlet	4.8e-16 kg
Min time in the domain	1.4e-01 sec
Max time in the domain	4.6 sec

5.4.4 Effect of heat sink cutouts

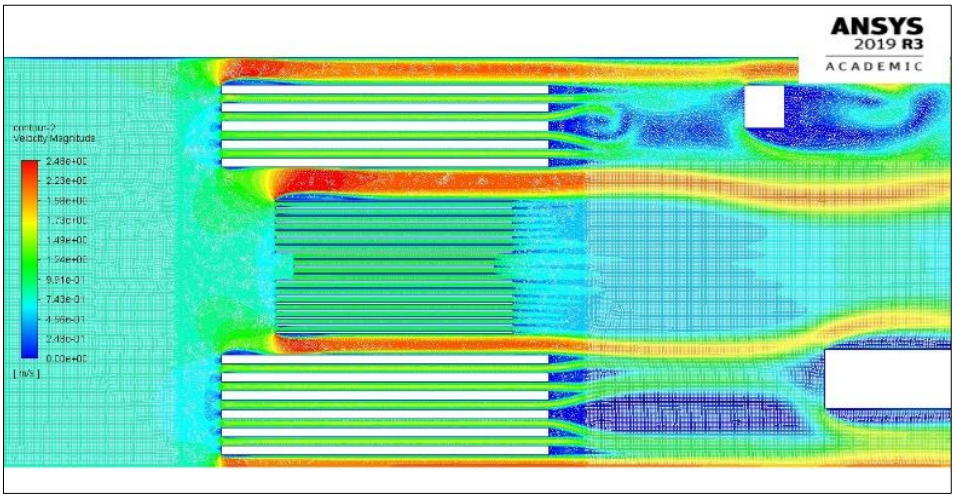

Figure 5-8: Velocity profile of airflow inside the server with a center cut-out in the heat-sink

Cutouts can be provided on narrow as well as high form factor heat sinks to reduce system pressure drops. To observe the effect of change of geometry within the heat sink, a heat sink cutout was provided at the center of the sink as shown in Figure 5-8. As can be seen in Table 5, the heat sink cutout caused a reduction in total mass escaping the outlet meaning more particles are trapped within the flow domain. Although the total reduction might seem a very small number, this can be significantly higher over hours of operation. This increase in particle count within the flow domain might be due to a reduction in total static pressure value around the fins which might cause a local deposition of particles in the surrounding region. This was also observed in particle residence time plots.

Table 21: Particle summary for heat sink cutout case

With cutout	
Parameter	**Value**
Total mass injected	5e-16 kg
Escaped Outlet	4.2e-16 kg
Min time in the domain	4.1e-01 sec
Max time in the domain	4.9 sec
Without cutout	
Total mass injected	5e-16 kg
Escaped Outlet	4.4e-16 kg
Min time in the domain	4.1e-01 sec
Max time in the domain	4.98 sec

5.5 Results for 3-D simulations

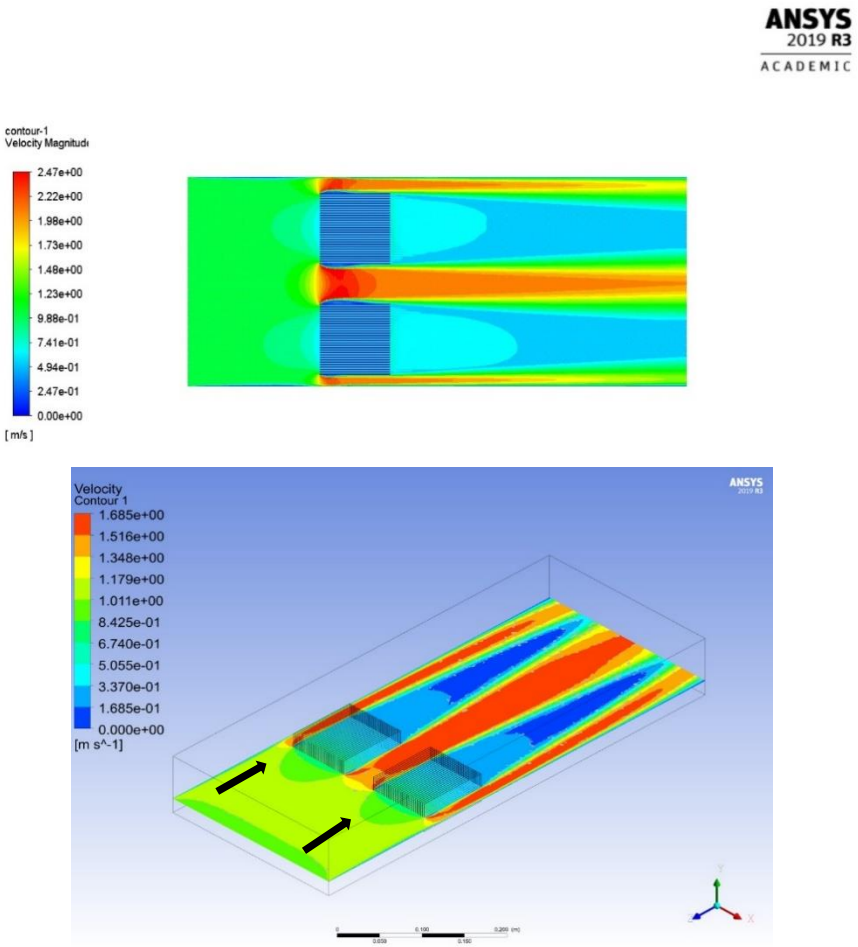

Figure 5-9: Comparison of velocity magnitude values obtained from (a) 2-D and (b) 3-D simulations

To comprehend the error in values obtained using 2-D geometries for simplification instead of 3-D geometries, the percentage variation in velocity and a visual comparison of the particle flow pattern were carried out. Figure 5-9 shows the velocity contours of 2-D and 3-D models of a server same geometric parameters. It can be seen that the airflow patterns in both cases are near similar, which is important from a particle dispersion point of view. The maximum velocity magnitude in the 2-D case was 2.47 m/s and 1.69 m/s for the 3-D model case. This means that the 2-D simulations show approximately a 30% increase value of velocity values. Observing the particle tracks in Figure 5-10, it was seen that the regions of maximum particle concentration were found in the trailing region behind both the heat sinks for both 2-D and 3-D modeling cases. This implies that while the simplification of using 2-D models

might not be accurate, it can aid in visualizing particle tracks with reduced computation time and resources.

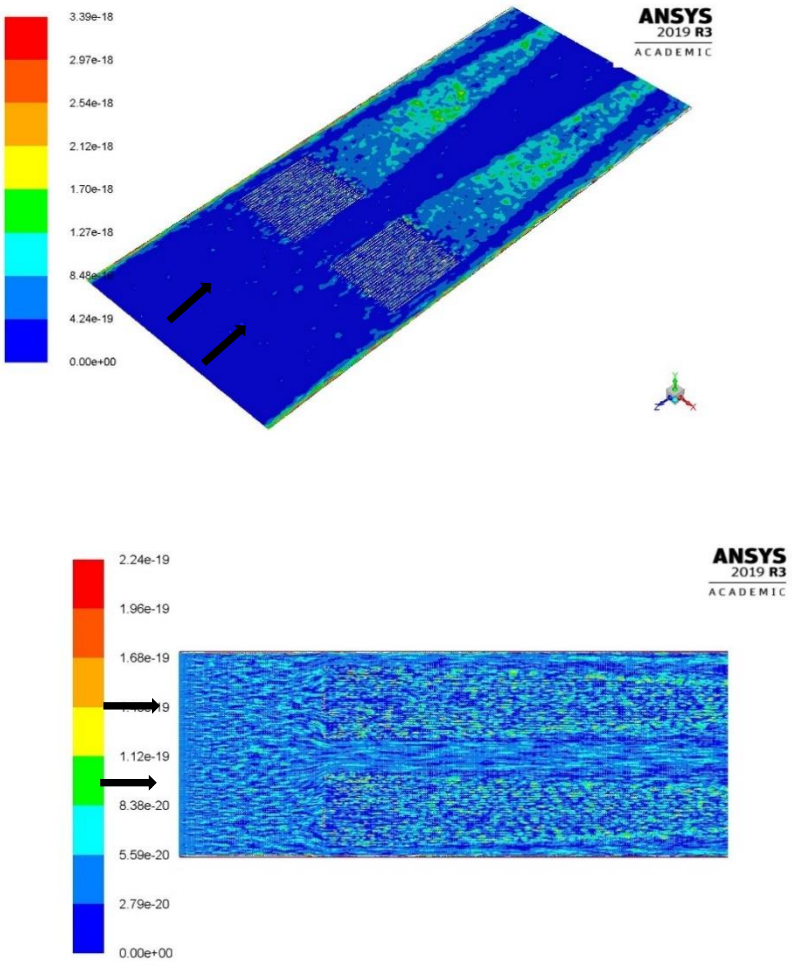

Figure 5-10: Comparison of the particle flow path for (top) 3-D simulation and (bottom) 2-D simulation cas

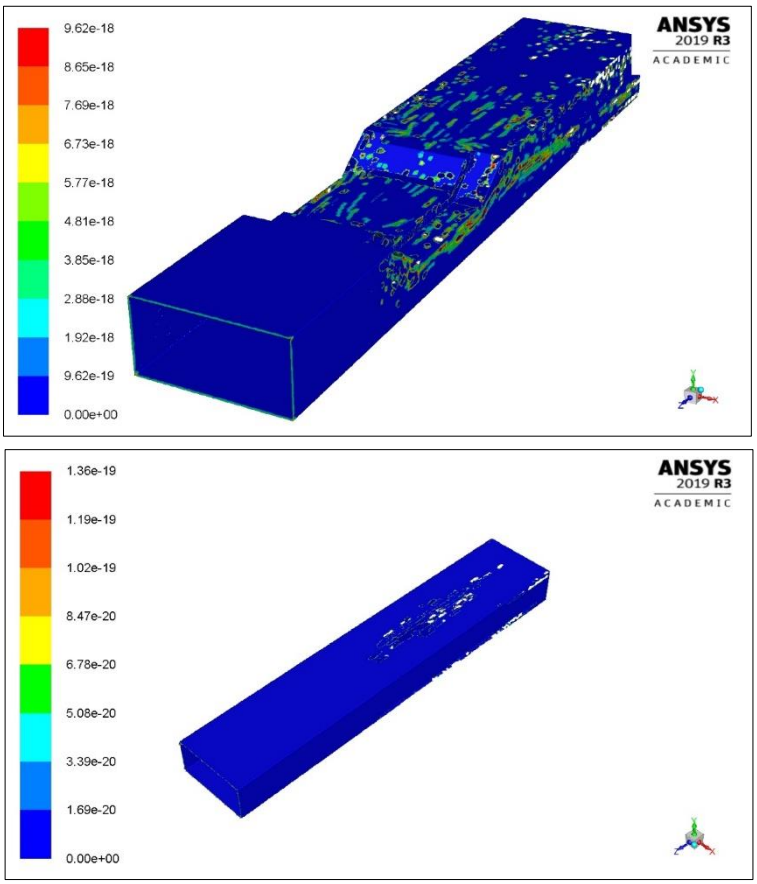

Figure 5-11: Results for particle concentration inside the server with and without flow hood

Figure 5-11 shows the impact of server flow hood on particle dispersion within the server. Flow hoods and baffles are used in servers to force the airflow through the heat sinks for maximum heat transfer and reduce the thermal shadowing effect between two heat sinks place inline. It was seen from simulations that in presence of flow hood the particle-laden airflow disperses more as the flow cannot pass through the path of least resistance. This leads to higher particle concentration around the flow hood walls and chassis frame around the flow hood. These findings are consistent with a previous experimental investigation done by Shah et al as shown in Figure 5-12 [22].

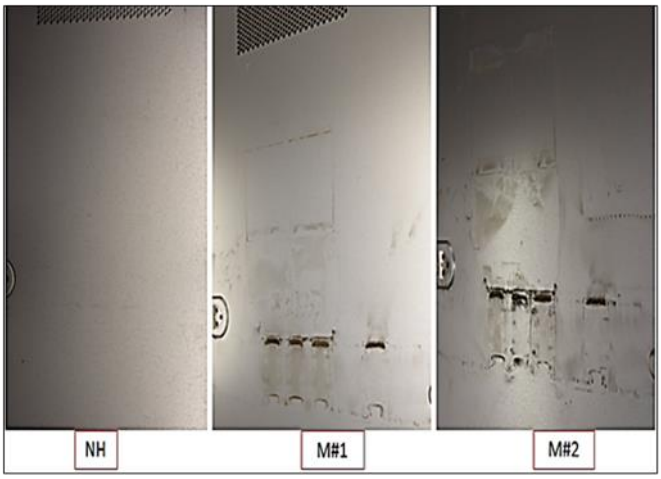

Figure 5-12: A comparison of dust deposition on the server chassis cover in (left) a clean laboratory data center (middle and right) in a modular data center located in polluted geography using an Indirect/Direct Airside economization unit [47]

As explained in section 4.1.1, a trade-off exists between using a curved edge heat sink which offers lower pressure drop and lower particle accumulation within the system. However, the thermal benefit of heat sinks with curved edges reduces due to a reduction of the total surface area of the fins, reducing its transfer capabilities as shown in Figure 5-13. To reduce particle concentration within the ITE room, similar tradeoffs should be quantified for the type or rating of the MERV filter to be used. Higher arresting efficiency MERV filters will lead to a higher pressure drop or power consumption penalty but can also enhance the equipment's reliability. This should be done by correlating the typical annual particle concentrations. Data centers in the coastal regions may experience higher sea salt concentrations. Therefore, air filtration strategies should be implemented based on a thorough knowledge of outdoor air quality in terms of both the size and chemical composition of particles.

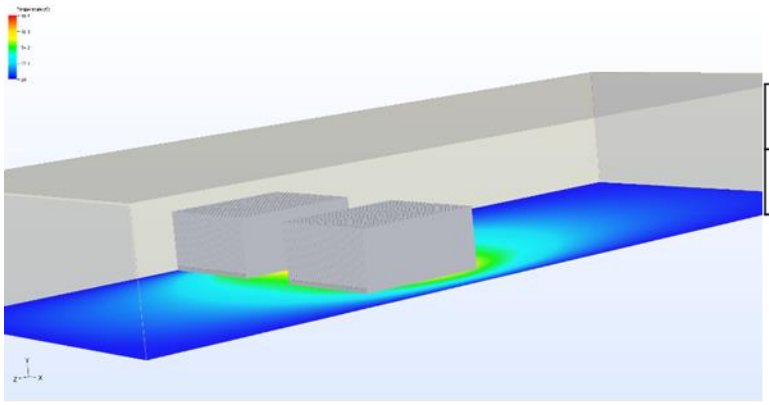

Max Temperature	Mean Temperature
38.2°C	25.2°C

Pressure Drop
2.03 kPa

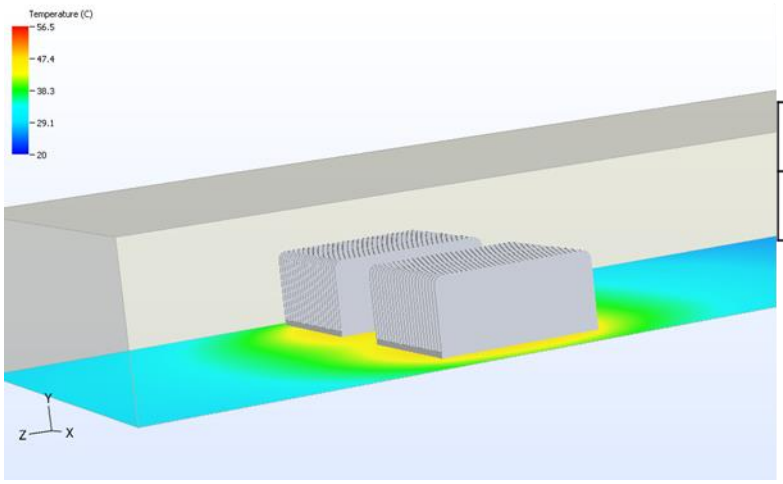

Max Temperature	Mean Temperature
47.3°C	33.2°C

Pressure Drop
1.9 kPa

Figure 5-13: Temperature contours showing thermal performance of (a) traditional heat sink (b) heat sink with curved edges for pressure drop reduction

5.6 Results for Room Level Particle Flow

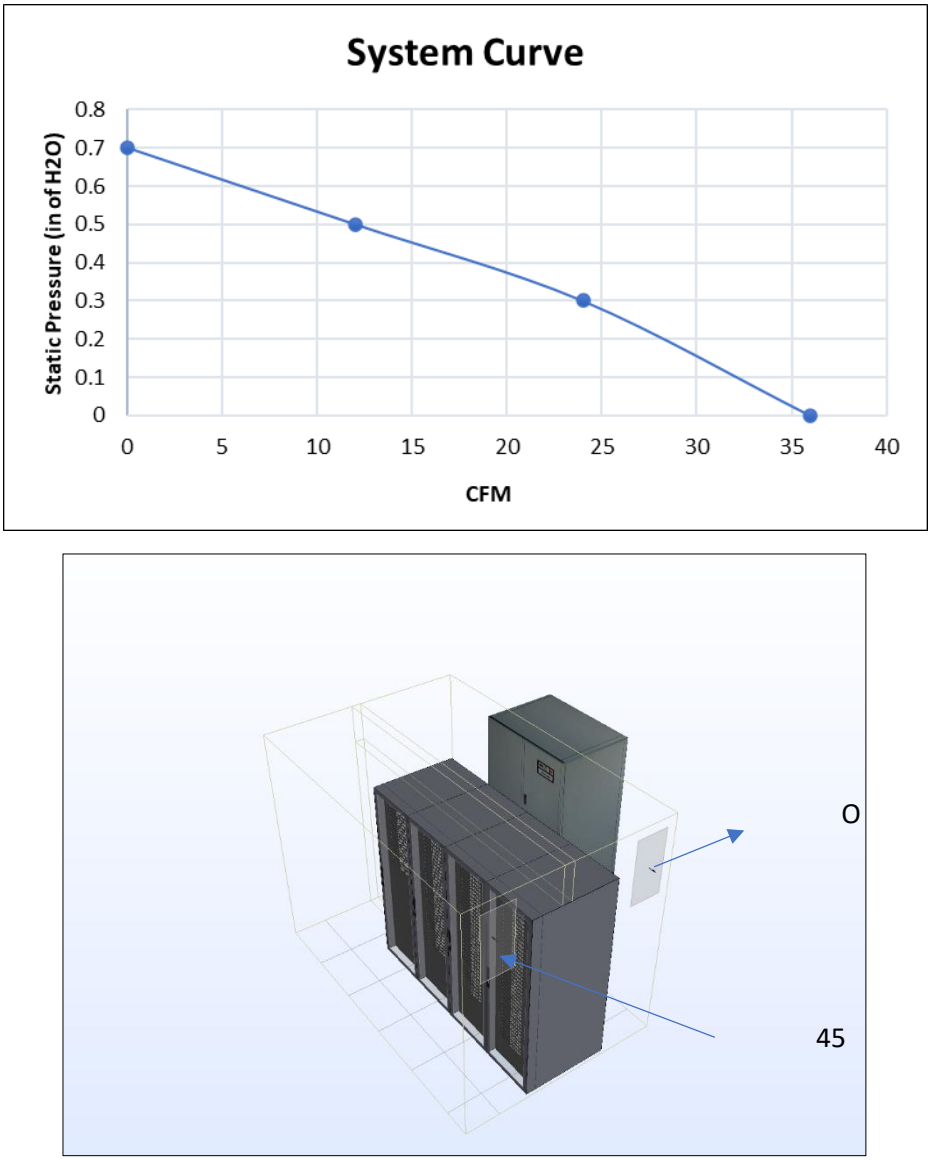

Figure 5-14: (a) Plot for system curve used in 6SigmaRoom for the servers (b) isometric view of the modular data center used in the study

For room-level simulations, a CFD model of a current research modular data center was used as a simulation case. This modular unit uses a direct/indirect airside economizer for cooling. As seen in Figure 5-14, a detailed model of the data center was first designed in 6Sigma Room, a commercially available data center design software. Server pressure drop characteristics were used as input conditions for the ITE populated in the racks. An array of sensors was placed in the simulation case to monitor the pressure drop across the rack for the given inlet cfm to the ITE space inside the IT pod. Based on this simulation, the pressure drop

for the entire rack was obtained, which was then used as a criterion for determining the viscous and inertial resistance coefficients for the rack for a simplified CFD modeling case in ANSYS FLUENT.

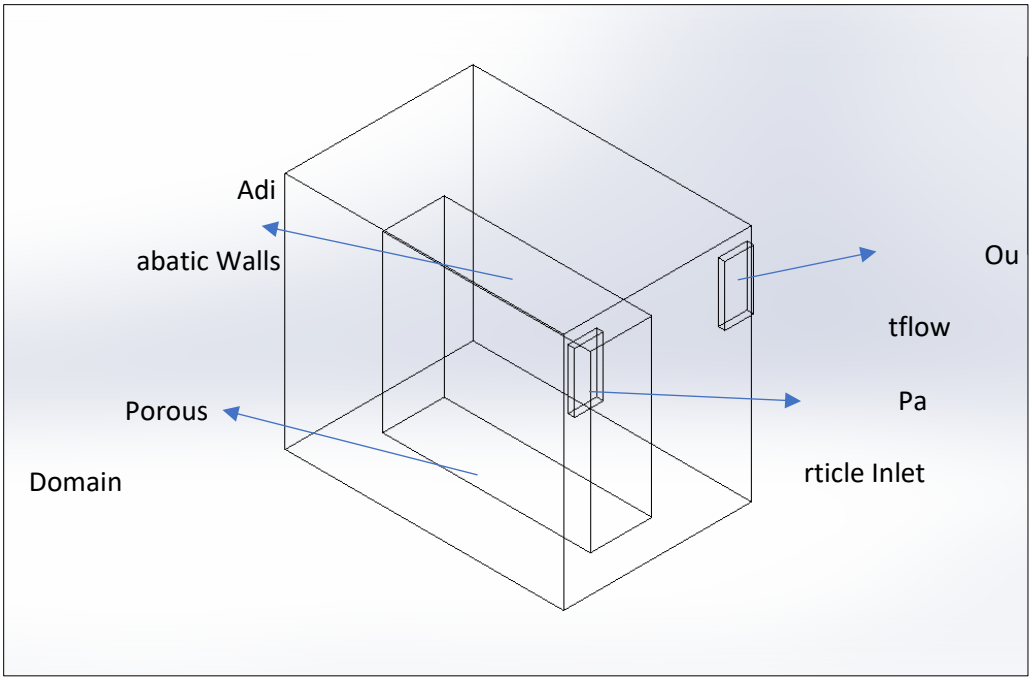

Figure 5-15: An overview of the boundary conditions used for particle flow pattern analysis at room level

As shown in Figure 5-15, the first case for room level simulations was carried out with a rack as sold obstruction with a hot aisle partition. Using a similar CFD model setup as in ITE simulations in section 3, the simulation results showed that the particles entering from the IT pod inlet, re-circulate and stagnate primarily around the rack frames. The transient simulation results, as shown in Figure 5-16 that the entire particle mass entering moves along with the airflow and moves toward the farther end of the pod. After striking this end, the particle mass circulates and reaches the bottom of the rack frames, rather than moving towards the outlet/hot-aisle side. A summary of particle flow data at room level is presented in Table 22.

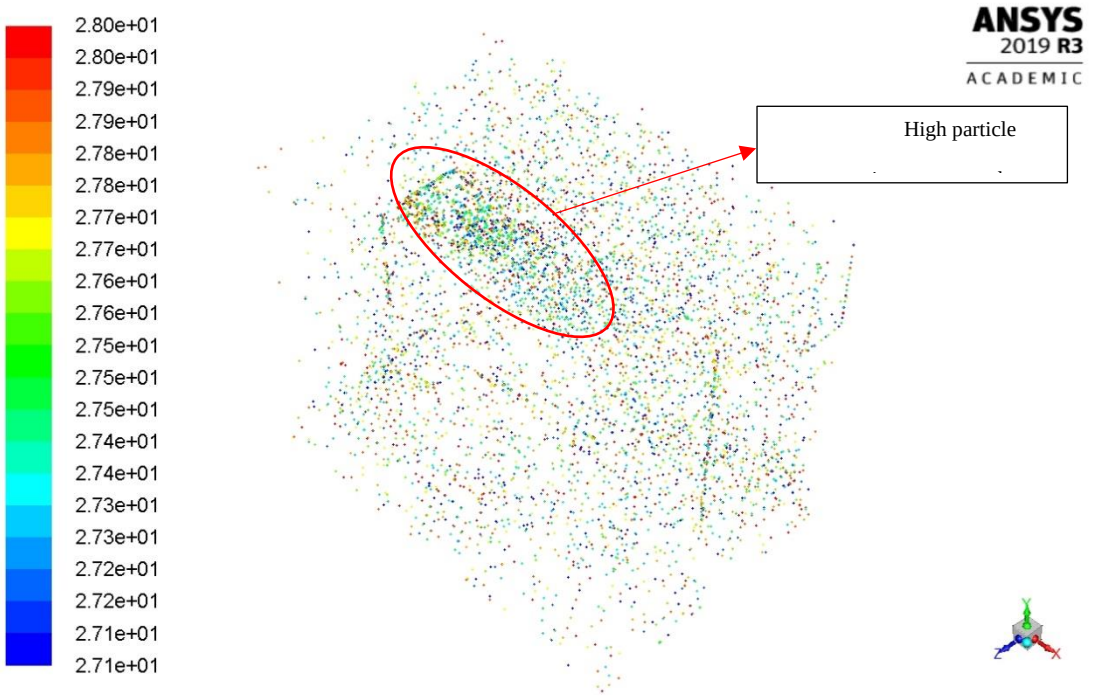

Figure 5-16: Distribution of particles inside the IT pod showing particle accumulation on top of the ITE rack

Table 22: Particle summary for room level simulation

Parameter	Value
Minimum Elapsed time	5.776 sec
Total Mass	2.8e-15 kg
Escaped outlet	6.121e-16 kg

5.7 Conclusion

This research presented a methodology for the assessment of particulate flow inside data center hardware and at room-level using simplified CFD models. Predictions for particle accumulation were made based on analysis of total elapsed time that the particles spend before escaping from the flow domain and by analyzing the difference of mass transferred between inlet and outlet of the flow domains. Based on the nature of flow obstructions present within the server, it was observed that while there might be little accumulation near thin features like DIMMS and heat sinks, the presence of other components and smaller features can significantly increase it. Also, features with aspect ratios of any dimension closer to 1 may have significant particle accumulation around them. On the contrary, features with larger lengths

offer significantly less flow resistance and may be less vulnerable to deposition. Critical components, as per failure rates are concerned, are usually hard drives. Most of the storage servers today have separate hard drive bays. The servers where the hard drives are located towards the rear end might be more prone to exposure to particulates. It was also seen that higher velocities tend to increase accumulation on flat surfaces like fins and the DIMMs, therefore, for computational servers that are air-cooled, they might experience increased exposure to particles when the data center is operating in free air-cooling mode.

Further simplifications can be added to the modeling to reduce simulation time and resources. Based on accurate system pressure drop curves of real servers, multi-phase simulations can be carried to represent the particle concentration distribution with the server as well as data center space. While there are methods and techniques to experimentally characterize the particulate contamination severity in the field environment [23-25], simple design and modeling-based CFD methods can be integrated with the data center HVAC design process to ascertain the contaminant flow path in data centers using airside economization. This will help in identifying the locations inside the data center that can be critical in terms of contaminant concentrations and can help in mitigating the exposure of airborne contaminants to the ITE. Similar simulations for large-scale data centers need to be performed to formulate best practices for airside economized data centers.

REFERENCES

[1] Niazmand, A, Chauhan, T, Saini, S, Shahi, P, Bansode, PV, & Agonafer, D., 2020, "CFD Simulation of Two-Phase Immersion Cooling Using FC-72 Dielectric Fluid," Proceedings of the ASME 2020 International Technical Conference and Exhibition on Packaging and Integration of Electronic and Photonic Microsystems. ASME 2020 International Technical Conference and Exhibition on Packaging and Integration of Electronic and Photonic Microsystems. Virtual, Online. October 27–29, 2020. V001T07A009. ASME. https://doi.org/10.1115/IPACK2020-2595

[2] Niazmand, A., Murthy, P., Saini, S., Shahi, P., Bansode, P., & Agonafer, D., 2020, "Numerical Analysis of Oil Immersion Cooling of a Server Using Mineral Oil and Al2O3 Nanofluid," Proceedings of the ASME 2020 International Technical Conference and Exhibition on Packaging and Integration of Electronic and Photonic Microsystems. ASME 2020 International Technical Conference and Exhibition on Packaging and Integration of Electronic and Photonic Microsystems. Virtual, Online. October 27–29, 2020. V001T08A009. ASME. https://doi.org/10.1115/IPACK2020-2662

[3] Shah, J.M., Rizvi, S.H.I., Kota, I.S., Nagilla, S.R., Thakkar, D., & Agonafer, D., 2016, "Design Considerations Relating to Non-Thermal Aspects of Oil Immersion Cooling." *Proceedings of the ASME 2016 International Mechanical Engineering Congress and Exposition. Volume 10: Micro- and Nano-Systems Engineering and Packaging*. Phoenix, Arizona, USA. November 11–17, 2016. V010T13A054. ASME. https://doi.org/10.1115/IMECE2016-67320

[4] Shahi, P., Saini, S., Bansode, P., and Agonafer, D., 2021 "A Comparative Study of Energy Savings in a Liquid-Cooled Server by Dynamic Control of Coolant Flow Rate at Server Level,"

in IEEE Transactions on Components, Packaging and Manufacturing Technology, doi: https://doi.org/10.1109/TCPMT.2021.3067045

[5] Shahi, P., Deshmukh, A., Hurnekar, H., Saini, S., Bansode, P. V., Kasukurthy, R., and Agonafer, D., 2021, "Design, Development, and Characterization of a Flow Control Device for Dynamic Cooling of Liquid-Cooled Servers." ASME. J. Electron. Packag. doi: https://doi.org/10.1115/1.4052324

[6] ASRAE, 2015, "Thermal Guidelines for Data Processing Environments," ASHRAE Datacom Series, 3rd Edition, Atlanta, GA, USA

[7] Open Compute Project, "Cooling an OCP Data Center in a Hot and Humid Climate" Accessed January 20th, 2021, https://www.opencompute.org/blog/cooling-an-ocp-data-center-in-a-hot-and-humid-climate

[8] Google, "Efficiency," accessed January 2021, https://www.google.com/about/datacenters/efficiency/

[9] "Microsoft Shares Video Tour of its Cloud Datacenters," accessed January 2021, https://blog.insideo365.com/2011/07/microsoft-shares-video-tour-of-its-cloud-datacenters/

[10] ASHRAE Technical Committee 9.9. 2011. "2011 Particulate and Gaseous Contamination Guidelines for Data Centers," ASHRAE Inc., Atlanta, GA

[11] Shah, J.M., Anand, R., Saini, S., Cyriac, R., Agonafer, D., Singh, P., & Kaler, M., "Development of a Technique to Measure Deliquescent Relative Humidity of Particulate Contaminants and Determination of the Operating Relative Humidity of a Data Center," *Proceedings of the ASME 2019 International Technical Conference and Exhibition on Packaging and Integration of Electronic and Photonic Microsystems*. *ASME 2019 International Technical Conference and Exhibition on Packaging and Integration of Electronic*

and Photonic Microsystems. Anaheim, California, USA. October 7–9, 2019. V001T02A016. ASME. https://doi.org/10.1115/IPACK2019-6601

[12] Thirunavakkarasu, G., Saini, S., Shah, J.M., & Agonafer, D., 2018, "Air Flow Pattern and Path Flow Simulation of Airborne Particulate Contaminants in a High-Density Data Center Utilizing Airside Economization," Proceedings of the ASME 2018 International Technical Conference and Exhibition on Packaging and Integration of Electronic and Photonic Microsystems. ASME 2018 International Technical Conference and Exhibition on Packaging and Integration of Electronic and Photonic Microsystems. San Francisco, California, USA. August 27–30, 2018. V001T02A011. ASME. https://doi.org/10.1115/IPACK2018-8436

[13] Seymour, M.J., A. A. M. A., and Jiang, J., 2000, "Cfd based airflow modelling to investigate the effectiveness of control methods intended to prevent the transmission of airborne organisms". Air Distribution in Rooms, (ROOMVENT 2000).

[14] Jones, P.J., and Whittle, G.E, 1992, "Computational fluid dynamics for building air flow prediction- current status and capabilities," Building and Environment, 27(3), pp. 321–338, https://doi.org/10.1016/0360-1323(92)90033-L

[15] Chen, Q., and Zhang, Z., 2005, "Prediction of particle transport in enclosed environment," China Particuology, 3(6), pp. 364–372, https://doi.org/10.1016/S1672-2515(07)60216-4

[16] Saini, S., Shahi, P., Bansode, P., Siddarth, A., and Agonafer, D., "CFD Investigation of Dispersion of Airborne Particulate Contaminants in a Raised Floor Data Center," *2020 36th Semiconductor Thermal Measurement, Modeling & Management Symposium (SEMI-THERM)*, San Jose, CA, USA, 2020, pp. 39-47, doi: https://doi.org/10.23919/SEMI-THERM50369.2020.9142865

[17] *ANSYS® ANSYS FLUENT Theory Guide, Chapter 16, Release 2019 R3*

[18] *ANSYS® ANSYS FLUENT User's Guide, Chapter24, Release 2019 R3*

[19] Ibrahim, M., Shrivastava, S., Sammakia, B., Ghose, K., 2012, "Thermal mass characterization of a server at different fan speeds." 13th InterSociety Conference on Thermal and Thermomechanical Phenomena in Electronic Systems, 2012, pp. 457-465, doi: 10.1109/ITHERM.2012.6231467.

[20] Lu, H., Wang, Y., 2019, "Particle deposition in ventilation ducts: A review," Building Simulation, 12, pp. 723–734 https://doi.org/10.1007/s12273-019-0522-8

[21] Frankenthal, R. P., Siconolfi, D. J., and Sinclair, J. D., 1993, "Accelerated Life Testing of Electronic Devices by Atmospheric Particles: Why and How," Journal of The Electrochemical Society, 140(11), pp. 3129-3134, https://doi.org/10.1149/1.2220997

[22] Shah, J. M., Awe, O., Gebrehiwot, B., Agonafer, D., Singh, P., Kannan, N., and Kaler, M., 2017, "Qualitative Study of Cumulative Corrosion Damage of Information Technology Equipment in a Data Center Utilizing Air-Side Economizer Operating in Recommended and Expanded ASHRAE Envelope." ASME. J. Electron. Packag., 139(2): 020903. https://doi.org/10.1115/1.4036363

[23] Shah, J.M., Anand, R., Saini, S., Cyriac, R., Agonafer, D., Singh, P., & Kaler, M., 2019, "Development of a Technique to Measure Deliquescent Relative Humidity of Particulate Contaminants and Determination of the Operating Relative Humidity of a Data Center," *Proceedings of the ASME 2019 International Technical Conference and Exhibition on Packaging and Integration of Electronic and Photonic Microsystems*. *ASME 2019 International Technical Conference and Exhibition on Packaging and Integration of Electronic and Photonic Microsystems*. Anaheim, California, USA. October 7–9, 2019. V001T02A016. ASME. https://doi.org/10.1115/IPACK2019-6601

[24] Shah, J. M., Anand, R., Singh, P., Saini, S., Cyriac, R., Agonafer, D., and Kaler, M. 2020, "Development of a Precise and Cost-Effective Technique to Measure Deliquescent Relative Humidity of Particulate Contaminants and Determination of the Operating Relative Humidity of a Data Center Utilizing Airside Economization." ASME. *J. Electron. Packag*. December 2020; 142(4): 041103. https://doi.org/10.1115/1.4047469

[25] Saini, S., Shah, J. M., Shahi, P., Bansode, P., Agonafer, D., Singh, P., Schmidt, R., and Kaler, M., 2021, "Effects of Gaseous and Particulate Contaminants on Information Technology Equipment Reliability—A Review," ASME. J. Electron. Packag., 144(3): 030801. https://doi.org/10.1115/1.4051255

[26] Saini, S., Shahi, P., Bansode, P., Shah, J. M., and Agonafer, D., 2022, "Simplified and Detailed Analysis of Data Center Particulate Contamination at Server and Room Level Using Computational Fluid Dynamics." ASME. *J. Electron. Packag*. June 2022; 144(2): 024501. https://doi.org/10.1115/1.4053363

Chapter 6 A Numerical Study on Multi-objective Design Optimization of Heatsinks for Forced and Natural Convection Cooling of Immersion Cooled Servers

6.1 Introduction

Data centers have quickly become the backbone of any modern economy with the emergence of technologies like cloud computing, online media, and social networking, ArtiFicial Intelligence (AI), and Machine Learning. Active internet user statistics suggest that at any given time, around 5 billion users are active on the internet which sheds ample light on the reliance on network servers and data centers [1]. Data center energy trends, while have slowed down due to efficient IT equipment [2], continue to rise every year. It is however uncertain if the cooling and energy efficiency enhancements can continue to offset the rapid growth in computing workloads [3]. Power densities in typical data centers maybe 15-100 times greater than generic commercial buildings [4]. The growth in this demand has also environmental implications like an increase in greenhouse emissions and excessive water usage, both direct and indirect [5].

In the last decade, as the energy demands and processor power densities increased due to higher processing demands, traditional air cooling methods have been limited to cooling processors with lower Thermal Design Power (TDP) limits. With rising energy consumption and increasing complexity in thermal management, researchers have proposed various strategies to enhance thermal performance [6,7], increase power savings using different operation strategies of current cooling techniques [8,9], or use liquid-based cooling technologies [10, 11]. Among the popular liquid-cooling technologies, Single-Phase

Immersion Cooling stands out owing to its ease of deployment, low costs of dielectric fluids, and low-complexity cooling infrastructure [12]. Many of the present proprietary cooling solutions have established the efficacy of single-phase immersion cooling in terms of low Power Usage Effectiveness [13] values and enhanced reliability of server components [14]. A key direct advantage of complete submersion of servers in dielectric fluids is that it disconnects the server components from the harsh environment such as gaseous contaminants, reduces failures due to fan vibrations, and removes the necessity of cooling peripheral components as hot components are in direct contact with the coolant. Immersion cooling offers significant advantages as compared to air-cooling but requires careful thermal and non-thermal design considerations for air-cooled hardware. As an example, when immersing air-cooled hardware, fans should be removed from the server, hard drives need to be sealed, material compatibility issues should be addressed and the heat sink design should be optimized, which is the objective of this study.

To achieve consistently reliable and peak performance from Central Processing Unit (CPU) or (Graphics Processing Unit) GPU in immersion cooling, an optimized heat sink needs to be utilized, rather than using an air-cooled heat sink. Design optimizations for parallel plate-fin heat sinks have been widely studied including optimization of geometric properties [15, 16] and also from a single or multi-objective optimization point of view [17, 18]. Optimum geometric parameters such as fin spacing, fin thickness, base thickness, and fin count play an important role in maximizing the thermal performance of the heat sink as well as the processors. Current literature shows an increasing number of studies related to the optimization of heat sink solutions for both air and liquid-cooled systems using various CFD-based and analytical methods.

Chen and Chen used a multi-objective and novel direction-based algorithm to optimize plate-fin heat sinks integrated with an impingement fan using a commercially available

Multiphysics tool [19]. The optimized parallel plate heat sink showed both superior heat transfer performance and reduced weight. Fuzzy logic-based approaches have also been used to quantify the effect of heat sink design parameters on thermal performance [20]. Design parameters of a pin-fin heat sink such as fin spacing, pin-fin diameter, and height were investigated experimentally. Analysis of Variance (ANOVA) was then used to explore the effect of these design parameters on heat sink characteristics like thermal resistance, pressure drop, and average heat transfer coefficient. Response Surface Method (RSM) was used by Chaing and Chang [21] used to obtain optimum design parameters for pin-fin heat sinks to achieve higher thermal performance. Minimizing entropy generation rate as an objective function was done by Chen et al. [22]. They optimized a plate-fin heat sink for a CPU using a coded genetic algorithm for obtaining optimum design parameters for the heat sink. In terms of objective functions, Devi et al. [23] used a Taguchi-based non-gradient method for minimizing three objective functions namely, radiation emission, thermal resistance, and heat sink mass.

However, these studies are very generic in terms of the application of the heat sinks and it is to the best of the authors' knowledge, no study in the literature discusses the heat sink optimization specific to immersion-cooled servers for both natural and forced convection cooling. The main purpose of this investigation is to dive deep into different design parameters and objective functions combinations for optimizing a parallel plate-fin heat sink of an air-cooled Open Compute server that is used for immersion cooling. A CFD model of the server was developed using ANSYS Icepak and was validated against the experimental data in a previously published work for thermal performance. Baseline CFD simulations were first done using the air-cooled heat sink in the dielectric fluid, EC-100 [24], for both natural and forced convection cooling modes. The heat sink material was also varied from aluminum to copper in the baseline simulations for both the cooling modes. OptiSLang, a dedicated design

optimization and analysis tool inside the ANSYS platform was used for heat sink design optimization. Heat sink fin thickness, fin count, fin height, and base thickness were optimized in different combinations at constant pumping power. The objective functions, heat sink pressure drop, and thermal resistance, are defined in Icepak and set to be minimized for an optimized design. A range of values of the heat sink design parameters is defined in Icepak which are exported to OptiSLAng along with the information related to objective functions and design parameters. OptiSLang then creates a Design of Experiment (DOE) based on the input range of the design variables using a full-factorial approach to create multiple design points. These design points are then solved iteratively and the response surfaces, effect plots, and Pareto fronts are generated by OptiSLang based on the results from each of the design points. Analysis of the effect of each of the design variables on the objective functions is done to establish which parameters have a greater impact on the performance of the optimized copper and aluminum heat sinks under natural and forced convection.

6.2 Numerical Modeling Setup

6.2.1 CFD Model Validation

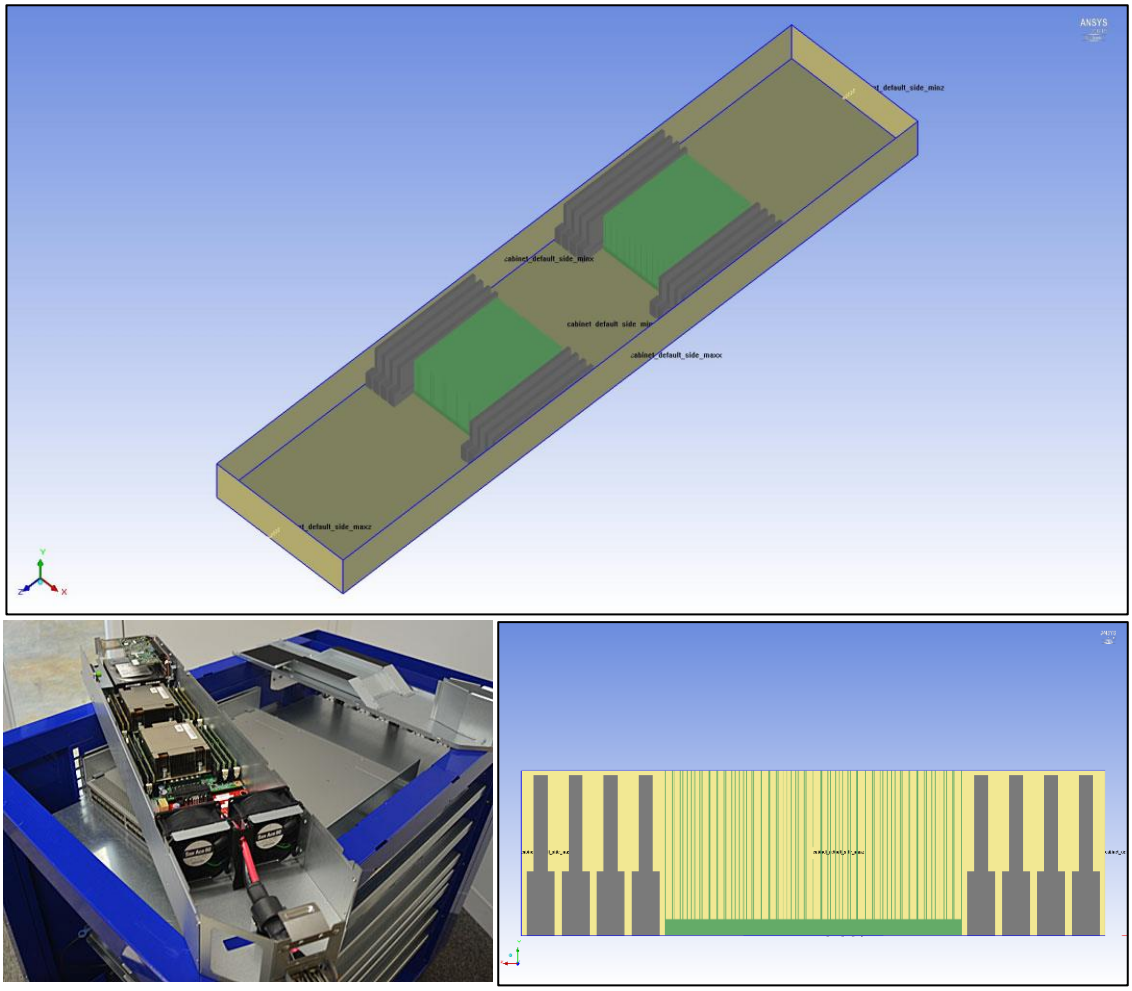

Figure 6-1: Computational model of the server showing the heat sinks and the memory modules and (Bottom Left) air-cooled version of the real server

A computational model of an Open Compute server was designed in ANSYS Icepak by simplifying the server and considering components critical to the heat transfer process like CPU, heat sinks, and Dual In-line Memory Modules (DIMMs) as shown in Figure 6-1. Each CPU unit in the CFD model is designed to dissipate 115W. The thermal stack representing the CPU consists of a 2-D heat source at the bottom of a heat sink with a Thermal Interface Material (TIM) of thickness 0.2 mm with a thermal conductivity value of 3.8 W/mK. The CFD model was first validated against an experimental study done by our research group on the same server [25]. Figure 6-2 shows the difference in the values of the maximum temperature at different

flow rates between the benchmark experimental study and the CFD simulation data. A maximum variation of 2% was observed in the maximum temperature value between the CFD and the experimental study. Some differences seen in the results could be because the heat sinks in the server used during the experiments have embedded heat pipes in them. However, heat pipes were not modeled in the CFD study to keep the heat sink design simpler and accelerate the optimization process.

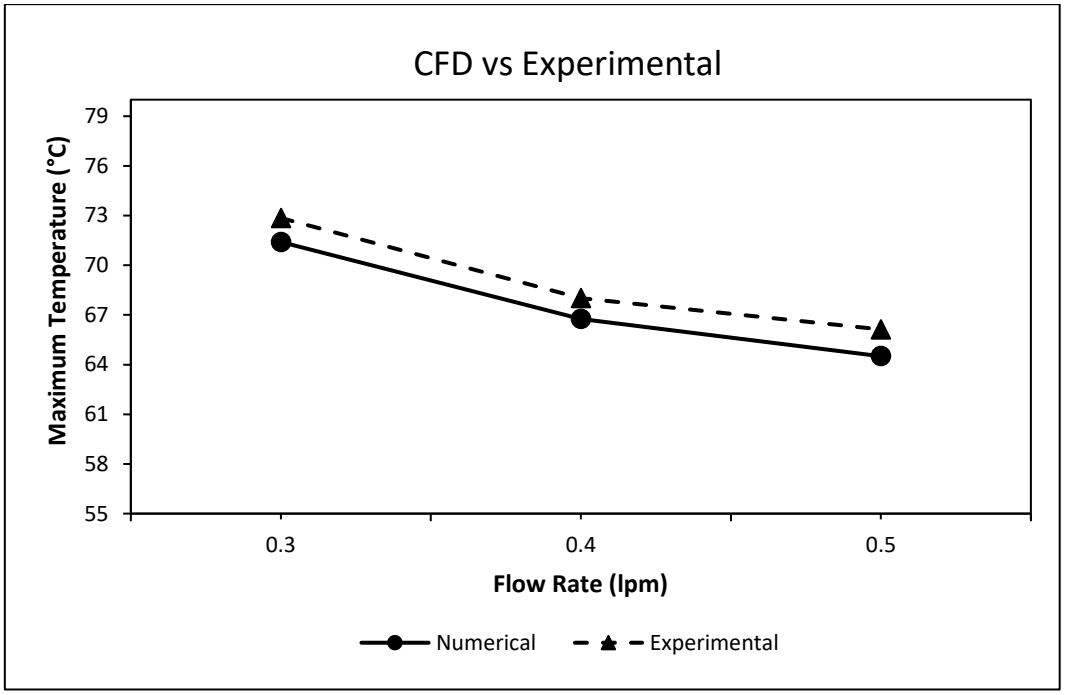

Figure 6-2: A comparison of the average junction temperatures (maximum source temperatures in case of CFD model) between the experimental and simulation data

A grid independence study was also done for the baseline CFD model to determine the validity and precision of the results obtained. A coarse to a fine level meshes were generated by reducing the minimum element size in each of the three directions. ANSYS Icepak, by default, generates a minimum element size of 1/20 of the length in that specific direction. For the grid independence study, this element size was reduced to 1/5 of the length for a coarse mesh. For a refined grid, minimum mesh element sizes of 1/30, 1/40, 1/50, and 1/60 of the length were generated. To verify the grid independence, both pressure drop across the server

and thermal resistance of the heat sink was monitored for different mesh element count as shown in Figure 6-3. It can be seen that both the pressure drop and thermal resistance show a non-varying trend at all the mesh counts. Therefore, the default meshing size of 1/20 was used for the simulations.

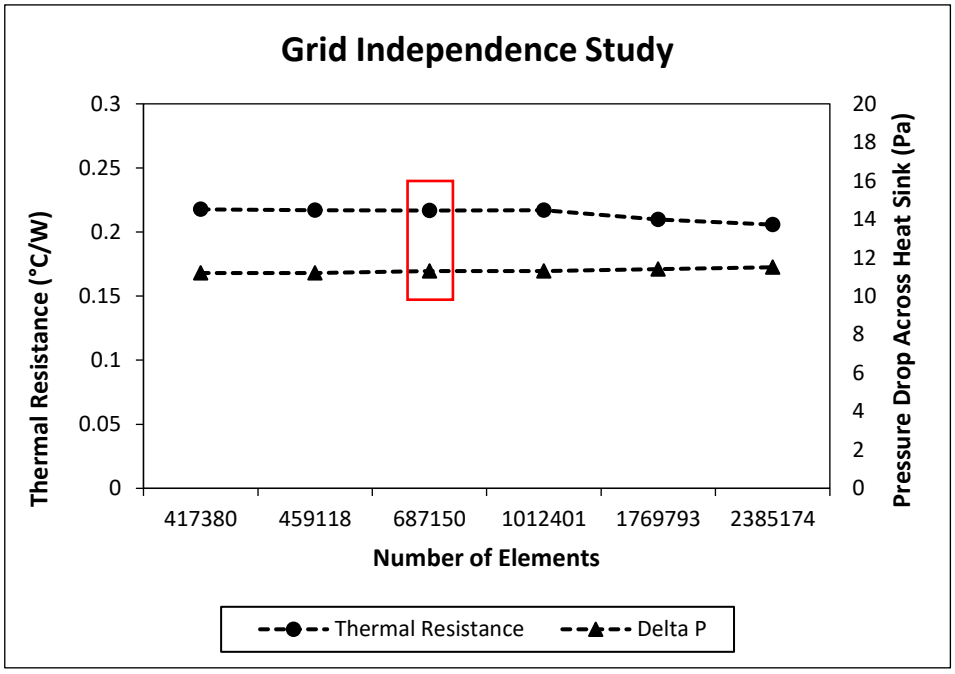

Figure 6-3: Variation of the pressure drop and thermal resistance values with changing mesh element count

6.2.2 optiSLang Setup

OptiSLang is used as the design optimization tool in the present investigation. As a part of ANSYS Workbench, OptiSLang has the advantage that it can be used for direct integration with any of the ANSYS thermal, structure, electrical or fluid tools. The simulation model to be optimized is solved independently in any of the ANSYS tools or modules. Design parameters and their range or bounds for optimization are also defined in the simulation module itself and are then imported to OptiSLang. The software uses a meta-modeling approach for sampling the design space known as the Adaptive Meta-model of Optimal Prognosis (AMOP) which uses a Coefficient of Prognosis (CoP) for quality approximation of the model. It can be mathematically represented as:

$$CoP = 1 - \frac{SS_E^{Prediction}}{SS_T} \qquad (1)$$

Here, SS_T is equivalent to total variation and SS_E represents variation due to regression or sum of squared of prediction errors. The higher the value of CoP the more accurate is model's representation of the data. This reduces the post-processing of the output data from the design exploration space and helps in the direct assessment of the response surface models [26]. Also, typical meta-model approaches provide limited accuracy when the number of input variables starts increasing, thereby, making the design sample space increase exponentially. This can be overcome by using AMOP, which improves the prediction quality of an approximation model by eliminating the design variables that are not important in the model [27]. A summary of the simulation model setup and its integration with the design optimization tool is shown in detail using a schematic in Figure 6-4.

The objective functions and the constraints that control the optimization process can be defined in the simulation module as well as OptiSLang. Once the optimization process is completed, a sensitivity analysis is done to determine the effect of the chosen design variables on the objective functions. As the baseline design in the present investigation is fixed a pre-determined upper bound of the design variables was selected. Using a very large range of design variables also makes it difficult to assess the design exploration space. The optimized design points are visualized on a Pareto front for each of the optimizations run to determine the design points that offer the least thermal resistance and pressure drop.

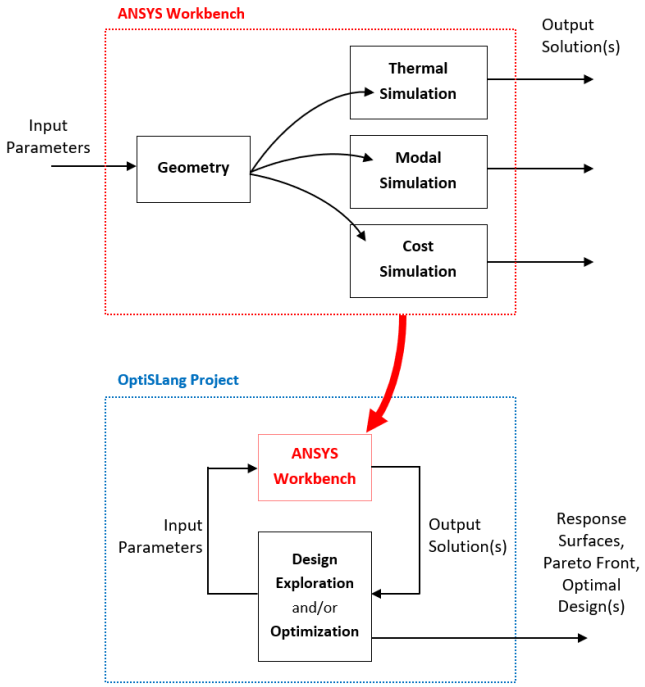

Figure 6-4: Overview of the integration of CFD simulation model setup and optimization setup in OptiSLang [28]

6.3 Methodology

The primary purpose of this study is to investigate various possible design optimization methodologies for heat sinks when transitioning from air-cooling to immersion cooling. In this section, the underlying methodology, assumptions, and different parametric cases run for the optimized heat sink are discussed. The optimization of the heat sinks was carried out for a constant flow rate of 2 lpm and peak utilization power for both the CPUs at 115W. The baseline air-cooled heat sink has a fin count of 41, a base thickness of 4 mm, 0.23 mm thick fins with a fin height of 37mm. The dielectric fluid selected for the CFD study is a commercially available synthetic fluid, EC100. The optimization was done for both copper and aluminum heat sinks under natural and forced convection flow regimes separately. This was done to quantify the differences in the optimized heat sink design and the effect of design variables on the objective functions when either the flow regime or heat sink material is changed. The results of doing these permutations of heat sink material under different cooling modes will also allow users to directly choose the design variables that have the most impact on the objective functions.

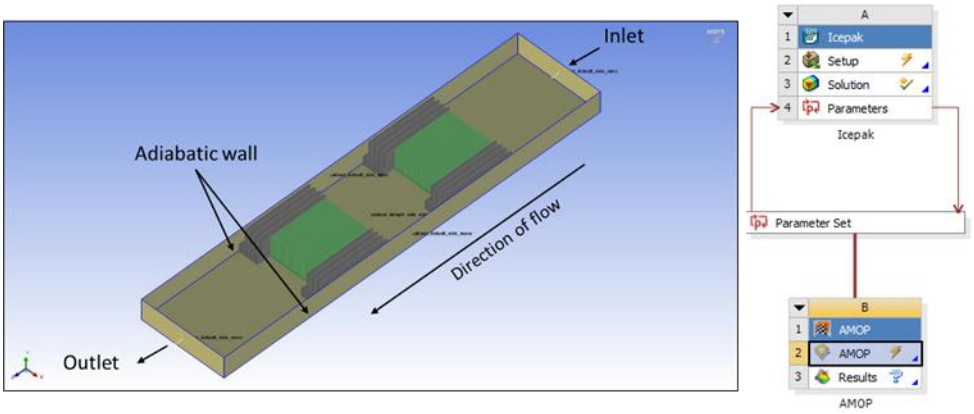

Figure 6-5: (Left) Boundary conditions used for the CFD simulations in ANSYS Icepak and (Right) Integration of OptiSLang module with Icepak in ANSYS Workbench

Figure 6-5 shows the boundary conditions used for thermal simulations in ANSYS Icepak. The gravity is set in the negative z-direction, representing the vertical orientation of the server, as in the case of typical immersion-cooled tanks. The first step in the design optimization process was validating the CFD data with the experimental results. After the baseline simulations for the air-cooled heat sink, the bounds for the design variables and the objective functions are defined. Thermal resistance and pressure drop are the typical performance metrics that define the heat sink performance. Both these functions were defined to be minimized during the optimization process. A summary of the bounds of the design variables, the objective functions, and other variable parameters used in this study is shown in Table 23. The final CFD results from thermal simulations along with the design variable bounds and objective functions are published to OptiSLang where the multi-objective optimization is performed.

Table 23: Variable input parameters used in ANSYS Icepak

No.	Parameters	Factor
1	Inlet Fluid Velocity	Varying cabinet height
2	Heat Sink Overall Height	Optimization design variable

3	Fin Thickness	Optimization design variable
4	No. of Fins	Optimization design variable
5	Mesh	Varying cabinet height
6	Thermal Resistance	Objective function
7	Pressure Drop	Objective function

Once the input parameters or the design variables are read in OptiSLang, a Design of Experiments (DoE) is created. Based on this DoE, a sensitivity analysis is first done to determine the effect of the chosen design variables on the objective functions of the study. This phase is also known as the design exploration phase where the solution space can be sampled using the available sampling methods in OptiSLang. For the current study, AMOP is used for this purpose. Figure 6-6 shows the criteria set up in OptiSLang showing the input design variable parameters and the objective function. The outputs from this stage are the response surfaces, response plots, and the total effects matrix. These results help in determining the relationships and the weightage of those relationships between the design variables and the objective functions. The final result of the optimization of the design space is directly obtained on a Pareto front with its axis as the two objective functions. The boundaries of the Pareto front represent the minimum values of the objective functions.

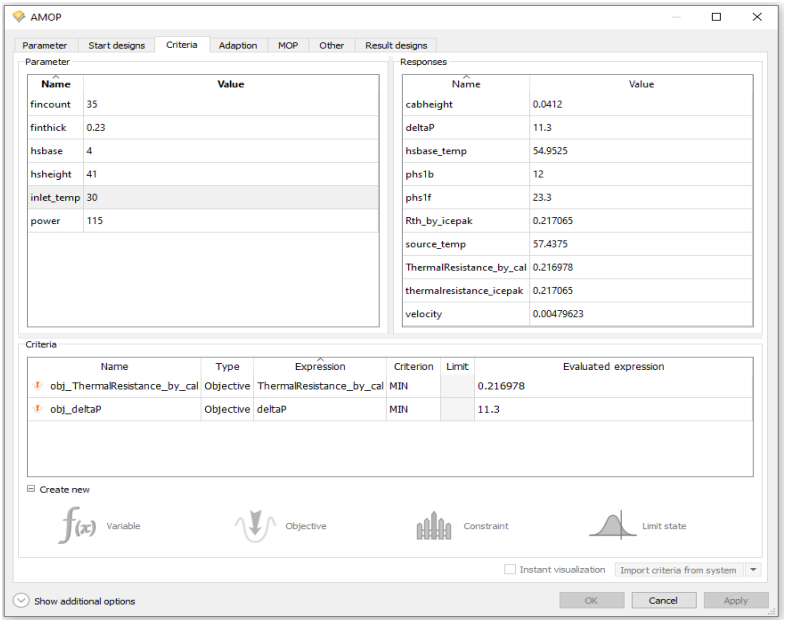

Figure 6-6: Setup of optimization parameters in OptiSLang using AMOP for design exploration:

Table 24: Inputs of design variables used for design exploration in OptiSLang (Bold + italics text shows baseline values of the parameters)

S.No	Overall Heatsink Height (mm)	Fin Thickness (mm)	No. of Fins	Fin Thickness
1	26	***0.23***	25	
2	29	0.32	27	
3	32	0.41	29	
4	35	0.5	31	
5	38	0.59	33	
6	***41***	0.68	***35***	
Step Size	3	0.09	2	
Discrete Values	6	6	6	
Total Number of Design Points (6 x 6 x 6) = 216				

6.4 Results

The optimization results presented in this section are divided into two sub-sections: the results for aluminum heat sink and copper heat sink. The results for both the heat sinks also include the results for natural and forced convection. Assessment of the optimized heat sink design is done based on analyzing surface response plots, CoP, and by compiling the complete design space on a Pareto front. It should be noted that the criteria for optimization of heat sinks and design variables were kept the same for both natural and forced convection heat sinks so that a comparison can be made under similar constraints. A total of 216 design points were generated for each simulation case with a total of 6 different simulation cases.

6.4.1 Optimization for Aluminum Heatsink

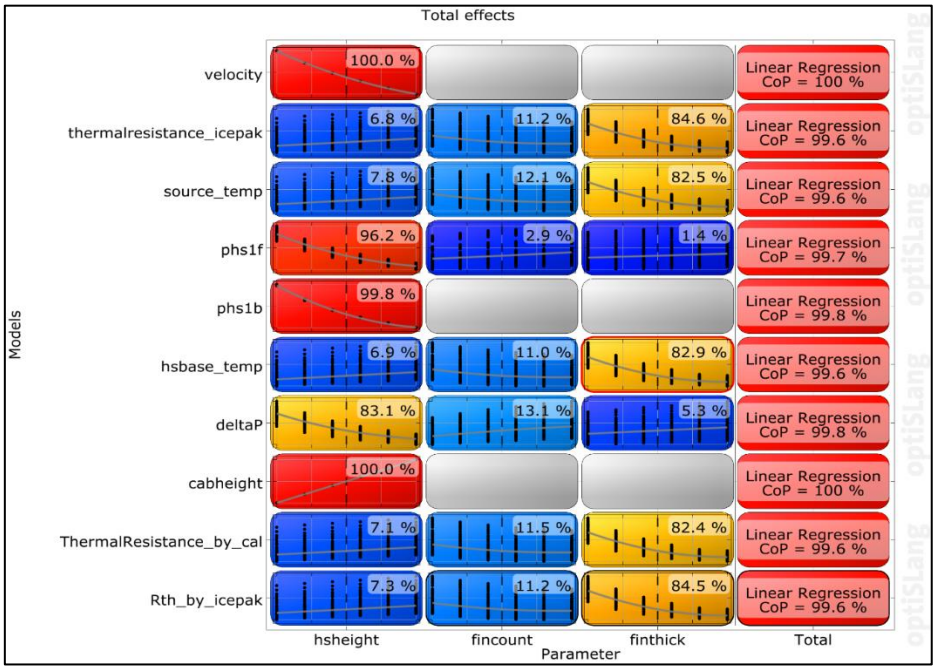

Table 25: Total effects plot for aluminum heat sink under forced convection

The first part of the optimization study was the sensitivity analysis of the design variables to the objective functions. Table 25 shows the total effects plots for the aluminum heat sink optimization case under forced convection flow. The effect plot essentially quantifies

the impact of each of the inputs on the outputs or post-processing functions. It can be seen that thermal resistance is primarily dependent on heat sink fin thickness. Similarly, in the case of pressure drop, heat sink height is a major factor. The fin count of the heat sink does not have a significant impact on both the pressure drop and thermal resistance. This was against the assumption that a large number of fins and a correspondingly larger surface area will improve heat transfer. This is also a part of the reason why heatsinks designed for air-cooling are typically not able to provide the expected heat dissipation in immersion cooling. It can be seen that a linear regression CoP value of greater than 99.6% is achieved for all model outputs. This indicates that the sample points generated based on the design variable inputs a highly robust model was created.

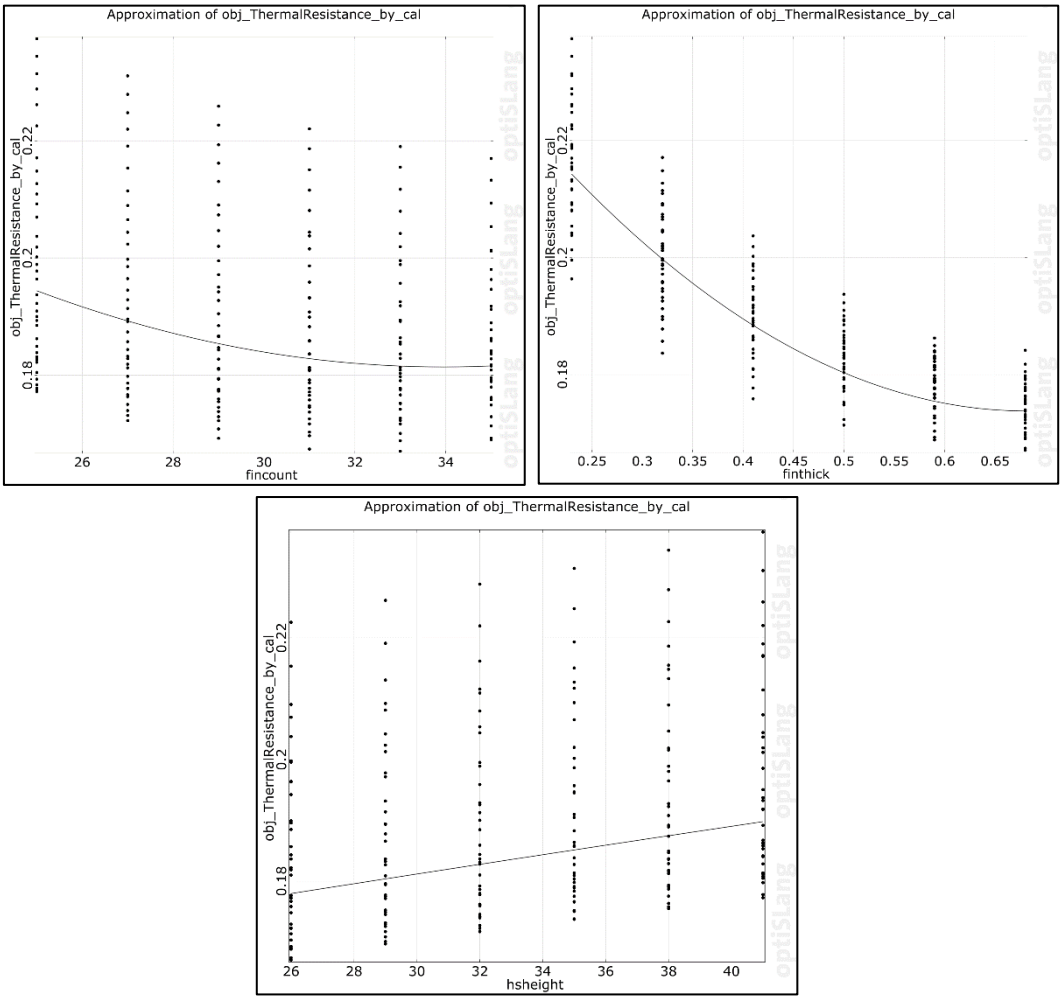

Figure 6-7: Relation between thermal resistance and different input variables in 2-D regression plot for the aluminum heat sink in forced convection

The 2-D and 3-D dependencies of the input design variables are visualized using linear regression-based plots and response surfaces. Figure 6-7 shows the dependency of the input variables on thermal resistance. As observed from the total effects matrix fin count has a very low impact on thermal resistance variation and tends to become asymptotic after a fin count of 33 fins in the current heatsink design. It should also be noted that discrete values of fin height and fin count were used in this study rather than giving a range of values in a smaller interval. This was done to restrict the design space to a certain number of design points and reduce simulation time. As expected, the pressure drop increases and thermal resistance reduces with the fin thickness of the heat sink. It was, however, observed that the variation in thermal resistance becomes less than 1% after a fin thickness of 0.6 mm. The same variation between 0.25mm to 0.6mm fin thickness is around 17%. This means a final optimized design of the heat sink will require a trade-off between the pressure drop and thermal resistance values.

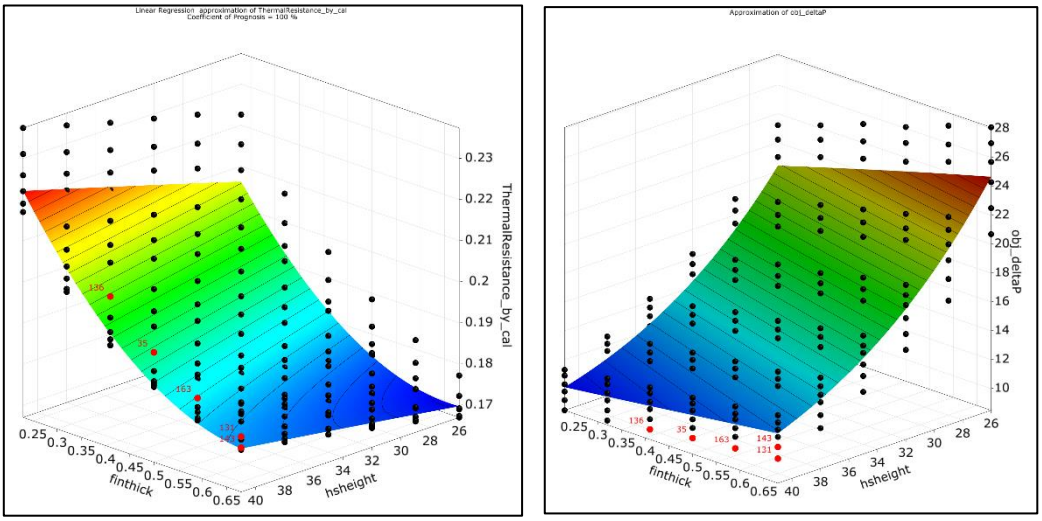

Figure 6-8: Comparison of 3-D response surfaces of the objective functions with varying fin thickness and heat sink height

To observe the coupled effect of more than one design variable on the objective function, 3-D response surface plots. Figure 6-8 shows the response plots for the variation of two objective functions with heatsink fin thickness and fin height. It is clear from the response plots that both the objective functions have an inverse relationship with each other. This would

mean that to achieve better thermal performance, a pumping power penalty would be incurred at some point. The CoP values of 100% were obtained for all the response surfaces of both the objective functions which depict the quality of the model approximation of the input design space. The optimization solver uses the design space created by the sensitivity analysis and plots the solution of the objective functions as outputs on a Pareto front as shown in Figure 6-9. Each point on this Pareto front represents a solution for the objective functions based on a design space point. The best design points from the Pareto front are those that lie along the red boundary. It can be seen that a vast majority of the design points were clustered in a region with a pressure drop of less than 20 Pa and a thermal resistance value between 0.2-0.18 W/mK. After analyzing all of the best Design Points (DP), five design points have both low pressure drop and thermal resistance as shown in Table 26. Out of the selected points, DP 163 showed the most optimum value for pressure drop, source temperature, and thermal resistance. When compared to the baseline heatsink design, the optimized heat sink offers a 15.3% less pressure drop and approximately 15% lower thermal resistance for the same fin height.

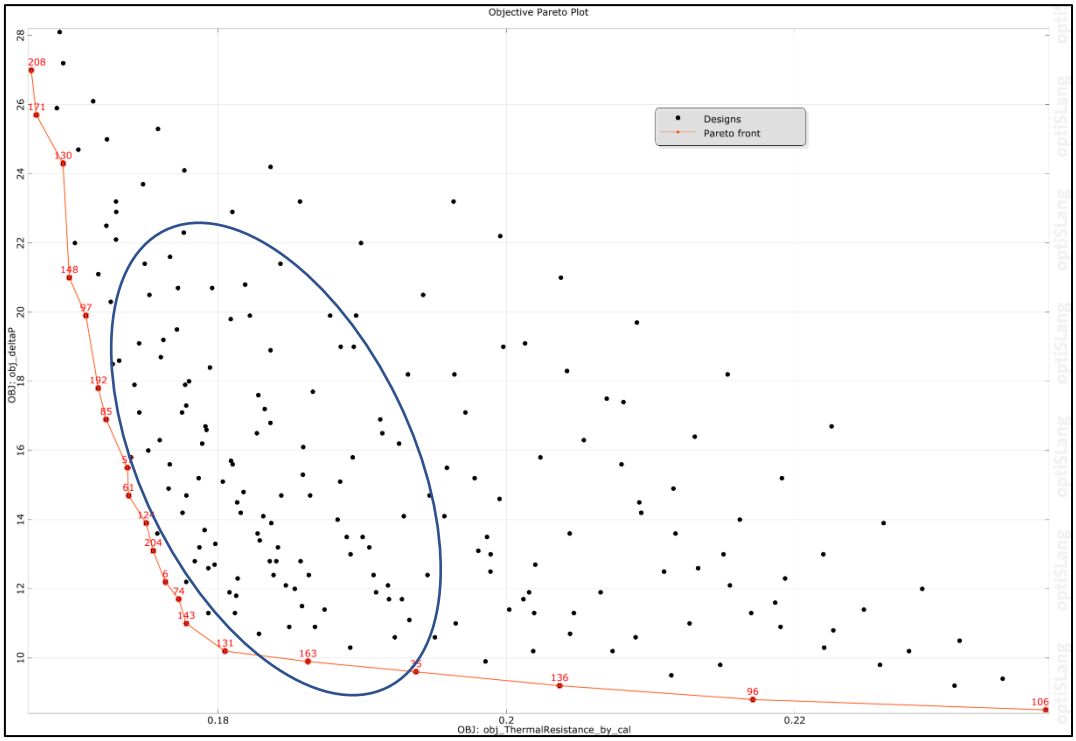

Figure 6-9: Pareto front showing the entire design space of 216 points and the red boundary depicting the best design points where the objective functions have a minimum value

Table 26: Summary of best design points showing the values of corresponding objective functions and source temperature

Design Point	**HS Height(mm)**	**Fin Count**	**Fin Thickness (mm)**	**R_{th} (W/mK)**	**ΔP (Pa)**	**T_{source}** (°C)
Base Line	41	35	0.23	0.22	11.3	57.4
35	41	25	0.5	0.19	9.6	54.8
131	41	25	0.68	0.18	10.2	53.3
136	41	27	0.41	0.20	9.2	55.9
143	41	27	0.68	0.18	11	52.9
163	***41***	***25***	***0.59***	***0.19***	***9.9***	***53.9***

In the data center industry, server heights are typically denoted in terms of form factor. A form factor of 1U represents a server height of 44.5mm. As discussed earlier, one of the main advantages of immersion cooling lies in the fact that it allows a higher heat transfer rate as compared to air-cooling technologies. Therefore, it is also possible to reduce the form factor or height of the heat sink itself to dissipate the same amount of heat flux from the processors. This allows the data center to pack more servers in the same space by utilizing efficient cooling methods like immersion cooling. The baseline heat sink used in this study is designed for a 2U air-cooled server. An investigation of reducing the heat sink height was also carried out from the optimization results. To do a fair comparison with the baseline design, the selection criteria was which heat sink would give a lower temperature than the baseline design for a reduced heat sink height. The optimization results of the heat sink with reduced height, show that the best DPs for a heatsink height equivalent to a 1U server, the optimized heat sink offers lower

thermal resistance and source temperature than the baseline design in a lower form factor for the same CPU power. This means that while the overall heat transfer area is being reduced, an optimized heat sink for immersion cooling offers better thermal performance as seen in Table 27. Although, it should be noted that the pressure drop or the pumping power will increase significantly for a smaller form factor server. The trade-off to be weighed here is the improvement in thermal performance and the ability to deploy more servers in the same volume of space in a data center. Further analysis of the reduced form factor heat sink also shows that a significant reduction in heat sink weight and production cost per unit can also be reduced.

Table 27: Overview of the results of design points with heat sink height for a 1U server

Design Point	**HS Height (mm)**	**Fin Count**	**Fin Thickness (mm)**	**R_{th} (W/mK)**	**ΔP(Pa)**	**T_{source}(°C)**
Base Line	41	35	0.23	0.22	11.3	57.4
120	26	35	0.68	0.17	28.1	51.9
99	***26***	***25***	***0.32***	***0.20***	***17.5***	***56.3***
41	26	27	0.23	0.21	18.2	57.2
171	26	31	0.68	0.17	25.7	51.7
24	26	33	0.41	0.18	24.1	56.5

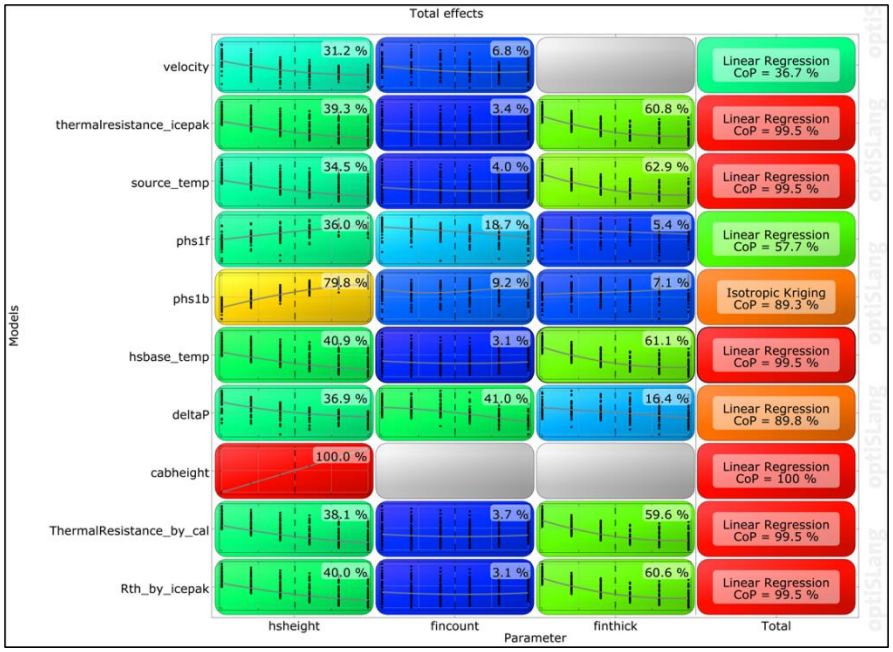

Figure 6-10: Total effects plot for aluminum heat sink under natural convection

As discussed earlier, after determining the optimized heat sink geometry for the baseline design, an optimization study was also done for natural convection immersion cooling. Figure 6-10 shows the total effects plot for the aluminum heat sink in natural convection. It is seen that unlike the case of forced convection, which is still very low Reynolds number flow in immersion cooling, the impact of fin thickness on thermal resistance reduces from 82% to 59%. Another difference observed when comparing the case of natural convection to forced convection is that the impact of heat sink height becomes at least 5 times more significant. At the same time, the effect of heat sink height becomes even less important in terms of optimization for natural convection. For pressure drop, it is observed that the impact number of fins increases almost threefold and the impact of overall heat sink height reduces by almost 50%.

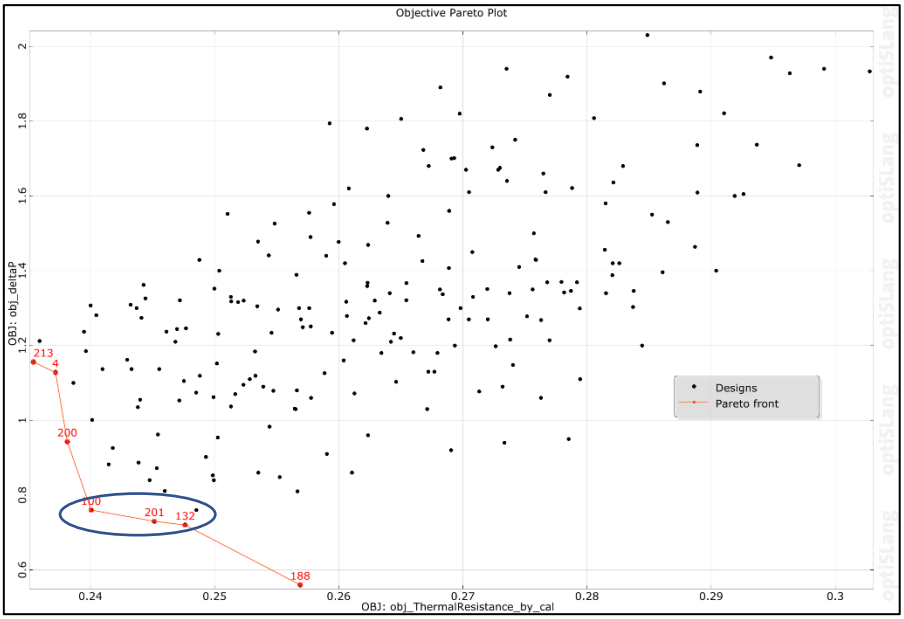

Figure 6-11: Pareto front showing the distribution of the solutions of the objective functions and the chosen DPs

The distribution of the solution for each DP on the Pareto front is shown in Figure 6-11. This is also different when compared to Figure 6-10 where a greater number of solutions satisfy the objective function constraints and are more uniformly distributed. As compared to the results of pressure drop and thermal resistance of the baseline design in natural convection, a maximum reduction of 32% was obtained in pressure drop and a 10% reduction in thermal resistance. Additionally, the optimized heatsink was able to reduce the source temperature by 3°C for the same fin height as the baseline design. An interesting observation made from the response graphs is that the thermal resistance value reduces to a certain fin count, and then starts creeping up as seen in Figure 6-12. This could be because a larger number of fins tend to choke the natural convection through the fins. This effect is also observed in thermal resistance response to fin thickness that plateaus out after 0.5mm fin thickness.

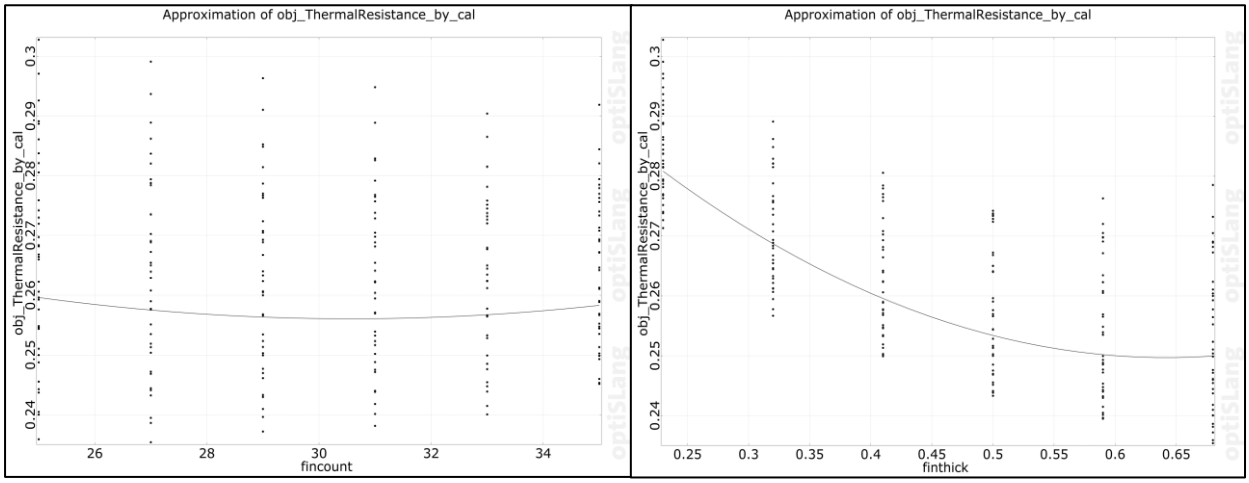

Figure 6-12: Response graph for variation of thermal resistance with the design points for heat sink fin count

6.4.2 Optimization for Copper Heatsink

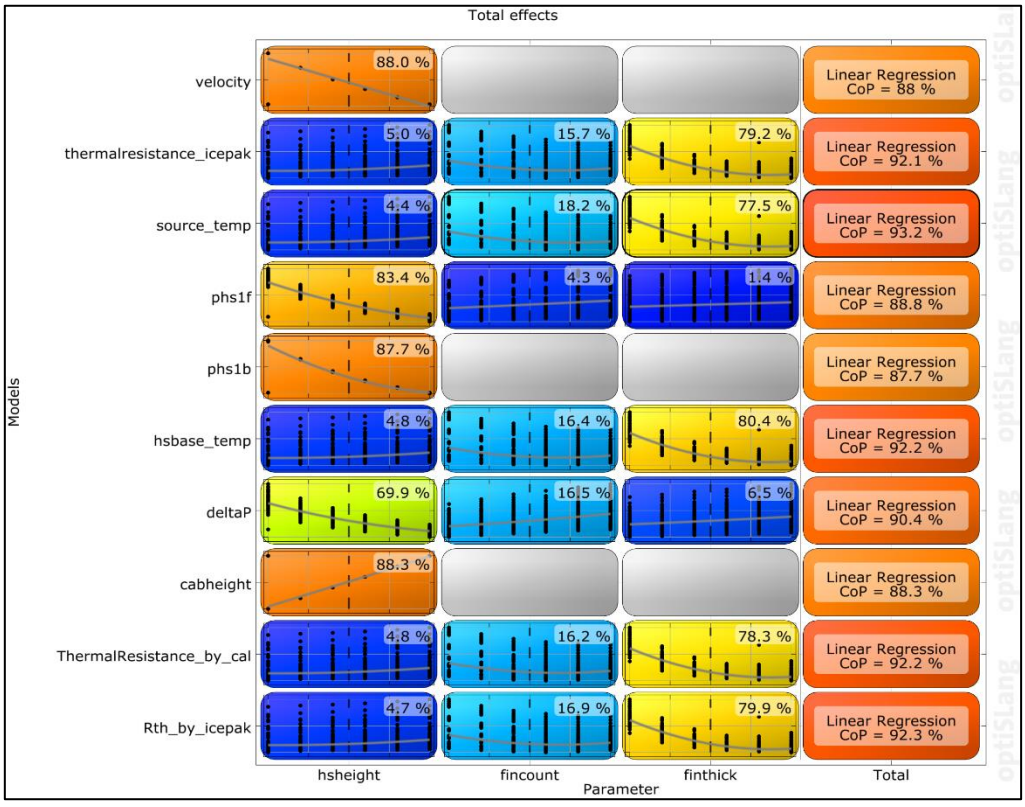

Figure 6-13: Total effects matrix for copper heat sink with forced convection cooling

Aluminum is typically used for heat sink applications as it offers lower weight and cheaper manufacturing options. Cooper heat sinks offer better thermal performance, especially

when the application is for high power density. Therefore, following the same methodology as for aluminum heat sinks, a design optimization was also done for the same heat sink with copper as the material. Both the design variables and the objective functions were kept the same as in the case of aluminum heat sinks. A baseline CFD simulation was first carried out to ascertain the values of the objective functions under both forced and natural convection cooling modes. Figure 6-13 shows the total effects matrix for the copper heat sink DoE. It can be seen from the matrix that fin thickness and fin height have a dominant impact on thermal resistance and pressure drop, respectively. The Pareto front distribution looks very similar to the forced convection case in the aluminum heat sink. A comparison of the objective function values of the best DPs from the Pareto front is shown in Table 28.

Table 28: Summary of the results of the optimized values of the objective function for forced convection cooling using copper heat sinks

Design Point	**HS Height (mm)**	**Fin Count**	**Fin Thickness(mm)**	**R_{th} (W/mK)**	**ΔP (Pa)**	**T_{source} (°C)**
Base Line	41	35	0.23	0.15	11.3	49.6
27	41	27	0.68	0.13	11	47.3
28	41	25	0.5	0.13	9.5	48.2
158	41	25	0.41	0.13	10.2	47.4
199	41	27	0.68	0.14	9.2	48.8
207	***41***	***25***	***0.59***	***0.13***	***9.2***	***47.7***

Also, as done in the case of the aluminum heat sink, an analysis was done to determine the performance of the optimized heat sink design for the same source power but a smaller 1U

form factor. As opposed to the case of the aluminum heatsink where the pressure drop increases significantly, an optimized heat sink design for copper showed negligible variation in pressure drop is observed. At the same time, the optimized 1U heat sink displayed the same thermal performance as the baseline heat sink as seen in Table 29.

Table 29: Results of the optimized values of the objective functions for 1U copper heat sink

Design Point	**HS Height (mm)**	**Fin Count**	**Fin Thickness (mm)**	**R_{th} (W/mK)**	**ΔP (Pa)**	**T_{source} (°C)**
Base Line	41	35	0.23	0.15	11.3	49.6
27	26	25	0.59	0.15	11.3	49.6

For the case of natural convection cooled copper heat sinks, the main difference in the total effects plot is in pressure drop where both the number of fins and fin height. Also, as opposed to forced convection, thermal resistance for natural convection copper heatsink is highly dependent on fin height. This is also different from the aluminum heatsink in natural convection where the thermal resistance is dominated by a variation in fin thickness. The Pareto front for the solution of the objective functions shows that the best DP for the heatsink design reduces the thermal resistance by approximately 6% and reduces the pressure drop by 27% as compared to the baseline design of copper heat sink in natural convection.

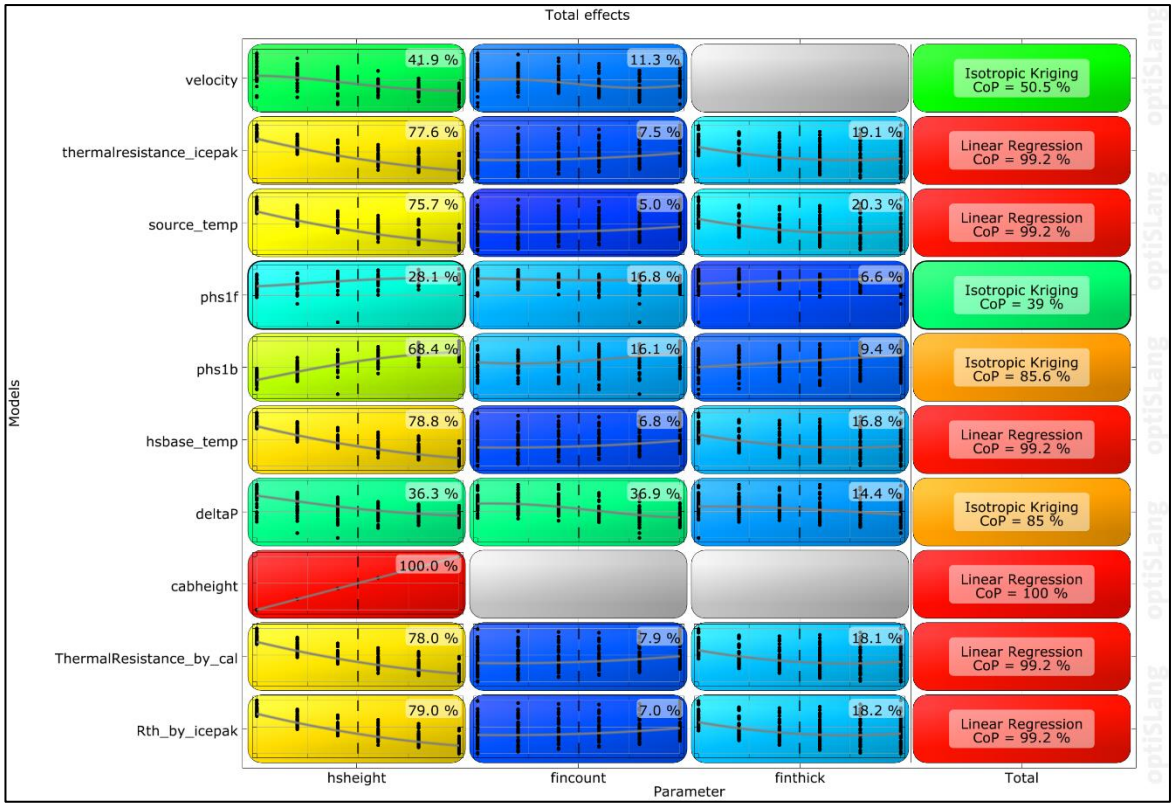

Figure 6-14: Total effects plot for copper heatsink under natural convection

6.5 Conclusion and Future Work

As the power densities for high-performance processors keep rising, the demands for the deployment of efficient cooling technologies are also increasing. Single-phase immersion cooling helps to address many shortcomings of traditional air-cooling and competitive liquid cooling technologies. As compared to air-cooling, immersion-cooling offers higher thermal mass, simplicity in cooling infrastructure, alleviation of airborne contamination issues, and is particularly suitable for edge data centers deployments. An in-depth study of different multi-objective and multi-design variable optimization schemes for heat sinks in immersion-cooled servers was investigated. Heat sink geometric parameters like heat sink fin height, fin thickness, and fin count were varied. Minimization of thermal resistance and pressure drop for constant pumping power was chosen as the objective function for the optimization study. As compared to the baseline heat sink design, the optimized heat sink was able to reduce the thermal resistance by 15% and a further 15.3% reduction in pumping power. A comparison of

the optimization results from the aluminum heat sink between forced and natural convection shows that the impact of fin thickness reduces significantly and the influence of heatsink height increases almost five times. This change of influence is even more pronounced for copper heat sink where the influence of heatsink height is negligible in forced convection but has the most dominant influence in natural convection.

The results of this study on the influence of the heatsink design variables on heat transfer and pumping power can be directly used for the optimization of typical parallel plate heat sinks for single-phase immersion cooling. There are more heat sink fin designs and configurations that can also be studied for optimization. As an example, pin-fin heat sinks are typically used in natural convection flows but offer a lower overall heat transfer surface area. An optimized pin-fin geometry can be obtained that not only offers lower pressure drop but also enhance their heat transfer performance. A further extension of this study can be to carry out a multi-disciplinary optimization where the optimization parameters can be thermal and flow physics, a cost model of the heat sink, and material optimization based on thermal profile at the heat sink base.

REFERENCES

[1] https://www.internetlivestats.com/

[2] Masanet, E., Shehabi, A., Lei, N., Smith, S. and Koomey, J., Recalibrating global data center energy-use estimates. *Science*, **vol** *367 no.* 6481, pp.984-986, https://doi.org/10.1126/science.aba3758, 2020

[3] Shehabi, A., Smith, S.J., Masanet, E. and Koomey, J., Data center growth in the United States: decoupling the demand for services from electricity use, *Environmental Research Letters*, **vol** *13* no. 12, p.124030, https://doi.org/10.1088/1748-9326/aaec9c, 2018

[4] Greenberg, S., Mills, E., Tschudi, B., Rumsey, P. and Myatt, B., Best practices for data centers: Lessons learned from benchmarking 22 data centers, *Proceedings of the ACEEE Summer Study on Energy Efficiency in Buildings in Asilomar, CA. ACEEE, August*, *3*, pp.76-87, 2006

[5] Siddik, M.A.B., Shehabi, A. and Marston, L., 2021, The environmental footprint of data centers in the United States. *Environmental Research Letters*, **vol** *16*(6), https://doi.org/10.1088/1748-9326/abfba1, 2021

[6] Shahi, P., Agarwal, S., Saini, S., Niazmand, A., Bansode, P., & Agonafer, D., CFD Analysis on Liquid Cooled Cold Plate Using Copper Nanoparticles, *Proceedings of the ASME 2020 International Technical Conference and Exhibition on Packaging and Integration of Electronic and Photonic Microsystems*. *ASME 2020 International Technical Conference and Exhibition on Packaging and Integration of Electronic and Photonic Microsystems*. Virtual, Online. October 27–29, 2020. V001T08A007. ASME. https://doi.org/10.1115/IPACK2020-2592, 2020

[7] Niazmand, A., Murthy, P., Saini, S., Shahi, P., Bansode, P., & Agonafer, D., Numerical Analysis of Oil Immersion Cooling of a Server Using Mineral Oil and Al2O3 Nanofluid, *Proceedings of the ASME 2020 International Technical Conference and Exhibition on Packaging and Integration of Electronic and Photonic Microsystems*. *ASME 2020 International Technical Conference and Exhibition on Packaging and Integration of Electronic and Photonic Microsystems*. Virtual, Online. October 27–29, 2020. V001T08A009. ASME. https://doi.org/10.1115/IPACK2020-2662, 2020

[8] Shahi, P., Saini, S., Bansode, P., Agonafer, D., A Comparative Study of Energy Savings in a Liquid-Cooled Server by Dynamic Control of Coolant Flow Rate at Server Level, in *IEEE Transactions on Components, Packaging and Manufacturing Technology*, vol. 11, no. 4, pp. 616-624, doi: 10.1109/TCPMT.2021.3067045, 2021

[9] Shahi, P., Deshmukh, A. P., Hurnekar, H. Y., Saini, S., Bansode, P., Kasukurthy, R., and Agonafer, D., Design, Development, and Characterization of a Flow Control Device for Dynamic Cooling of Liquid-Cooled Servers, ASME. *J. Electron. Packag*., **vol** 144(4): 041008. https://doi.org/10.1115/1.4052324, 2022

[10] Niazmand, A., Chauhan, T., Saini, S., Shahi, P., Bansode, P.V., & Agonafer, D., CFD Simulation of Two-Phase Immersion Cooling Using FC-72 Dielectric Fluid, *Proceedings of the ASME 2020 International Technical Conference and Exhibition on Packaging and Integration of Electronic and Photonic Microsystems*. *ASME 2020 International Technical Conference and Exhibition on Packaging and Integration of Electronic and Photonic Microsystems*. Virtual, Online. October 27–29, 2020. V001T07A009. ASME. https://doi.org/10.1115/IPACK2020-2595

[11] Hoang, C.H., Hoang, C.H., Tradat, M., Manaserh, Y., Ramakrisnan, B., Rangarajan, S., Hadad, Y., Schiffres, S. and Sammakia, B., A Review of Recent Developments

in Pumped Two-Phase Cooling Technologies for Electronic Devices," in *IEEE Transactions on Components, Packaging and Manufacturing Technology*, vol. 11, no. 10, pp. 1565-1582, doi: 10.1109/TCPMT.2021.3117572, 2021

[12] Shah, J.M., Eiland, R., Siddarth, A. and Agonafer, D., Effects of mineral oil immersion cooling on IT equipment reliability and reliability enhancements to data center operations. In *2016 15th IEEE Intersociety Conference on Thermal and Thermomechanical Phenomena in Electronic Systems (ITherm)*, 31 May-3 June, pp. 316-325, IEEE, https://doi.org/10.1109/ITHERM.2016.7517566, 2016

[13] Eiland, R., Fernandes, J., Vallejo, M., Agonafer, D. and Mulay, V., "Flow Rate and inlet temperature considerations for direct immersion of a single server in mineral oil," *Fourteenth Intersociety Conference on Thermal and Thermomechanical Phenomena in Electronic Systems (ITherm)*, 2014, pp. 706-714, doi: 10.1109/ITHERM.2014.6892350, 2014

[14] Shah, J. M., Padmanaban, K., Singh, H., Duraisamy Asokan, S., Saini, S., and Agonafer, D., Evaluating the Reliability of Passive Server Components for Single-Phase Immersion Cooling, ASME. *J. Electron. Packag.*, 144(2): 021109. https://doi.org/10.1115/1.4052536, 2022

[15] Yazicioğlu, B. and Yüncü, H., 2007. Optimum fin spacing of rectangular fins on a vertical base in free convection heat transfer. *Heat and Mass Transfer*, *44*(1), pp.11-21, https://doi.org/10.1007/s00231-006-0207-6, 2007

[16] Jang, D., Yu, S.H. and Lee, K.S., 2012. Multidisciplinary optimization of a pin-fin radial heat sink for LED lighting applications. *International Journal of Heat and Mass Transfer*, *55*(4), pp. 515-521, https://doi.org/10.1016/j.ijheatmasstransfer.2011.11.016, 2012

[17] Kim, D.K., Thermal optimization of plate-fin heat sinks with fins of variable thickness under natural convection, *International journal of heat and mass transfer*, *55*(4), pp.752-761, https://doi.org/10.1016/j.ijheatmasstransfer.2011.10.034, 2012

[18] Subasi, A., Sahin, B. and Kaymaz, I., Multi-objective optimization of a honeycomb heat sink using Response Surface Method. *International Journal of Heat and Mass Transfer*, *101*, pp.295-302, https://doi.org/10.1016/j.ijheatmasstransfer.2016.05.012, 2016

[19] Chen, C.T. and Chen, H.I., 2013. Multi-objective optimization design of plate-fin heat sinks using a direction-based genetic algorithm. *Journal of the Taiwan Institute of chemical Engineers*, *44*(2), pp.257-265, https://doi.org/10.1016/j.jtice.2012.11.012, 2013.

[20] Chiang, K.T., Chang, F.P. and Tsai, T.C., 2006. Optimum design parameters of Pin-Fin heat sink using the grey-fuzzy logic based on the orthogonal arrays. *International communications in heat and mass transfer*, *33*(6), pp.744-752, https://doi.org/10.1016/j.icheatmasstransfer.2006.02.011, 2006

[21] Chiang, K.T. and Chang, F.P., 2006. Application of response surface methodology in the parametric optimization of a pin-fin type heat sink. *International communications in heat and mass transfer*, *33*(7), pp.836-845, https://doi.org/10.1016/j.icheatmasstransfer.2006.04.011, 2006

[22] Chen, C.T., Wu, C.K. and Hwang, C., 2008. Optimal design and control of CPU heat sink processes. *IEEE Transactions on components and Packaging Technologies*, *31*(1), pp.184-195, https://doi.org/10.1109/TCAPT.2008.916855, 2008

[23] Devi, S.P., Manivannan, S. and Rao, K.S., 2012. Comparison of nongradient methods with hybrid Taguchi-based epsilon constraint method for multiobjective optimization of cylindrical fin heat sink. *The International Journal of Advanced Manufacturing Technology*, *63*(9-12), pp.1081-1094, DOI 10.1007/s00170-012-3985-7, 2012

[24] Engineered Fluids, EC-100 Dielectric Coolant, https://engineeredfluids.store/products/ec-100

[25] McWilliams, T.D., Evaluating Heat Sink Performance in an Immersion-Cooled Server System, M.S Thesis, The University of Texas at Arlington, USA, 2014

[26] Will, J. and Most, T., 2009, Metamodell of optimized prognosis (MoP)-an automatic approach for user friendly parameter optimization, 6th *Optimization and Stochastic Days*, October 15-16, Weimar, Germany, 2009

[27] Most, T. and Will, J., 2011. Sensitivity analysis using the Metamodel of Optimal Prognosis. 8th *Optimization and Stochastic Days*, November 24-25, Weimar, Germany, pp.24-40,

[28] Mimery, D.R., *Multidisciplinary design optimization of part geometry in CAD*, M.S. Thesis Massachusetts Institute of Technology, USA, 2020

[29] Bar-Cohen, A., Iyengar, M. and Kraus, A.D., 2003. Design of optimum plate-fin natural convective heat sinks. *J. Electron. Packag.*, Vol *125*(2), pp. 208-216, https://doi.org/10.1115/1.1568361, 2003

[30] Teertstra, P., Yovanovich, M.M. and Culham, J.R., 2000. Analytical forced convection modeling of plate fin heat sinks. *Journal of Electronics Manufacturing*, vol *10*(04), pp. 253-261, https://doi.org/10.1142/S0960313100000320, 2000

[31] Saini, S., Wagh, T., Bansode, P., Sahi, P., Herring, J., Lamotte-Dawaghreh, J., Shah, J., Agonafer, D., 2022, "A Numerical Study on Multi-objective Design Optimization of Heatsinks for Forced and Natural Convection Cooling of Immersion Cooled Servers," Journal of Enhanced Heat Transfer.

Chapter 7 Numerical Investigation Of Influence Of Tank Design On Thermal And Flow Performance Of A Server In Single-Phase Immersion Cooling

7.1 Introduction

Data center proliferation and data center platform power densities continue to rise with increasing data storage and data processing demands. The increased processing demands have also given impetus to increased deployment of high-performance and high-power central processing units (CPUs) or graphic processing units (GPUs) based server platforms. These performance gains in these processing units over generations are bring realized by increasing compute, memory, and storage subsystem powers [1]. For future high-performance and high-power server platforms, air-cooling may not be the most efficient cooling method for maintaining optimum server component and subsystem temperatures. Additionally, large cooling energy consumption and lower possibility for waste heat recovery further reduce the benefits of air-cooling [2].

Liquid coolants offer superior thermal properties such as thermal conductivity and specific heat by unit volume, thus, yielding higher convective heat transfer coefficients. Liquid cooling not only allows better heat removal from the chips but further allows the chips to be overclocked as well [3]. Liquid cooling for data centers is deployed either using direct to chip method that uses cold plates mounted on chips or by direct immersion of servers in thermally conductive dielectric fluids. In both these cooling technologies, the coolant used may be single or two-phase. For the scope of this study, we will only focus on the single-phase immersion technique. This cooling methodology involves direct contact of the dielectric fluid with the

server and its components. One of the fundamental advantages of this approach is that it allows complete removal of fan-based cooling inside the server, enabling a significant reduction in cooling power consumption and subsequently in power usage effectiveness (PUE). Single-phase immersion cooling also allows isolating the servers from harsh environmental impacts of temperature and humidity transients as well as airborne contaminants which may otherwise deteriorate in the air especially if the data center is operating in free air-cooling mode. With the increased utility of the Internet of Things (IoT) and low latency demands, immersion cooling will also enable easily deployable edge infrastructure in urban areas.

In addition to the many advantages that single-phase immersion cooling offers, some inherent thermo-mechanical considerations should be addressed. Most of the commercially available tank-based solutions typically comprise a manifold system that can deliver the desired volume flow rate of the coolant to the immersed servers. While it is easy to predict the total volume flow rate of the coolant such a manifold can deliver, it may become extremely difficult to quantify what fraction of the flow is being delivered to the severs. This issue becomes even more complicated when not all the servers may be necessarily operating under the operational workloads. This may, in turn, cause non-homogeneous flow distribution in the tank where some servers may drive a large volumetric flow rate while others may be deficient. Under such conditions, it may become difficult to predict if the primary heat-dissipating components inside a server will operate under optimal conditions and will be able to deliver peak performance. Another unknown that may cause a change in CPU thermal performance is variation in the bypass flow due to spacing between two consecutive server chassis. This change may alter the flow boundary condition at the server inlet. The primary fluid distribution manifold should also be designed in a way that it has minimum impact on flow distribution to each server. Therefore, it is imperative to develop and utilize fluid delivery solutions that will efficiently and reliably dispense coolant to each server.

This paper uses a commercially available computational fluid dynamics (CFD) tool to quantify the variations in CPU thermal performance due to the aforementioned unknowns for a simplified server and tank design. The numerical analysis is divided into two parts. The first part of this study describes the analysis of the tank-level distribution manifolds and their impact on the server inlet boundary conditions. This is done by analyzing three different manifold configurations for an arbitrary 10U tank containing simplified servers. Total power to each server is varied so that a different value of flow rate is driven through each server chassis. The uniformity in the flow rate through each chassis is calculated by quantifying the flow rates inside the server at a location 1/3rd downstream of the server inlet location. To assess the server-level cooling capability, a numerical model of a 1U server with memory modules and two CPUs in a spread-core version is developed. Three different configurations of server supply manifold designs are analyzed and the influence of the fluid delivery mechanism on CPU thermal performance is recorded. To quantify this influence, CPU case temperatures and the pressure drop across the server are recorded under different flow rate conditions. The manifold design that offers lower case temperature and pressure drop is concluded to deliver better performance. To assess the influence of changing coolant bypass around the server, the flow domain design was modified and the CPU case and sink temperatures were noted for any variation.

7.2 Numerical Modeling Setup

The numerical study presented in this investigation is divided into two parts. The first part characterizes the performance of different distribution manifold schemes at the tank level by determining the homogeneity of flow delivery to each server in the tank. The second part quantifies the efficiency of the said flow delivery schemes on the server and CPU cooling capability by comparing the case temperatures of the two CPUs inside the server.

7.2.1 Tank Level Modeling

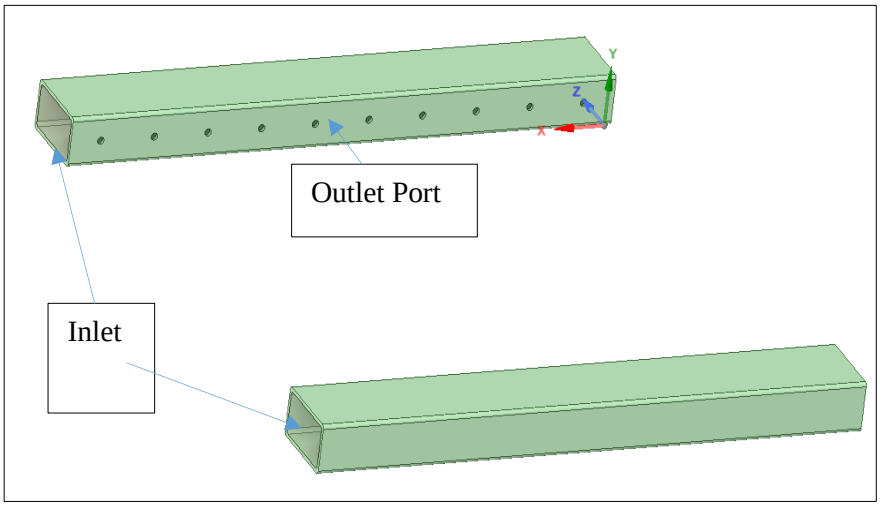

Figure 7-1: CAD geometry of one of the manifolds studied in this investigation showing the outlet ports on the manifoldsCAD geometry of one of the manifolds studied in this investigation showing the outlet ports on the manifolds

For the tank level study, a custom 10U tank is designed with two different fluid delivery mechanisms. The first is where the manifold is located on one side of the tank at the bottom and the flow delivery is in a direction perpendicular to vertically immersed servers (server inlet at the tank bottom and power supply at the top near the outlet). The second configuration is where a single manifold is located in the middle of the tank and delivers flow vertically upwards through the server. The third configuration analyzed, as shown in Figure 7-1, is where the two manifolds are integrated into the tank and deliver the fluid using the aforementioned fluid delivery mechanisms. The final manifold configuration investigated is identical to the first fluid delivery scheme, but with a centrally located inlet on the manifolds, as shown in Figure 7-2. Each manifold design contains a primary inlet of an identical cross-section area from one side and ten identical outlet ports, 6 mm in diameter, that cater to each 1U server immersed in the tank. The impact of having two outlets in the tank as compared to a single overflowing outlet is also investigated.

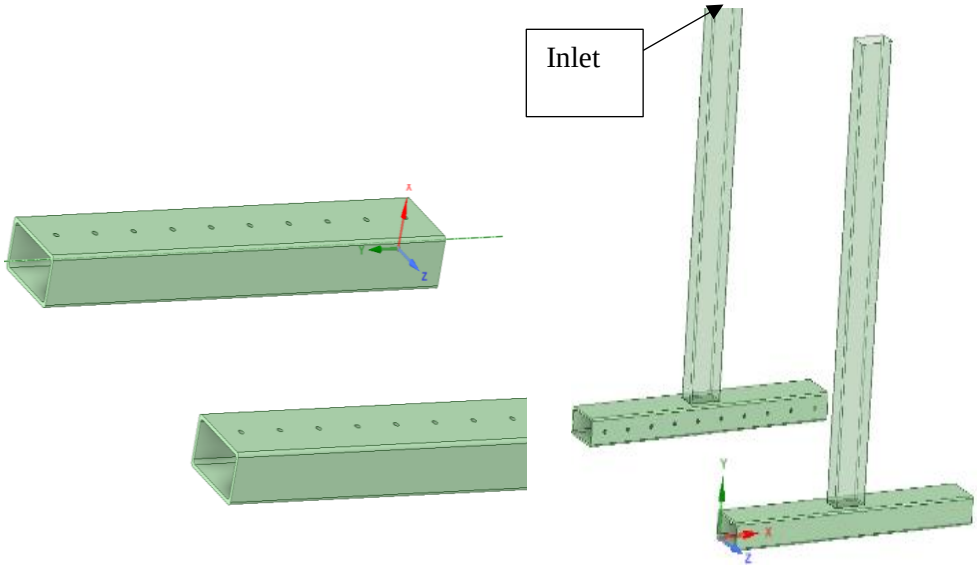

Figure 7-2: (Left) Two-inlet manifold configurations with vertical flow delivery and (right) Inlet location in the middle of the distribution manifold

These CAD models of the distribution manifolds were then integrated and populated with ten representative 1U server models using commercially available electronics thermal management CFD tool ANSYS Icepak [4]. These representative server geometries were modeled to emulate real servers in an immersion tank with known heat dissipation value that drives the flow through the server. Each simplified server geometry contains two high-power 2-D heat sources that represent CPUs inside a server, 2-D inlet and outlet perforations vents, and power supply units (PSU). The volume flow rate calculation through each server enclosure was done by numerically determining the outlet flow rate and flow rate value through the server backplane location. An overview of the one such server enclosure with all the components is shown in Figure 7-3 depicting the inlet manifold location, the simplified server containing 2-D heat sources, and the flow direction from the distribution manifold, through the servers, and

out from the tank. The geometry and the components of the simplified 1U server in the tank are kept the same for all the tank configurations investigated.

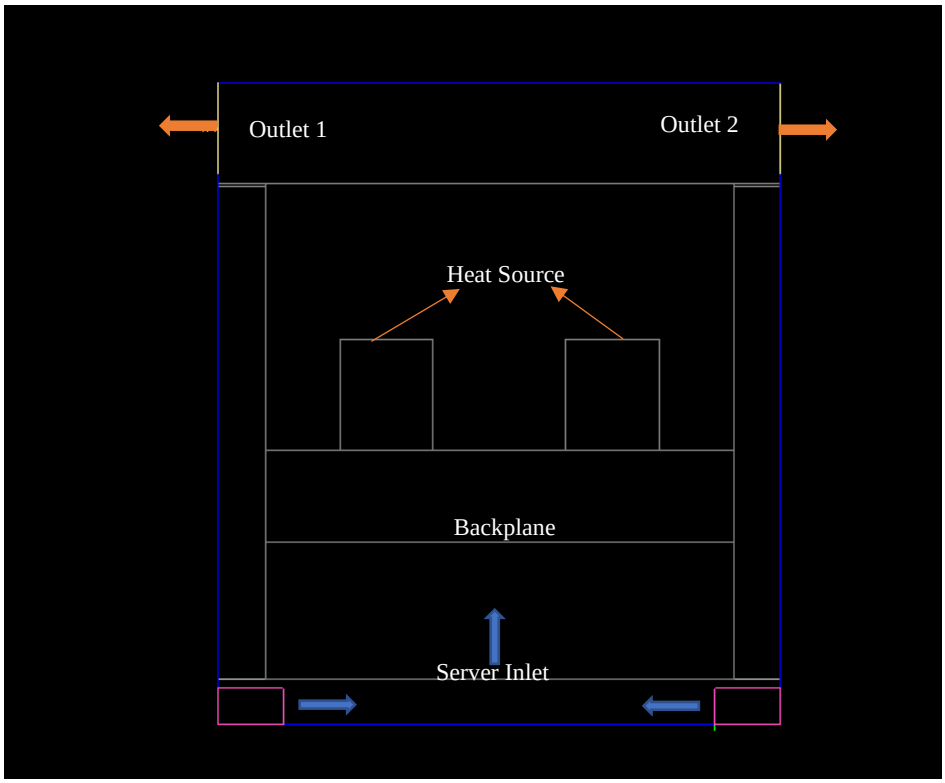

Figure 7-3: Overview of the cfd model of the tank and simplified server showing the server location in the tank, components, and numerical model boundaries

7.2.2 Server-Level Modeling

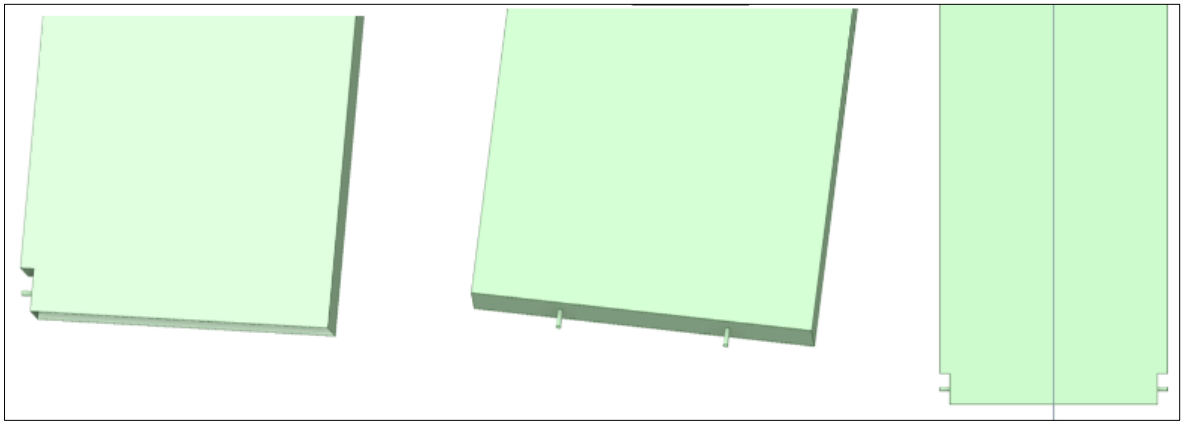

Figure 7-4: CAD models of the representative server enclosures used for determining the influence of the fluid delivery scheme on CPU cooling

To analyze the impact of the flow delivery schemes at the server level, a detailed CFD model of an Intel 1U server (Coyote Pass) was developed [5]. Different flow delivery

mechanisms are represented at the server level by creating representative server enclosures that house the detailed components of the server such as memory modules, PSUs, and combined heat sink and CPU assembly as shown in Figure 7-4. The inlets connected to the server enclosure depict the type of flow delivery scheme and the overhanging server length on top of the manifold in the tank is represented by the stair-stepped cutout on the enclosure side. It was ensured that the same clearance between the server inlet location and the tank bottom is used. Additionally, the diameter of the inlet is also the same as the diameter of the outlet ports on the distribution manifold in the tank. As an example, the case of the single distribution manifold in the tank is represented at the server level as seen in the geometry labeled '(a)' in Figure 7-4. The server components were modeled as native objects in the CFD tool after importing the outer server enclosure with the connected inlet. Figure 7-5 shows the final CFD model of the server containing all the detailed components for one of the flow delivery schemes and the flow direction.

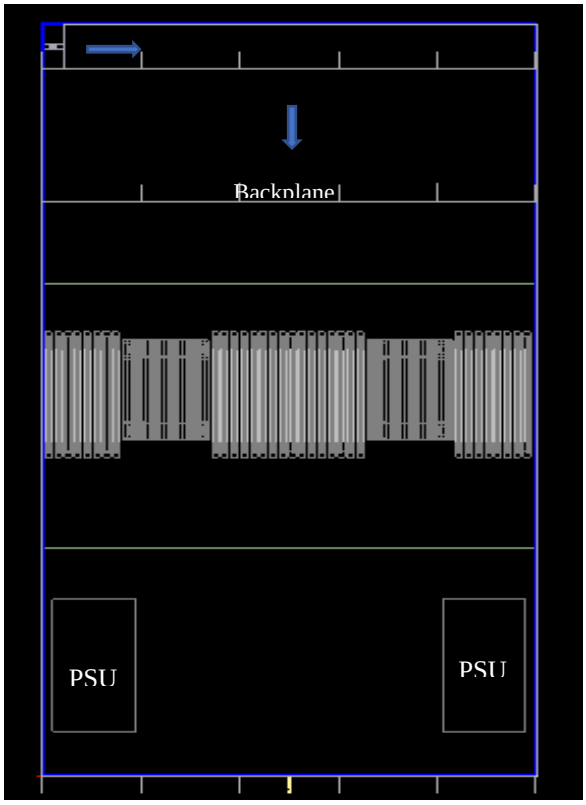

Figure 7-5: CFD model of the server showing detailed heat sink and memory modules for single inlet configuration

7.3 Simulation Methodology

As described earlier, this study is divided into a tank-level analysis of the flow uniformity through the server and a server-level analysis of the influence of the flow delivery scheme on the CPU cooling capability. A single-phase immersion synthetic dielectric fluid PAO 6 [6] was used as the cooling fluid for this investigation. PAO6 is a non-proprietary and cost-effective dielectric fluid that offers a good range of thermo-physical properties for single-phase immersion cooling of servers and is also available worldwide. A constant fluid temperature of 40°C was used for all the simulation cases with a velocity inlet boundary condition in the manifolds corresponding to three flow rate values of 14, 7, and 3 GPM per manifold. Three power values of 750 W, 450 W, and 150 W per server were used to simulate the server under operation. The manifold flow rates were decided based on the system energy balance equation for 750 W power per server.

The approach followed to quantify the differences in the flow delivery schemes investigated involved first, quantifying the volumetric flow rate values from each of the outlet ports when no servers are present in the tank. The tank was then populated with ten 1U simplified servers with 2-D heat sources to simulate the impact of flow being driven through the server under operating conditions. Detailed server geometries were not modeled at tank level as it would increase the simulation time significantly. The volume flow rate through each server was calculated numerically from the CFD modeling data at the backplane location and compared for different server power and manifold total flow rates. Boussinesq approximation was used to simulate the buoyancy-driven flow inside the servers for low tank flow rate conditions.

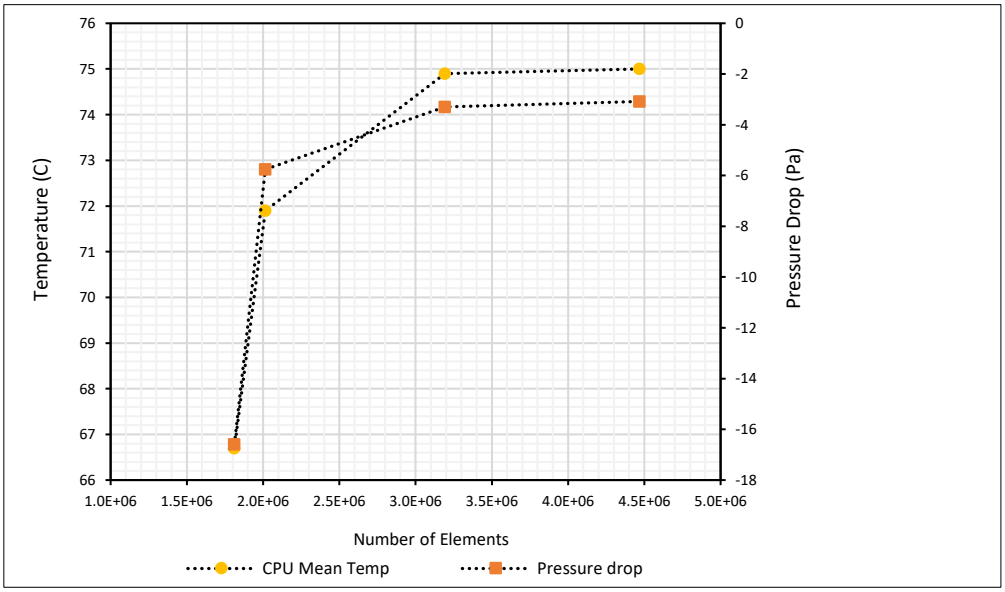

Figure 7-6: Results for grid independence for the server level study for a single inlet case

The influence of the flow delivery schemes at the server level was analyzed in a numerical model of a 1U Intel Coyote Pass server with two Intel 3rd generation Xeon Scalable Family Processors with a TDP value of 205 W each. Immersion optimized heat sink specific to this processor TDP and server flow rates were used instead of the air-cooled heat sink. The details of the heat sink geometry and comparison of thermal performance with the baseline air-

cooled heat sink design can be found in a recently published study by Sarangi et al. [7]. It should however be noted that the heat sink in this study did not have a heat pipe integrated with the base. The case temperature for each of the fluid delivery schemes was analyzed at three different coolant flow rates of 1 GPM, 0.7 GPM, and 0.35 GPM at a constant fluid inlet temperature of 40°C. The value of these flow rates was chosen to reflect a flow regime dominated by forced to near natural convection conditions. A grid independence study was also conducted for one of the server configurations. An optimum mesh value of 3.2 million elements was chosen for all the simulation cases as the server geometry, other than the inlet was fixed for all simulation cases.

7.4 Results And Discussion

This section summarizes the key results obtained for both the tank-level flow distribution study and the server-level thermal performance study. The results at the tank level are discussed in terms of the volume flow rates distribution manifold outlet ports and through the server. For the server level study, the results are discussed in terms of the case temperature and heat sink flow rate values for different flow delivery schemes. The case temperatures are calculated on the integrated heat spreader (IHS) and the heat sink flow rate is obtained by calculating the coolant mass flow rate through the heat sink channels.

7.4.1 Distribution Manifold Study

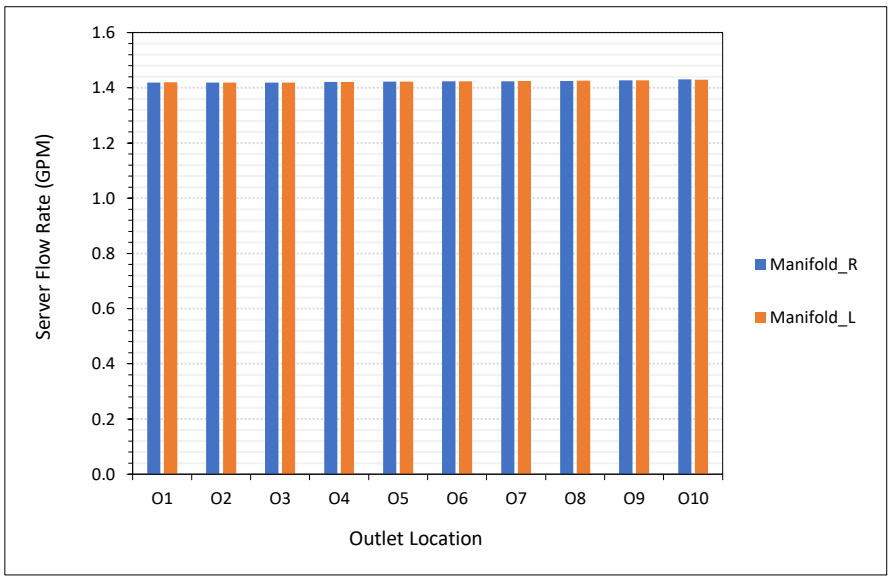

Figure 7-7: volume flow rates through manifold outlet ports for the case of two opposing manifolds with flow delivery transverse to the server

To assess the efficiency of the distribution manifold designs, the volume flow rate values through each of the outlet ports of the manifold were quantified. Figure 7-7 describes the variation of the outlet flow rates with outlet port location in the tank for the two-manifold configuration where the flow delivery is transverse to the flow direction through the sever. It can be seen that the volume flow rates from both the manifolds show near similar values. A similar trend is also observed in the case of a single manifold where the outlet flow rates show a maximum variation within 0.1 GPM only with or without the tank being populated by servers. This variation is also consistent in all other distribution manifold designs investigated in this study. These results imply that the flow rate distribution through the manifold is independent of the type of manifold designs considered in this study. This may however change if the outlet port area to manifold inlet area ratio which may need further analysis.

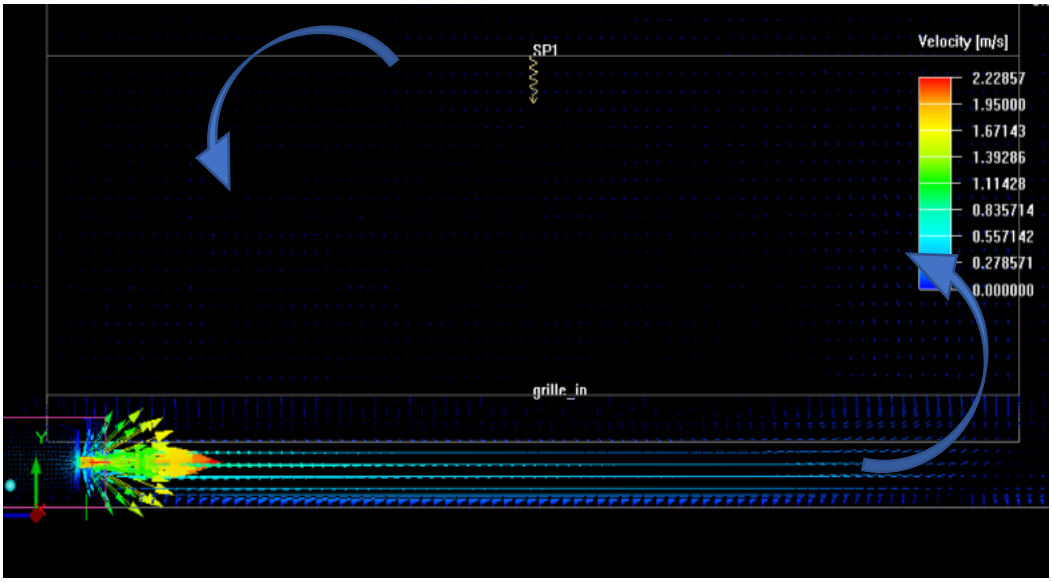

Figure 7-8: Velocity vectors for single manifold for 14 gpm flow rate showing recirculation pattern at the server inlet

When the tank is populated with representative server enclosures, it was observed that the flow distribution through each server, when measured at different locations, is rather erratic. The primary reason for this distribution is the manifold design with small diameter outlet ports that allow forcing enough flow through the server. A downside of this design is that the jet exiting from the outlet ports at high flow rates results in large recirculation at the sever inlet at the bottom of the tank. Figure 8 shows this recirculation pattern for the single manifold case. This recirculation pattern causes the flow distribution to vary throughout the tank resulting in a large flow rate variation in the tank as seen in Figure7- 9. Here the flow rates are calculated at the server backplane location and the value of the flow rate represents the net flow rate through a 2-D plane (mathematical difference in flow rate values in positive direction and negative direction). The sever location S1 in Figure 7-9 represents the server located closest to the main inlet of the distribution manifold and S10 is the farthest. The velocity vectors plotted in the middle of each server along the flow direction also show that there is a large downflow pattern through the server at location S1 and it reduces when moving towards location S10.

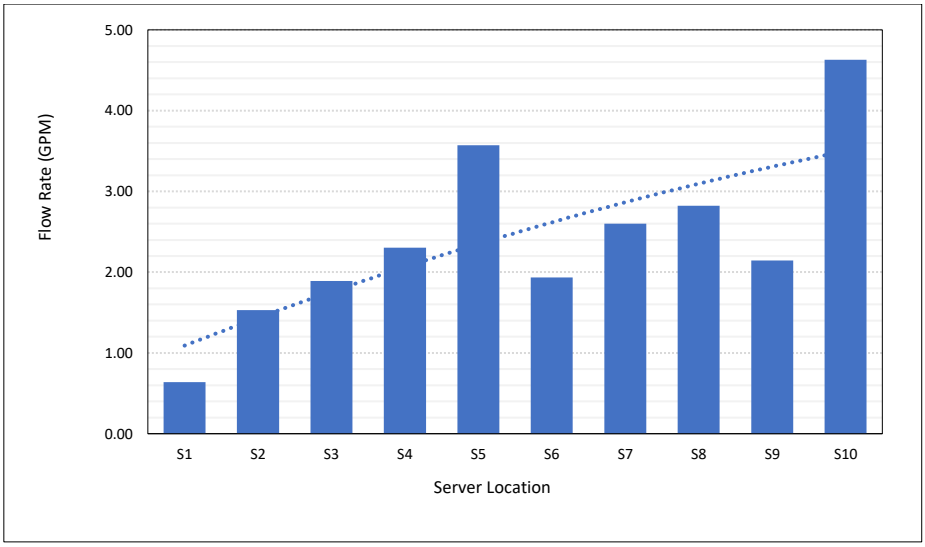

Figure 7-9: Volume flow rates through manifold outlet ports for the case of a single distribution manifold with flow delivery transverse to the server

Another key observation made was that as the manifold flow rates are reduced from 14 GPM per manifold to 3 GPM per manifold, an improvement in the flow uniformity through the servers is achieved. This improvement is depicted in Figure 7-10 showing the volume flow rates through each server when the server power is at 450 W and the flow rate is reduced to its minimum value. This is primarily because the contribution of natural convection at low tank flow rates becomes significant. Also, the recirculation at the server inlet is reduced leading to a more uniform flow through the server backplane towards the heat sink location. These observations are consistent with other distribution manifold designs investigated in this study.

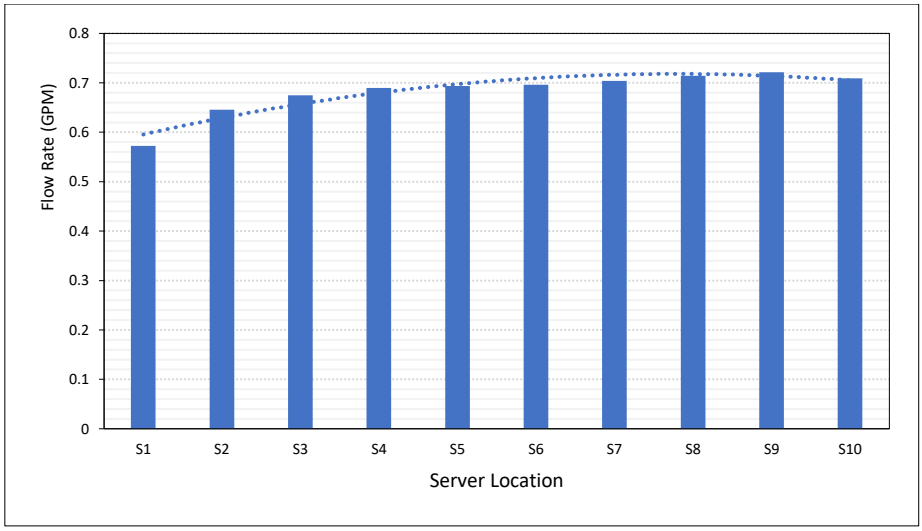

(A)

(B)

Figure 7-10: volume flow rates through manifold outlet ports for the case of a single distribution manifold with flow delivery transverse to the server with 450 W per server at (a) 3 gpm manifold flow rate and (b) 14 gpm manifold flow rate

Figure 7-11 shows a comparison of the server flow rate for a two-manifold configuration where one manifold has the primary inlet in the middle of the manifold and the second manifold has the inlet on one end. Both manifolds have the same flow delivery scheme which is transverse to the server flow direction. It was observed that the manifold with an inlet in the middle of the manifold yields better flow uniformity inside the tank as compared to the

case when the primary inlet is on one side when the flow rate through each distribution manifold is14 GPM per manifold. This could be a possible design solution for a tank design where forced flow is required through the server due to high component TDP requirements.

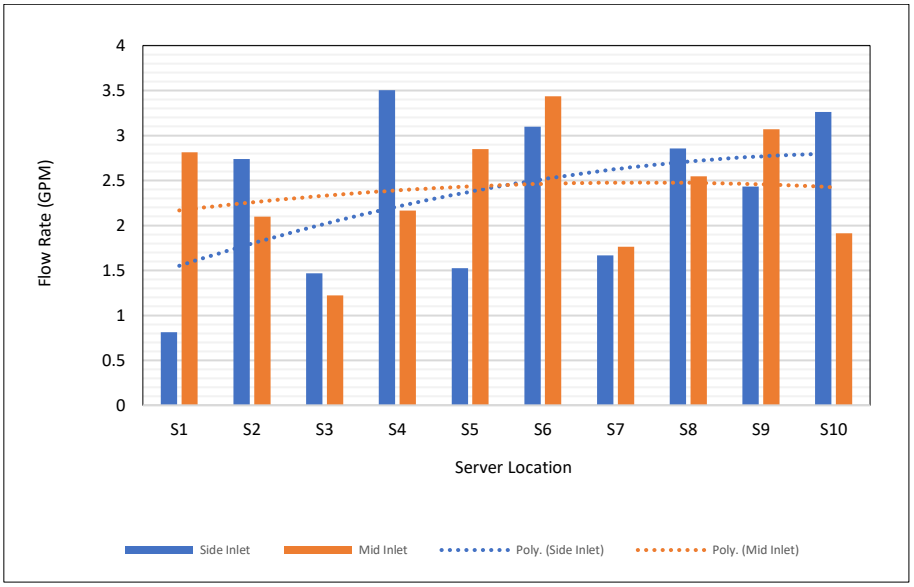

Figure 7-11: Comparison of the volume flow rates through the server at 14 gpm per manifold for a manifold with an inlet on one side vs. a manifold with a primary inlet located in the center of the manifold

7.4.2 Server-Level Study

The influence of the fluid delivery schemes at the sever level is presented in this section. As discussed in section 3, three different flow rates very investigated and a comparison of the case temperature values was obtained to assess the influence of the fluid delivery schemes on server cooling capability. Figure 7-12 shows the comparison of the case temperature values of both the CPUs. The CPU case labeled as 'L' represents the CPU located closer to the inlet for the single distribution manifold as shown in Figure 7-5. It was observed that there is a case temperature mismatch between both the CPUs for the case of the single inlet on one side. At the tank level, this represents the case for a single distribution manifold with the fluid delivery transverse to flow direction through the server. The difference in the case temperature value increases as the flow rate is reduced. The disparity in the case temperature values is not

observed for any other case of fluid delivery schemes. Therefore, although this fluid delivery scheme results in the lowest case temperature value, the issue of inequality in the case temperature values can be significant for higher inlet temperatures or lower flow rate values.

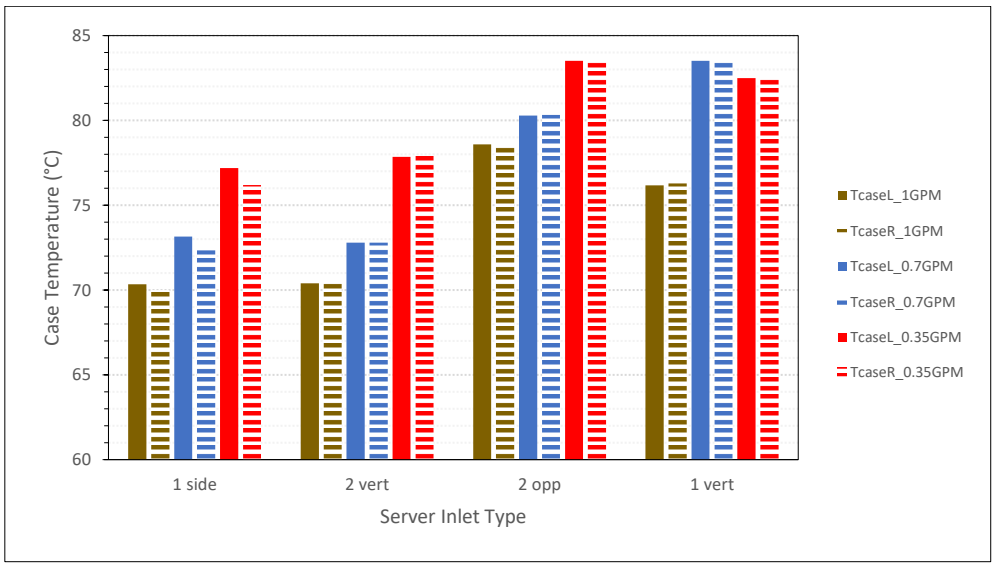

Figure 7-12: Case temperature values for different flow delivery schemes for varying server flow rates

The case of fluid delivery with two inlets located in front of the CPU heat sinks with fluid delivery in the same direction as flow movement through the server closely matches the case of a single inlet or single manifold in the tank. Additionally, this fluid delivery scheme alleviates the issue of case temperatures disparity. The results show that this disparity arises due to the maldistribution of the flow within the server as seen in Figure 7-13 for the case of a single inlet on the side. The other fluid delivery schemes enable symmetrical delivery of the coolant through the server causing near equal fluid flow through the heat sink. However, additional analysis of the pressure drop across the server in each of these fluid delivery schemes should be carried out. By doing so, both thermal and hydraulic performance of the server can be obtained and trade-offs in regards to pumping power requirements against the thermal performance enhancements can be quantified.

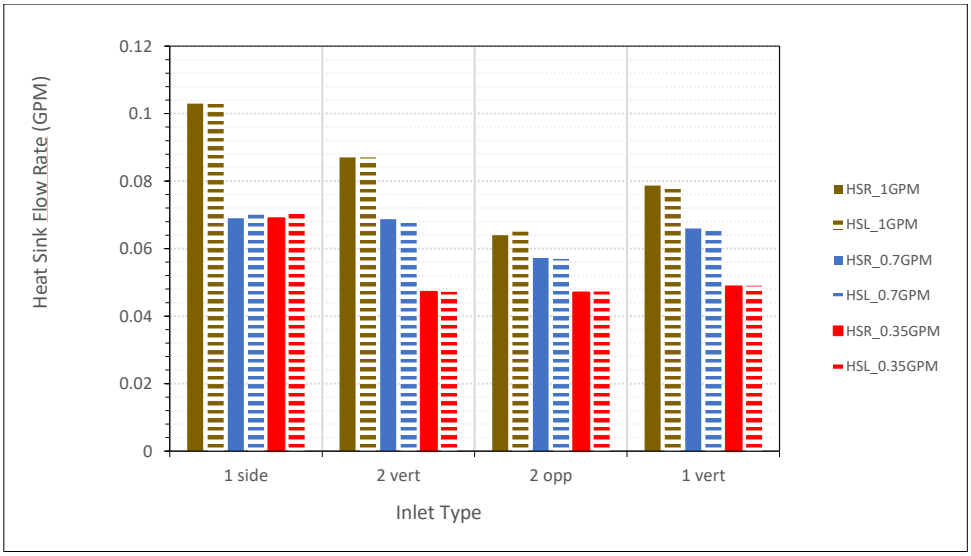

Figure 7-13: Comparison of the volume flow rates through the heat sink channels for different inlet configurations

7.5 CONCLUSION

In this paper, a numerical study on the influence of different fluid delivery mechanisms on server cooling capability and a comparison of the efficiency of these mechanisms on delivering were presented. It was observed that irrespective of the distribution manifold fluid delivery mechanism investigated in this study, each outlet port of the manifold can deliver near equal volumetric flow rate to each server in the tank. The non-homogeneity in the server flow rate arises when the tank is populated with the servers and peaks for high forced flow rate values in all the flow delivery schemes considered in this investigation. For near-natural convection flow rates, the flow rate through each server enclosure was observed to be highly uniform. The non-homogeneity is primarily caused due re-circulation patterns that develop due to the jet impingement action through the outlet ports at high flow rates. At the server level, the best server thermal performance was observed for the case of a single manifold in the tank. Future work on this investigation may involve analyzing if the non-homogeneity in server flow rates is independent of the tank size. Also, numerical modeling can be used to develop

strategies to minimize the flow maldistribution inside the tank. Detailed server geometries can be modeled to quantify the impact of flow maldistribution on server thermal performance.

REFERENCES

[1] ASHRAE Technical Committee 9.9, 2021, “Emergence and expansion of liquid cooling in mainstream data centers,” American Society of Heating, refrigeration and Air-Conditioning Engineers, Atlanta, GA

[2] Li, Z., & Kandlikar, S., 2015, “Current Status and Future Trends in Data-Center Cooling Technologies,” Heat Transfer Engineering, 36(6), pp. 523-538, DOI: 10.1080/01457632.2014.939032

[3] Ramakrishnan, B., Alissa, H., Manousakis, I., Lankston, R., Bianchini, R., Kim, W., Baca, R., Misra, P., Goiri, I., Jalili, M. and Raniwala, A., 2021, "CPU Overclocking: A Performance Assessment of Air, Cold Plates, and Two-Phase Immersion Cooling," in IEEE Transactions on Components, Packaging and Manufacturing Technology, 11(10), pp. 1703-1715, doi: 10.1109/TCPMT.2021.3106026.

[4] Ansys® Icepak, 2021 R1, ANSYS, Inc, PA, USA.

[5] Intel® Server System M50CYP1UR204, Intel Corporation, CA, USA

[6] “Synfluid PAO 6 cSt”, technical data sheet from Chevron Phillips Chemical Company LP, June, 2019. https://www.cpchem.com/sites/default/files/2020-12/Synfluid%20PAO%206%20cSt.pdf

[7] Sarangi, S., McAfee, E. D., Damm, D. G., and Gullbrand, J., 2022, "Single-Phase Immersion Cooling Performance in Intel Servers with Immersion Influenced Heatsink Design," *38th Semiconductor Thermal Measurement, Modeling & Management Symposium (SEMI-THERM)*, March 21-25, San Jose, CA, pp. 1-5.

[8] Saini, S., Gullbrand, J., Sarangi, S., McAfee, E., Damm, D., 2022, “Numerical Investigation Of Influence Of Tank Design On Thermal And Flow Performance Of A Server In Single-Phase

Immersion Cooling," *Proceedings of the ASME 2022 International Technical Conference and Exhibition on Packaging and Integration of Electronic and Photonic Microsystems*. *ASME 2022 International Technical Conference and Exhibition on Packaging and Integration of Electronic and Photonic Microsystems*, October 24-28, Paper No. IPACK2022-94537

Chapter 8 A Numerical Study On The Influence Of Mixed Convection Heat Transfer In Single-Phase Immersion Cooling

8.1 Introduction

Thermal management of data center electronics has become increasingly difficult over the last decade owing to an increase in the utilization of data-intensive technologies such as machine learning, the Internet of things, and cryptocurrency mining. Traditional data center cooling methods that utilize air for heat dissipation of server platforms consume significantly large energy and also water [1]. Liquid-based cooling technologies offer higher heat transfer coefficients and are being increasingly used to dissipate high power densities of the new generation central processing units (CPUs) and graphics processing (GPUs) [2]. Some of the popular liquid cooling technologies include cold plate-based single and two-phase cooling and direct contact single and two-phase immersion cooling. Additional benefits in these cooling technologies have also been proposed using optimized geometrical shape cold plates [3], the addition of nano-particles to base fluids to improve thermal properties of the base fluids specific to server platform cooling [4,5]

Advanced liquid cooling techniques such as single-phase immersion cooling allow data centers to not only dissipate high power densities but also enable high energy efficiency by offering very low PUE values [6]. The primary advantage of single-phase immersion (SPI) cooling lies in the fact that it allows complete removal of fan-based cooling from the servers and any of the synthetic dielectric fluids used are biodegradable with zero global warming potential (GWP). Also, in recent times significant attention has been given to addressing the material compatibility and reliability issues in this cooling technique that had been a major bottleneck in its widespread adoption [7-9]. With the reliability concerns being addressed, the

data center industry is now seeing an increase in SPI cooling deployments, especially due to its ease of deployment even in harsh environments where air and hybrid cooling systems cannot be used [7].

Coolant flow rates in typical SPI cooled servers usually fall under the laminar flow regime [6,11]. This means if the server is designed with an air-cooled heat sink, it needs to be optimized for lower flow rates and changes in convective heat transfer properties. It also means that under such low Reynolds number flow, it should be carefully analyzed whether the dominant heat transfer mode is forced or natural convection or a combination of both these modes known as mixed convection. Mixed convection is commonly found in cooling systems where the coolant flow rates or flow velocities are very low. In such flows, buoyancy forces have a significant impact on flow behavior and heat transfer rate [12]. Mixed convection is characterized by a dimensionless number known as the Richardson number (Ri) defined by the ratio Gr/Re2 which is a quantitative indicator of the balance between natural and forced convection in a flow. A value of $Ri<1$ depicts forced convection-dominated flow and a value of $Ri>1$ depicts natural convection-dominated flow.

An in-depth review of various convective heat transfer cooling options for electronic packages has been carried out by Incropera [13]. Papanicolaou and Jaluria [14] studied mixed convection in a horizontally oriented square enclosure for a single heat source. They varied the location of the outlet and size of the isothermal heat source assuming laminar 2-D flow with a Re range between 50-2000. It was observed that for Ri values between 0-10, the flow remained in the laminar regime and became oscillatory at higher values. Acharya and Ptankar [15] investigated the effect of buoyancy on laminar mixed convection for a fin-array placed in an enclosure using analytical methods. They observed that heat transfer is significantly affected by the buoyancy forces in laminar mixed convection for such an arrangement of a finned array. Also, an enhancement in heat transfer rate is obtained due to buoyancy-driven secondary flows.

Maughan and Incropera [16] experimentally investigated the effects of laminar mixed convection airflow on longitudinal fins between parallel plates where the bottom plate is isothermally heated and the top plate is isothermally cooled. A considerable enhancement in heat transfer was observed for low values of the Rayleigh number (Ra). It was also observed that closely spaced fins had a higher heat transfer rate due to enhanced surface area but this delayed the formation of secondary flows that also enhance heat transfer. Dogan and Sivrioglu [17,18] studied the influence of fin spacing, fin height, and heat flux on laminar mixed convection for longitudinal fins in a rectangular channel. Conclusions were made on optimum fin spacing that yields maximum heat transfer and it was concluded that optimum fin spacing depends on the value of modified Ra.

While there is a lot of studies that look into the impact of forced, natural, or mixed convection separately for finned-arrays in angular ducts and enclosures, there is no discussion about the influence of mixed convection in servers using SPI cooling. Characterization of mixed convection is significant for SPI as a server typically contains multiple heat-dissipating components that may also have an impact on convective heat transfer from the heat sinks. The present investigation aims at characterizing the influence of mixed convection heat transfer in a single server for SPI cooling. A commercially available computational fluid dynamics (CFD) tool, ANSYS Icepak [19], was used to develop the server model and carry out the conjugate heat transfer simulations. The baseline version of the server design is a 2U open rack unit air-cooled chassis design with an air-cooled heat sink. The server was subjected to varying inlet flow rates boundary conditions from fully natural convection to highly forced flow ($0<Re<2000$). The analysis of mixed convection flow was done by identifying important dimensionless parameters such as Nusselt number, Richardson number, and Rayleigh number. The variation in the influence of mixed convection was observed by varying the geometry of the heat sink to make it more optimized for low flow rate viscous flows. The orientation of the

server was also varied from vertical (same direction of flow and natural convection) to horizontal (transverse flow and natural convection directions) to quantify the variation in mixed convection heat transfer. For a constant heat source area (representing the CPU), the source power was also varied at two values of 115W and 160W where 115W is the thermal design power of the current CPU design in the server.

8.2 Numerical Model And Analytical Relations

This section describes the details of the numerical modeling, its boundary conditions, and the required mathematical background on mixed convection.

8.2.1 Numerical Modeling and Methodology

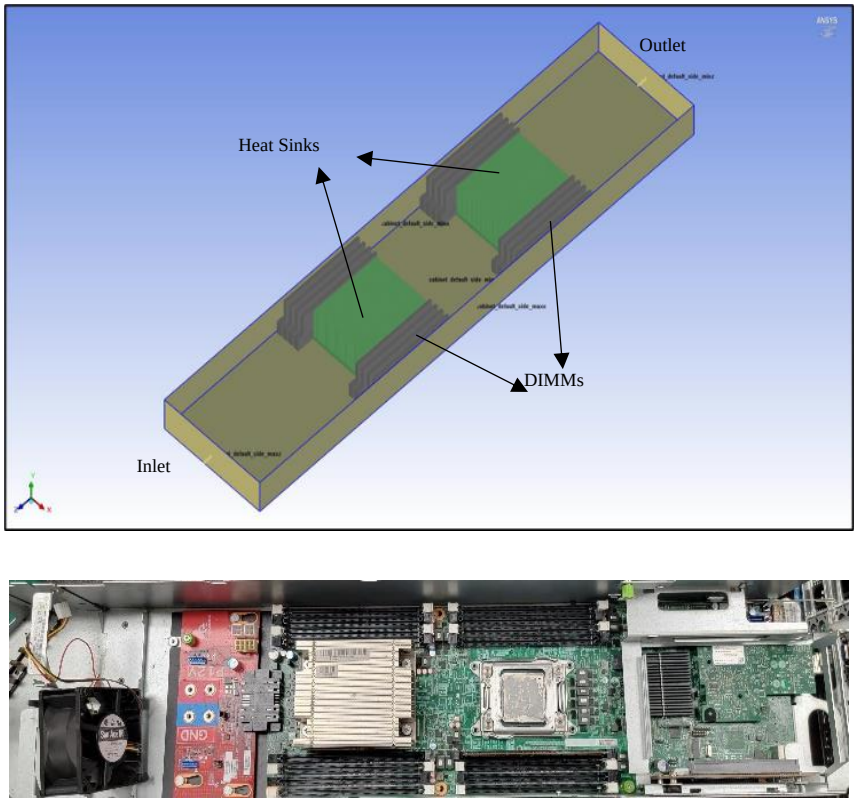

Figure 8-1: Overview of the CFD model showing the server components and boundary conditions

Figure 8-1 shows the overview of the numerical model and physical layout of the server used in this study. The server is a 3rd generation Intel-based 3rd generation open compute server

with dual CPU sockets, each with maximum thermal design power (TDP) of 115W, in a thermally shadowed configuration [20]. The simplified numerical model of the server was developed with only the CPU as a 2-D heat source under the heat sink base accompanied by the memory modules with no heat dissipation given to the memory modules. Thermo-physical properties of pure aluminum are imparted to the heat sink which was also modeled without the cutouts and the embedded heat pipe. The heat transfer fluid used for the CFD modeling is a synthetic dielectric fluid EC-100. Table 30 shows the overview of the known temperature-dependent properties of the fluid used for the simulation study. A constant value of density for the inlet temperature of 30°C is used during the study due to the limitation of the CFD tool. The thermal performance of this server in SPI with the baseline air-cooled heat sink was experimentally characterized by McWilliams with mineral oil [22]. The results of this experimental study were used to benchmark the baseline CFD model.

Temperature	**Kinematic Viscosity**	**Density**	**Thermal Conductivity**	**Specific Heat**
°C	**m^2/s ($x10^{-6}$)**	**kg/m^3**	**W/mK**	**J/kgK**
30	17.14	839.3	0.138	~2100
40	11.99	832.6	0.130	2209
50	9.52	825.3	0.136	-
60	6.68	819.5	0.135	-
70	5.24	812.9	0.135	-
80	4.22	806.3	0.134	-
90	3.48	799.7	0.133	-
100	2.92	739.1	0.132	2436

Table 30: Summary of the temperature-dependent properties of the fluid

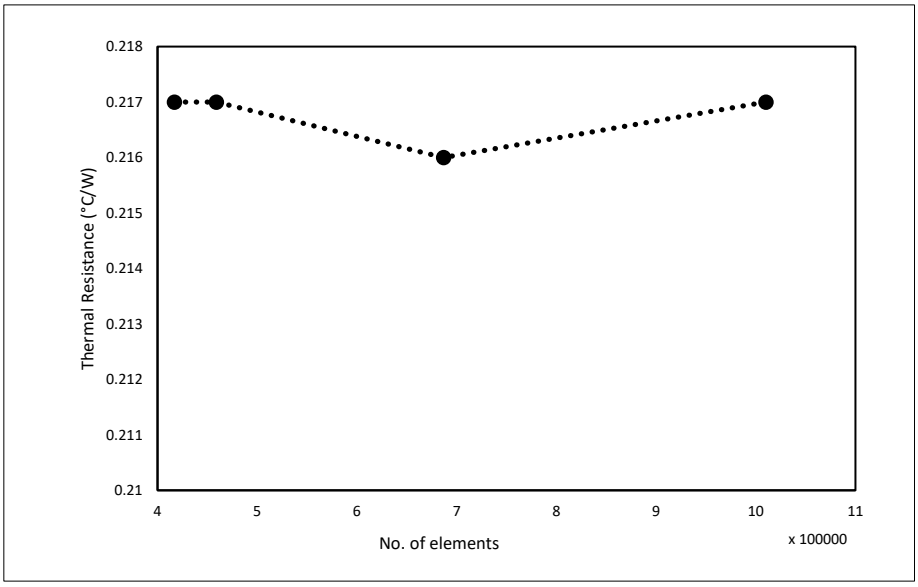

Figure 8-2: Results of grid independence study showing the variation in thermal resistance value with number of mesh elements

A grid independence study was first carried out for the baseline CFD model developed as shown in Figure 8-2. The value of thermal resistance of the heat sink was used to ascertain the grid independence results. The thermal resistance value was observed to be independent of the global mesh size outside of the heat sink and the- base value of mesh elements was used for the simulations. For benchmarking the CFD model, the source temperature value was compared with the junction temperature of the server for different inlet flow rates. As it can be seen in Figure 8-3, a close agreement is observed between the experimental data and the CFD modeling results. The maximum difference between the experimental data and the numerical model was observed to be less than 3% for all the simulation cases. The slight variation could be attributed to different fluids being used in both the experimental and numerical study.

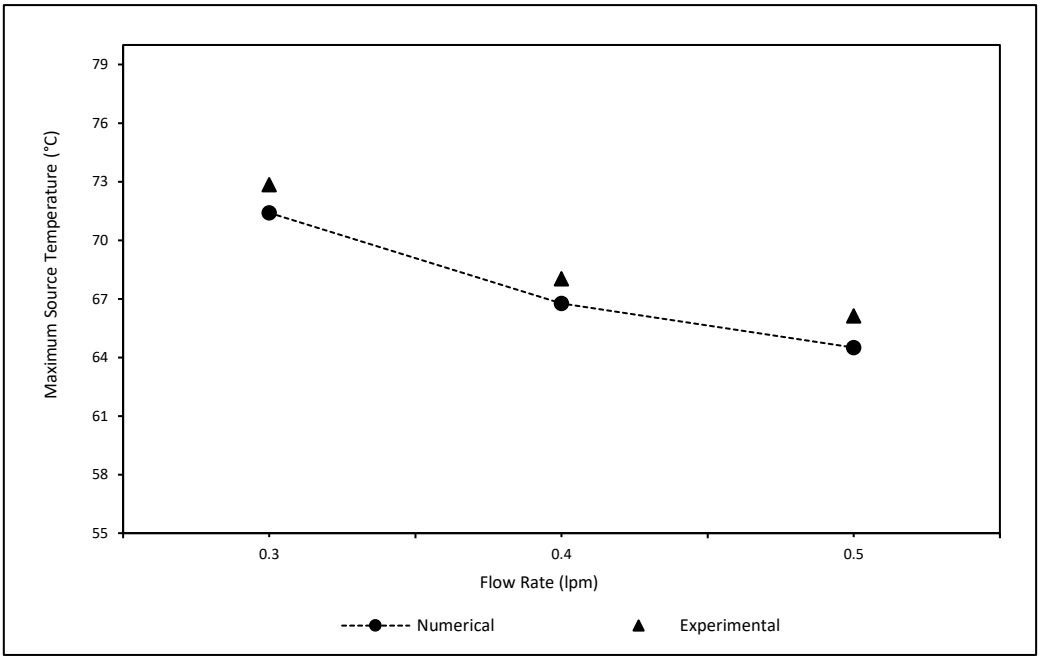

Figure 8-3: Comparison of the experimental results and results from numerical model

To vary the Re values, the inlet flow rate was varied by defining a velocity inlet boundary condition between the values of 0 to 2000. The source power is varied for two values of 115 W and 160 W. To quantify the participation of mixed convection in the heat transfer behavior the server is first analyzed in a vertical orientation as in the case of typical immersion cooling deployments. In the next step, the server was oriented in such a way that the flow direction is perpendicular to the direction of gravity. For low flow rate viscous flows where natural convection may be assumed to be the dominating heat transfer mode. Therefore, the baseline air-cooled heat sink design was assumed to be not beneficial and was also compared with an immersion optimized heat sink for the aforementioned cases.

8.3 Results and Discussion

Figure 8-4 the variation of the modified Nusselt number with varying modified Reynolds numbers for the immersion optimized heat sink when the server is immersed vertically. The modified Nusselt and Reynolds numbers are calculated using the channel width as the hydraulic diameter instead of the wetted channel cross-section and perimeter. It was

observed that the heat transfer behavior at low Reynolds number values is initially better for the 160 W CPU power for the same heat sink than 115 W CPU power. This could be due to the fact that at very low flow rates, higher CPU power induces a greater amount of natural convection behavior that assists in better heat transfer. After that, as the heat sink has been optimized for a power value of 115 W, the heat sink produces better heat transfer for that power value thereon.

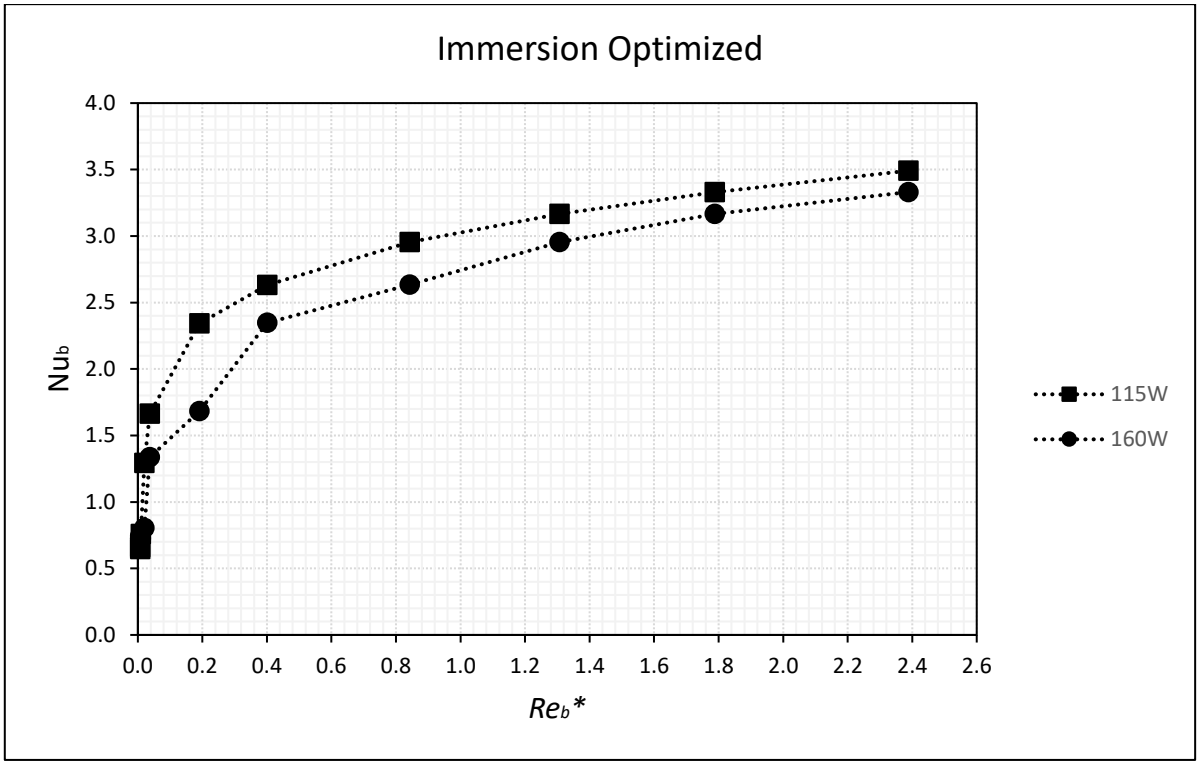

Figure 8-4: Results for heat transfer behavior for the immersion optimized heat sink with varying modified Reynolds number when the server is

It was also observed that the heat transfer behavior saturates after a certain flow rate or Reynolds number value. This Reynolds number value occurs at a very high flow rate which will be redundant for the current server's total heat dissipation value. It should also be noted that an optimized heat sink for 160W may give a better thermal performance as opposed to the current trend. Figure 8-5 shows the heat transfer behavior for the baseline heat sink at both 160W and 115 W. It is seen that the value of the modified Nusselt number reduces to almost

half of the value in the immersion optimized heat sink case implying that the heat transfer behavior is significantly impacted if an unoptimized heat sink is used, especially for low flow rate values.

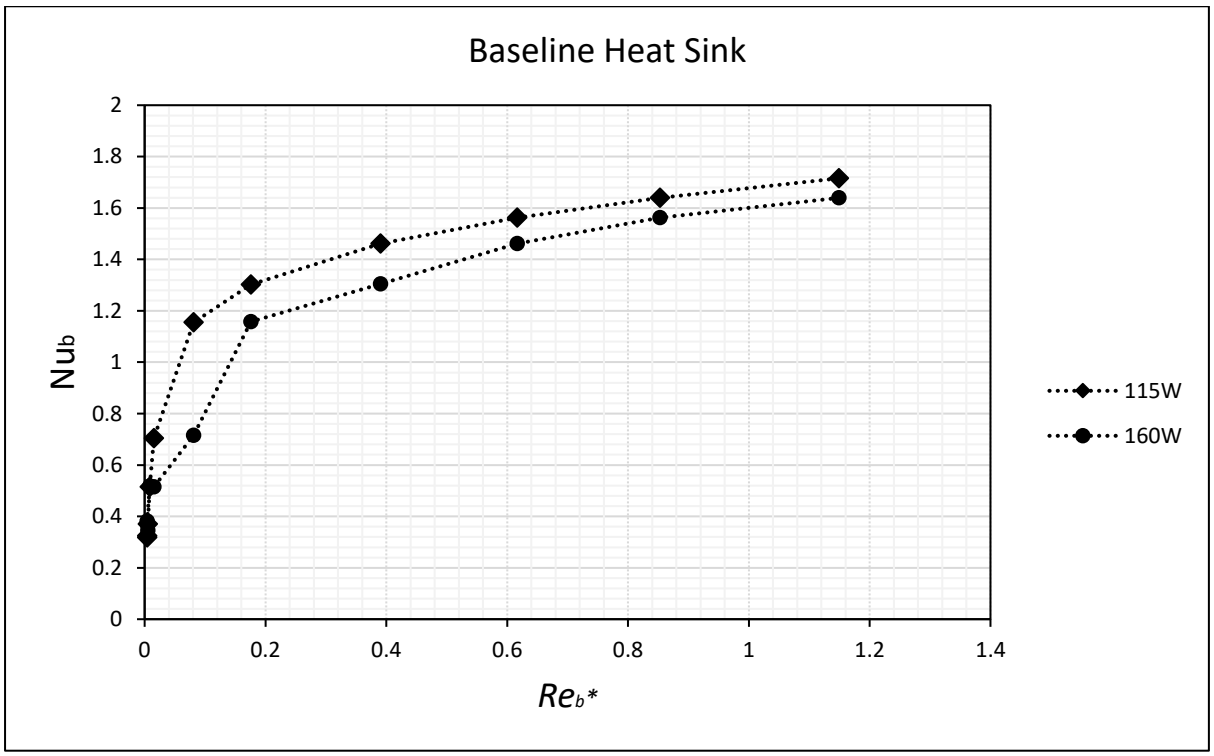

Figure 8-5: Result of the heat transfer behavior of the baseline air-cooled heat sink with varying modified Reynolds number

Figure 8-6 shows the variation of the average convective heat transfer coefficient with the ideal Nusselt number value. The ideal Nusselt number is calculated based on the heat sink geometry and flow parameters. It is seen that at lower values of the ideal Nusselt number, the heat transfer coefficient for 160W is higher than the 115 W case due to higher natural convetion at low near-natural convection flow rates. Lower heat transfer at 160W could be due to the fact that the current HS design was optimized to provide minimum R_{th} at 115W and not 160W.

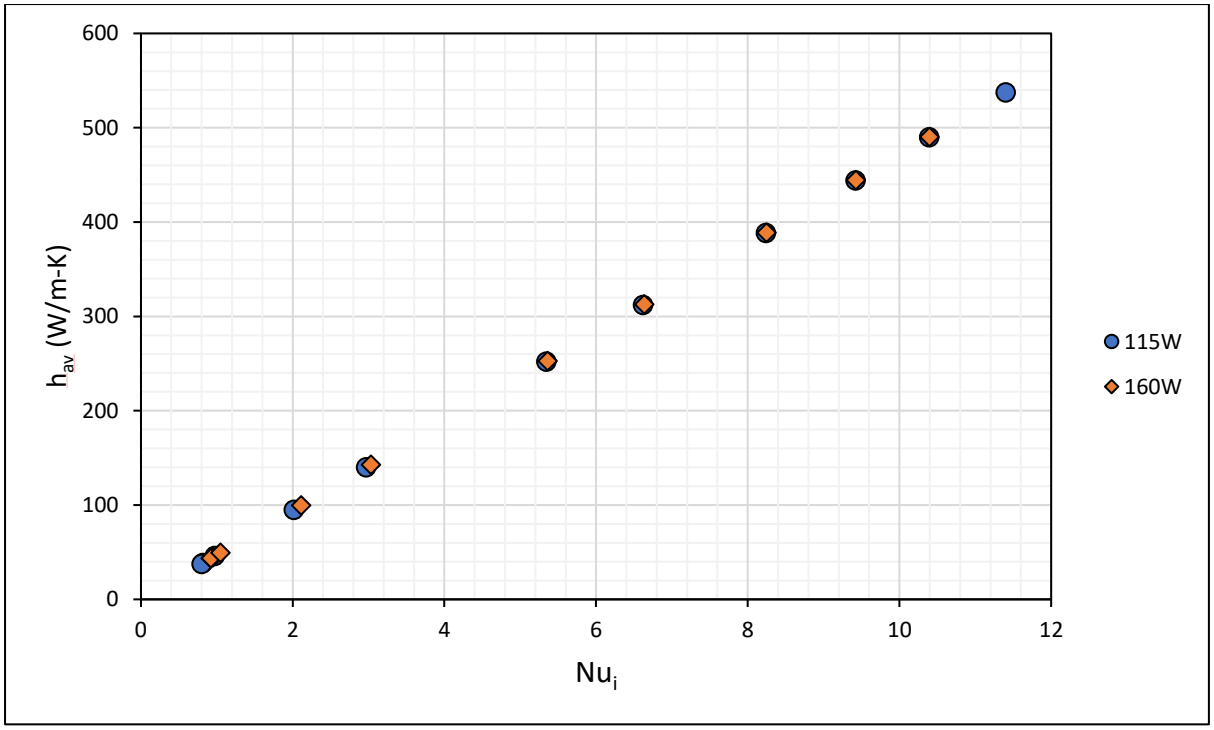

Figure 8-6: Variation of the average convective heat transfer coefficient for the two power values considered for immersion optimized heat sink

Figure 8-7 shows the variation of the mixed convection behavior for the optimized heat sink at 115 W and 160W CPU power. Mixed convection behavior is quantified by calculating the value of the Richardson number which is the ratio of the Grashof number to the square of the Reynolds number value. A value of Ri=1 depicts that both force and natural convection are balanced. A value of Ri<1 indicates that the heat transfer is dominated by forced convection and a value of Ri>1 indicates natural convection dominated flow. It was observed that the heat transfer inside the given server is dominated by natural convection until a Reynolds number value of approximately 730 for both the power values investigated. This value of Reynolds number depicts a very large flow rate which for this heat server will be redundant. Thus it can be assumed that the heat transfer behavior in this server is dominated by natural convection.

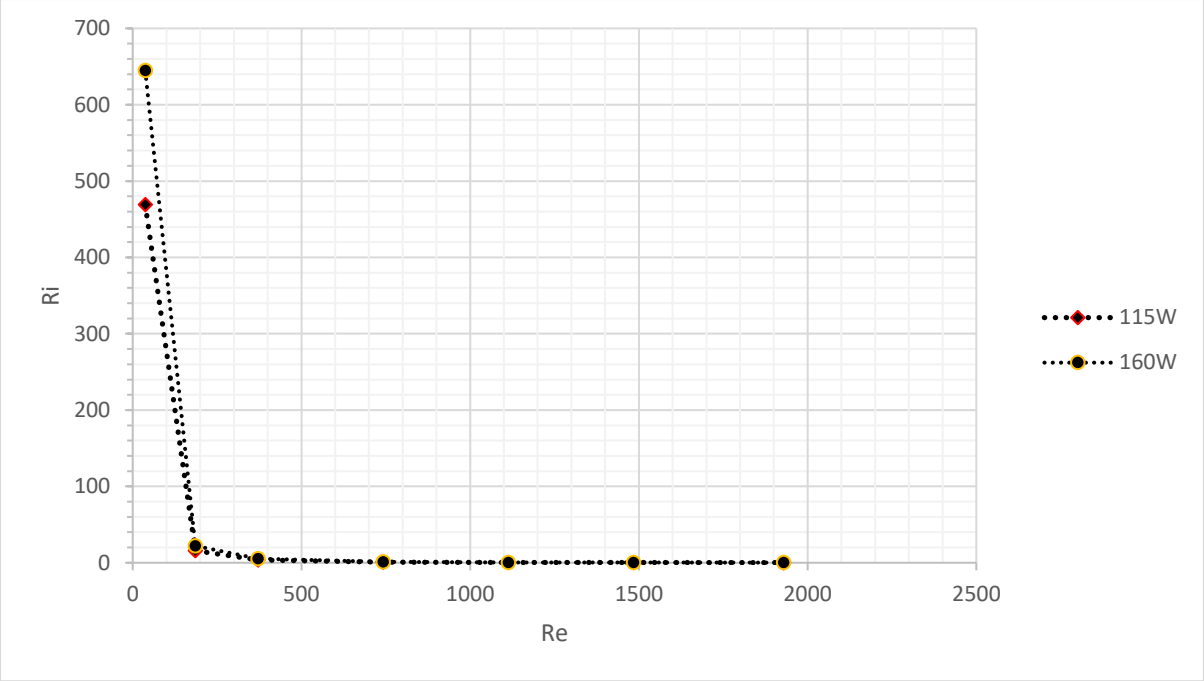

Figure 8-7: Variation of the Richardson number with the server Reynolds number for the immersion optimized heat sink at 115 W and 160 W

Figure 8-8 shows the influence of server orientation on heat transfer behavior for the immersion optimized heat sink for 115W CPU power. It can be seen that for the optimized heat sink in the vertical orientation, the heat transfer rate keeps increasing even though it appears to be saturating for high flow rate values. When the server is kept in horizontal orientation, depicting that the forced flow direction is orthogonal to the direction of the gravity vector. For the horizontal immersion case the heat transfer behavior saturates after increasing rapidly and then starts reducing as the flow rate is increased further. This means, that for horizontal orientation if the impact of natural convection is reduced, the overall heat transfer will reduce after a certain flow rate. This flow rate must be quantified for the servers if a horizontal immersion case so that the thermal performance of the server is not compromised.

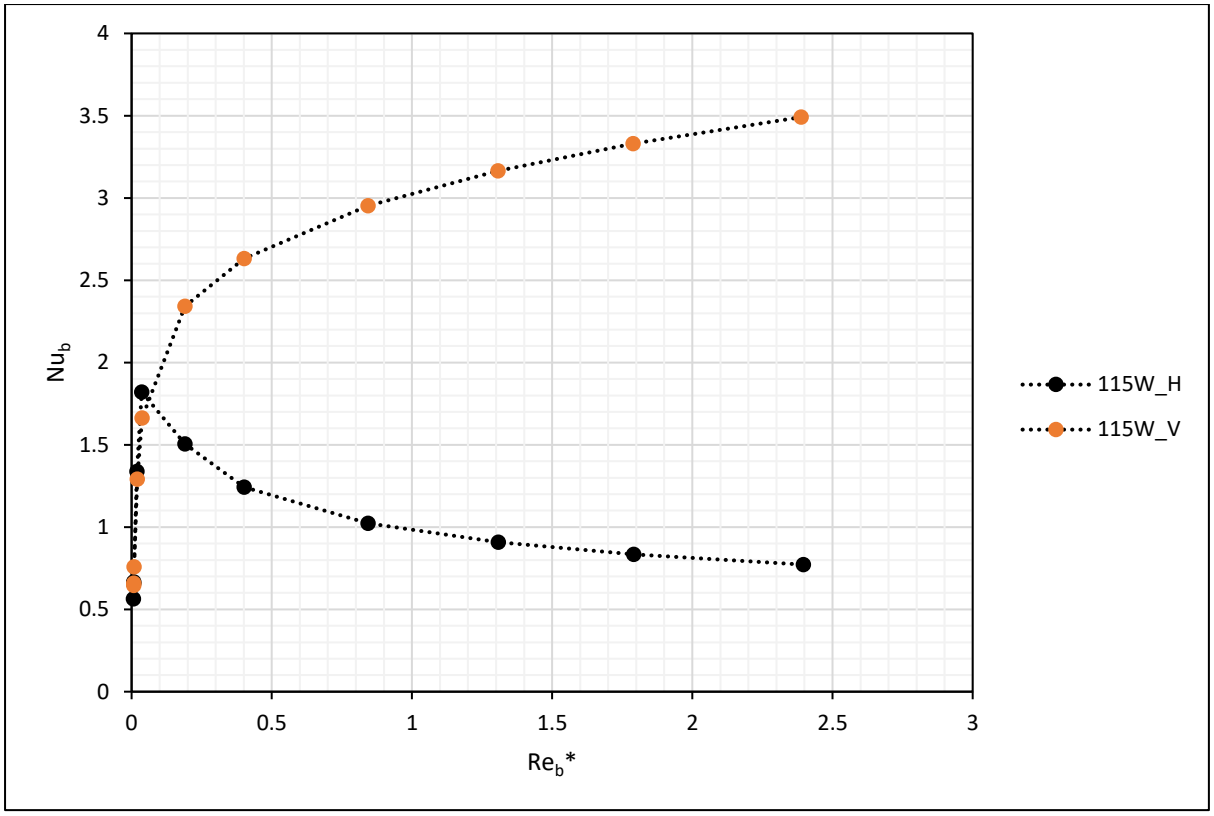

Figure 8-8: Effect of server orientation on the heat transfer behavior of the server for immersion optimized heat sink at 115 W CPU power

8.4 Conclusion and Future Work

This study numerically investigated the influence of mixed convection heat transfer in a single server SPI cooling. With increasing, edge deployments and expansion of 5G, natural convection-based immersion tanks operating at elevated ambient temperatures will be useful owing to simple cooling infrastructure and high heat capture capabilities. The following conclusions were drawn from this investigation:

- For the current server design and power values analyzed, natural convection is concluded to be the dominant heat transfer mode
- Mixed convection conditions are observed at very high liquid flow rate conditions that are operationally not feasible in single-phase immersion cooling

- Immersion optimized heat sink performs better in both vertical and horizontal server orientations
- Immersion optimized heat sink also outperformed baseline heat sink outside the optimized power range
- The point at which natural and forced convection are balanced occurs at a very large flow rate value for the current server
- For server horizontally immersed server, peak heat transfer point should be characterized as sharp decrease in heat transfer occurs thereafter

REFERENCES

[1] Li, Z., & Satish G. Kandlikar, S.G., 2015, “Current Status and Future Trends in Data-Center Cooling Technologies,” Heat Transfer Engineering, 36(6), 523-538, DOI: 10.1080/01457632.2014.939032

[2] ASHRAE 2021, Emergence and expansion of liquid cooling.

[3] Hoang, C.H., Rangarajan, S., Khalili, S., Ramakrisnan, B., Radmard, V., Hadad, Y., Schiffres, S., Sammakia, B., 2021, “Hybrid microchannel/multi-jet two-phase heat sink: A benchmark and geometry optimization study of commercial product,” International Journal of Heat and Mass Transfer, Volume 169, 120920, ISSN 0017-9310,

https://doi.org/10.1016/j.ijheatmasstransfer.2021.120920.

[4] Shahi, P., Agarwal, S., Saini, S., Niazmand, A., Bansode, P., & Agonafer, D., 2020, "CFD Analysis on Liquid Cooled Cold Plate Using Copper Nanoparticles." Proceedings of the ASME 2020 International Technical Conference and Exhibition on Packaging and Integration of Electronic and Photonic Microsystems. ASME 2020 International Technical Conference and Exhibition on Packaging and Integration of Electronic and Photonic Microsystems. Virtual, Online. October 27–29, V001T08A007. ASME. https://doi.org/10.1115/IPACK2020-2592

[5] Niazmand, A., Murthy, P., Saini, S., Shahi, P., Bansode, P., & Agonafer, D., 2020, "Numerical Analysis of Oil Immersion Cooling of a Server Using Mineral Oil and Al2O3 Nanofluid." Proceedings of the ASME 2020 International Technical Conference and Exhibition on Packaging and Integration of Electronic and Photonic Microsystems. ASME 2020 International Technical Conference and Exhibition on Packaging and Integration of Electronic and Photonic Microsystems. Virtual, Online. October 27–29, V001T08A009. ASME. https://doi.org/10.1115/IPACK2020-2662

[6] Eiland, R., Fernandes, J., Vallejo, M., Agonafer, D., and Mulay, V., 2014, "Flow Rate and inlet temperature considerations for direct immersion of a single server in mineral oil," Fourteenth Intersociety Conference on Thermal and Thermomechanical Phenomena in Electronic Systems (ITherm), May 27-30, Orlando, FL, pp. 706-714, doi: 10.1109/ITHERM.2014.6892350.

[7] Shah, J. M., Padmanaban, K., Singh, H., Duraisamy Asokan, S., Saini, S., and Agonafer, D., 2021, "Evaluating the Reliability of Passive Server Components for Single-Phase Immersion Cooling." ASME. J. Electron. Packag., 144(2): 021109. https://doi.org/10.1115/1.4052536

[8] Shah, J.M., Eiland, R., Siddarth, A., and Agonafer, D., 2016, "Effects of mineral oil immersion cooling on IT equipment reliability and reliability enhancements to data center operations," 15th IEEE Intersociety Conference on Thermal and Thermomechanical Phenomena in Electronic Systems (ITherm), May 31-3, Las Vegas, NV, pp. 316-325, doi: 10.1109/ITHERM.2016.7517566.

[9] Open Compute Project, 2022, “Immersion Requirements Revision 2.0,” Available at: https://www.opencompute.org/documents/ocp-acs-immersion-requirements-rev-2-v1-00-pdf

[10] Verma, D., 2020, “ Air-Based Cooling vs. Liquid-Based Cooling – Newly Updated,” Green revolution Cooling, Austin, TX, https://www.grcooling.com/air-based-cooling-vs-liquid-based-cooling/

[11] Cheng, C.C., Chang, P.C., Li, H.C., Hsu, F.I., 2020, “Design of a single-phase immersion cooling system through experimental and numerical analysis,” International Journal of Heat and Mass Transfer, 160, 120203, ISSN 0017-9310, https://doi.org/10.1016/j.ijheatmasstransfer.2020.120203

[12] S.G. Taji, G.V. Parishwad, N.K. Sane, Enhanced performance of horizontal rectangular fin array heat sink using assisting mode of mixed convection, International Journal of Heat and Mass Transfer, Volume 72, 2014, Pages 250-259, ISSN 0017-9310, https://doi.org/10.1016/j.ijheatmasstransfer.2014.01.012

[13] Incropera, F. P. (November 1, 1988). "Convection Heat Transfer in Electronic Equipment Cooling." ASME. J. Heat Transfer. November 1988; 110(4b): 1097–1111. https://doi.org/10.1115/1.3250613

[14] Papanicolaou, E., and Jaluria, Y., 1991, "Mixed Convection From an Isolated Heat Source in a Rectangular Enclosure," Numer. Heat Transfer, Part A, 18(4), pp. 427-461, DOI: 10.1080/10407789008944802

[15] Acharya, S., and Patankar, S. V., 1981, "Laminar Mixed Convection in a Shrouded Fin Array," ASME. J. Heat Transfer, 103(3): 559–565. https://doi.org/10.1115/1.3244502

[16] Maughan, J. R., and Incropera, F. P., 1990, "Mixed Convection Heat Transfer With Longitudinal Fins in a Horizontal Parallel Plate Channel: Part II—Experimental Results," ASME. J. Heat Transfer, 112(3): 619–624. https://doi.org/10.1115/1.2910432

[17] Dogan, M. and Sivrioglu, M., 2010, "Experimental investigation of mixed convection heat transfer from longitudinal fins in a horizontal rectangular channel," International Journal of Heat and Mass Transfer, 53(9-10), pp.2149-2158, https://doi.org/10.1016/j.ijheatmasstransfer.2009.12.031

[19] Ansys® Icepak, Release 2021R1, ANSYS, Inc.

[20] Ning, J., "Intel server in open Rack Hardware v 0.3," https://www.yumpu.com/en/document/read/29317108/intel-server-in-open-rack-hardware-v03-open-compute-project

[21] Saini, S., Bansode, P., Shahi, P., Gupta, G., Simon, V.S., Agonafer, D., 2022, "A Numerical Study On The Influence Of Mixed Convection Heat Transfer In Single-Phase Immersion Cooling," *Proceedings of the ASME 2022 International Technical Conference and Exhibition on Packaging and Integration of Electronic and Photonic Microsystems*. *ASME 2022 International Technical Conference and Exhibition on Packaging and Integration of Electronic and Photonic Microsystems*, October 24-28, Paper No. IPACK2022-94640

[22] McWilliams, T.D., 2014. Evaluating Heat Sink Performance In An Immersion-cooled Server System, M.S. Thesis, The University of Texas at Arlington, TX, USA